THERMOCHRONOLOGY AND COOLING HISTORIES OF PLUTONS: IMPLICATIONS FOR INCREMENTAL PLUTON ASSEMBLY

Jesse W. Davis

A dissertation submitted to the faculty of the University of North Carolina at Chapel Hill in partial fulfillment of the requirements for the degree of Doctor of Philosophy in the Department of Geological Sciences.

Chapel Hill
2010

Approved by:

Drew Coleman

Allen Glazner

John Bartley

Jonathan Lees

Lara Wagner

ABSTRACT

JESSE W. DAVIS: Thermochronology and cooling histories of plutons: implications for incremental pluton assembly.
(Under the direction of Drew S. Coleman)

Zircon U-Pb geochronology results indicate that the John Muir Intrusive Suite of the central Sierra Nevada batholith, California, was assembled over a period of at least 9 m.y. between 96 and 87 Ma, and the nearby Mount Whitney Intrusive Suite was assembled over at least 7 m.y. between 90 and 83 Ma. Bulk mineral thermochronology (U-Pb titanite, $^{40}Ar/^{39}Ar$ hornblende and biotite) of rocks from both suites indicate rapid cooling through titanite and hornblende closure following intrusion and subsequent slow cooling through biotite closure. Thermochronologic data are consistent with thermal cycling between hornblende and biotite closure temperatures for millions of years following intrusion.

Assembly of intrusive suites over millions of years favors growth by incremental intrusion. Estimated long-term pluton assembly rates for the John Muir and Mount Whitney intrusive suites are on the order of 0.002 $km^3 \cdot yr^{-1}$ which is inconsistent with the rapid magma fluxes that are necessary to form large-volume magma chambers capable of producing caldera-forming eruptions. If large shallow crustal magma chambers do not typically develop during assembly of large zoned intrusive suites, it is doubtful that the intrusive suites represent cumulates left behind following caldera-forming eruptions.

K-feldspar multi-diffusion domain (MDD) thermal modeling for samples from the John Muir Intrusive Suite suggests that the central Sierra Nevada batholith underwent a

period of accelerated cooling in the Late Cretaceous. In combination with previously published low-temperature thermochronologic data, the new data are consistent with a rapid cooling event that commenced around 76 Ma in the Sierra Nevada and Peninsular Ranges batholiths. Rapid cooling is apparently coincident with high erosion and sedimentation rates documented throughout this portion of the Cordilleran orogen. These observations, and the possibility that the Sierra Nevada range reached high elevations during the Late Cretaceous, indicate that the western edge of North America was tectonically active after the cessation of arc magmatism.

ACKNOWLEDGEMENTS

I would like to especially acknowledge my faculty advisor, Dr. Drew Coleman, for his guidance, helpful suggestions, and continual faith in my abilities during the course of this research effort. I am indebted to Drs. Allen Glazner, John Bartley, Jonathan Lees, and Lara Wagner for reviewing this manuscript and taking time to answer many questions. In particular, I would like to thank Drs. Matt Heizler, Ken Wohletz, and Danny Stockli. I greatly appreciate their technical support and willingness to help me maneuver through difficult subjects.

I would like to acknowledge all the students who supported the Isotope Geochemistry Lab. Their dedication and attention to detail have helped to establish this laboratory as a world class research facility. In particular, I would like to thank Russ Mapes, John Gracely, Ryan Mills, Breck Johnson, Mike Tappa, and Ayumi Shimokawa for providing stimulating discussion covering a wide variety of geological topics and for their tireless efforts pertaining to the maintenance and operation of the laboratory facilities. In addition, I would like to thank my family for their support throughout this endeavor.

Without generous financial support this project would not have been possible. The research was supported by National Science Foundation grants EAR-0538129 awarded to Drew S. Coleman. In addition, financial support from the following is greatly appreciated: University of North Carolina at Chapel Hill Martin Fellowship, University of North Carolina at Chapel Hill Charles S. Bartlett Graduate Student Field Fund, Sigma Xi Student Grants-in-Aid of Research Program, Geological Society of America Graduate Student Research Grants,

and White Mountain Graduate Student Research Fund. Logistical support from Yosemite and Kings Canyon Nation Park and the National Forest Service is greatly appreciated.

TABLE OF CONTENTS

LIST OF TABLES

Table

LIST OF FIGURES

Figure

LIST OF ABBREVIATIONS

a.s.l.	above sea level
ρ	density
Δx	grid spacing
Q	heat flux
HBr	hydrobromic acid
HCl	hydrochloric acid
dT/dz	initial geothermal gradient
zi	layer thickness
m.y.	million years
Ma	million years before present
MDD	multi-diffusion domain
A	radiogenic heat production
Cp	specific heat
T	temperature
T-t	temperature-time
k	thermal conductivity
κ	thermal diffusivity
TIMS	Thermal Ionization Mass Spectrometer
k.y.	thousand years

1. INTRODUCTION

Pluton Assembly Rates

During the Mesozoic, the western boundary of North America was an active continental magmatic arc. The Sierra Nevada and Peninsular Ranges batholiths, that are dominant features of the Cordilleran of the western United States, were assembled during subduction of an oceanic plate beneath continental North America (Fig. 1). Today, the Cordilleran orogen is exposed as a magnificent mountain range comprising some of the highest topography in the contiguous United States.

The processes by which plutons amalgamate into batholiths and are subsequently exposed are important to understanding continental crustal growth. Modern Cordilleran exposures are the result of dynamic processes that occurred at various crustal levels over hundreds of millions years. Fundamentally, pluton assembly and batholith development are tectonic issues because they are controlled by the ability of tectonic processes to produce magmas and the ability of the lithosphere to make space to accommodate these magmas. Although significant research has focused on the timescales and mechanisms by which batholiths grow, controversy remains. At the center of this controversy is understanding the rates that plutons are assembled, and the control that assembly rates have over the ability to sustain shallow crustal magma bodies with significant (>50%) proportions of liquid (Glazner et al. 2004; Lipman 2007).

Caldera collapse and associated ignimbrite eruptions demonstrate that large-volume magma chambers can exist in the upper crust (Lipman 2007). This has led to the view that

Fig. 1 Tapestry map of western United States and northern Mexico modified from Barton et al. (2003). Black outlines in main figure show the locations of the Sierra Nevada and the northern Peninsular Ranges batholiths.

plutons represent the remains of large-volume magma chambers and are genetically linked to caldera-forming eruptions (Hildreth 2004; Bachmann et al. 2007). In contrast, recent studies indicate that some plutonic suites were emplaced incrementally through amalgamation of intrusions over millions of years, and that plutons need not form from the crystallization of large-volume magma chambers (Coleman et al. 2004; Glazner et al. 2004). Seismic data are consistent with this view because geophysical studies have failed to locate large volumes of melt beneath active volcanic regions (Iyer 1984; Waite and Moran 2009).

Detailed geochronology and thermal modeling can be used to test these competing hypotheses. Magma fluxes during pluton assembly, in combination with the thermal history (T-t) of pluton assembly and subsequent cooling, can be compared to thermal models to evaluate whether large-volume magma chambers were present during pluton assembly.

Research Objective I

In order to investigate magma flux and T-t histories of zoned intrusive suites, crystallization ages and thermal histories (approximately 750-300°C) are determined for multiple plutons in the central Sierra Nevada batholith of California. The John Muir and Mount Whitney intrusive suites (hereafter referred to as the Muir suite and Whitney suite, respectively) are chosen as study areas because they provide excellent exposure and rock-types that contain minerals useful for quantifying T-t histories (zircon, titanite, hornblende and biotite). Furthermore, the intrusive suites are thoroughly mapped (Moore 1963, 1978, 1981; Bateman 1965; Bateman et al. 1964, 1965; Bateman and Moore 1965; Lockwood and Lydon 1975; du Bray and Moore 1985; Moore and Sisson 1985, 1987; Stone et al. 2000), and an existing U-Pb geochronological framework is established (Stern et al. 1981; Chen and

Moore 1982; Frost and Mattinson 1993; Coleman et al. 2004). The following methodologies are conducted to meet the study's objectives:

- Zircon U-Pb geochronology is combined with existing geologic mapping to determine long-term magma fluxes during the growth of the Muir and Whitney intrusive suites
- U-Pb zircon geochronology is combined with U-Pb titanite dates and $^{40}Ar/^{39}Ar$ thermochronology to evaluate the crystallization and T-t histories of the Muir and Whitney intrusive suites and their associated wall rocks
- Thermal models are calibrated against documented T-t histories to evaluate pluton emplacement geometries and to evaluate the volume of melt present during pluton assembly

Post-Magmatic History of the Sierra Nevada-Peninsular Ranges Arc

Magmatism in the Sierran arc ended abruptly in the Cretaceous following assembly of the zoned intrusive suites that dominate the high topography between Yosemite National Park and Mount Whitney (Stern et al. 1981; Chen and Moore 1982). Several studies suggested that the Sierra Nevada and northern Peninsular Ranges batholiths had similar post-magmatic T-t histories characterized by the onset of rapid cooling between approximately 80-67 Ma (Dumitru 1990; House et al. 1997; Grove et al. 2003). Dumitru (1990) suggested that this cooling event was caused by a shallow subducting oceanic plate resulting in significant cooling of the crust from below. Others suggested that this cooling phase expresses denudation that may have occurred in response to the removal of the subbatholithic mantle and lower crust during shallow subduction (Grove et al. 2003). However, because some of the age data from these studies have significant uncertainty, the timing and

synchroneity of this cooling event in the two batholiths remains uncertain. Consequently, the tectonic significance of these cooling patterns remains to be investigated.

The first step towards reconciling these issues is to better establish the timing of the cooling event in the Sierras. Once this is accomplished, data from other detailed studies can be combined, and the true nature and the tectonic significance of this Late Cretaceous cooling event can be investigated.

Research Objective II

In order to explore the regional tectonic significance of rapid post-magmatic cooling in the Sierra Nevada arc, I will better establish the timing of cooling by:

- Utilizing K-feldspar MDD thermal modeling to evaluate the low-temperature T-t history of the John Muir Intrusive Suite (and by inference the central Sierra Nevada batholith).
- Comparing K-feldspar MDD data from the central Sierra Nevada batholith to existing published T-t data to better determine the timing of a Late Cretaceous cooling event throughout the Sierra Nevada and Peninsular Ranges batholiths.

2. GEOLOGIC SETTING

The geology of east-central California is dominated by the Sierra Nevada batholith. The batholith formed in the Mesozoic during continental margin subduction beneath the North American plate (Fig. 2). The batholith includes over 40,000 km^2 of exposed plutonic rocks and extends approximately 600 km along the western edge of the North American craton (Kistler 1990; Bateman 1992). The majority of the exposed Sierra Nevada batholith intruded at depths around 4-15 km (Ague and Brimhall 1988); however, the southern 100 km exposes a southward transition from volcanic rocks to exposures of batholithic rocks intruded at depths as great as 35 km (Pickett and Saleeby 1993). Batholithic rocks range in composition from gabbro to leucogranite, with tonalite, granodiorite, and granite being the most abundant (Bateman 1992). Most plutons were emplaced during three major magmatic episodes: 225-195 Ma, 180-165 Ma, and 102-85 Ma (Stern et al. 1981; Chen and Moore 1982; Frost and Mattinson 1993; Saleeby et al. 1990, 2008; Coleman and Glazner 1998; Coleman et al. 2004).

In the eastern Sierra Nevada, the latest magmatic episode is characterized by intrusion of closely related plutons with similar composition, texture, fabric, age, and emplacement depth that Bateman (1992) assigned to intrusive suites (Fig. 2). From north to south these include the Tuolumne, Muir, and Whitney suites. There is also an informally named suite north of the Tuolumne Intrusive Suite (the Sonora pluton [Kistler et al. 1986]) and a poorly defined and unnamed suite south of the Whitney suite. The geology of the Muir suite,

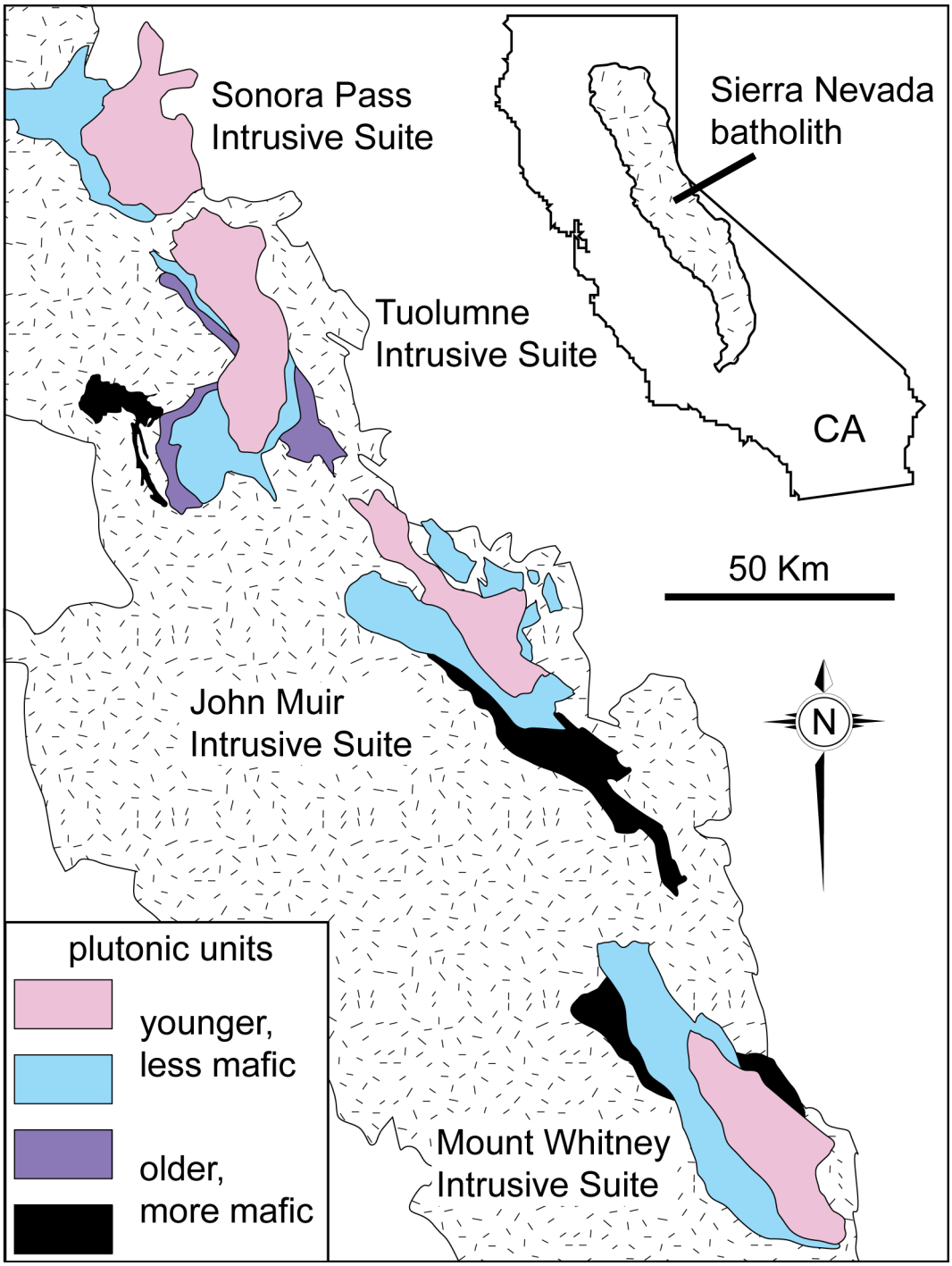

Fig. 2 Map of plutons in the eastern Sierra Nevada that are associated with the Cretaceous Sierra Crest magmatic event (Coleman and Glazner 1998). Plutonic units that are characterized by the intrusion of closely related plutons with similar composition, texture, fabric, age, and emplacement depth were assigned to intrusive suites (Bateman 1992). The Sonora Pass Intrusive Suite is an informally named suite (Kistler et al. 1986). Outcrop pattern after Bateman (1992) and Tikoff and Teyssier (1992).

originally called the John Muir sequence by Bateman and Dodge (1970), is mapped at a regional scale (Moore et al. 1963; Bateman et al. 1964, 1965; Bateman 1965, 1992; Lockwood and Lydon 1975; Frost and Mahood 1987) with local areas mapped in significant detail (Hathaway 2002; Mahan et al. 2003; Gracely 2006; Stearns and Bartley 2010). Following the original designation of the Muir suite, U-Pb zircon geochronology (Mahan et al. 2003; Gracely 2006) and field relationships (Mahan et al. 2003; Gracely 2006) suggest that the Inconsolable Quartz Monzodiorite and the McDoogle Quartz Monzodiorite be included in the Muir suite (Fig. 3). Originally, the Evolution Basin Alaskite was included with the Muir suite; however, portions of what were mapped as Evolution Basin Alaskite were recently reassigned to the Lamarck Granodiorite on the basis of field relations and geochronology (Gracely 2006). Also, preliminary zircon U-Pb geochronology from the western portion of the Evolution Basin Alaskite suggests a crystallization age of approximately 150 Ma (J. Wenner, unpublished data). Consequently, I do not include the alaskite in the Muir suite here. The Mt. Givens pluton is also excluded from discussion of the Muir suite because the pluton and Muir suite are separated by a large mass of Jurassic and older rocks.

All of the plutons in the Muir suite have elongate map patterns (Fig. 3) However, plutons exposed in the northern portion of the suite (including the northern Lamarck Granodiorite, Lake Edison Granodiorite, Mono Creek Granite, and the Round Valley Peak Granodiorite) have ages, textures, and compositional variations that mimic those of concentrically zoned, nested intrusions, such as the Tuolumne and Mount Whitney intrusive suites (Bateman 1992; Hirt 2007). Geobarometry data suggest that the exposed surface of the

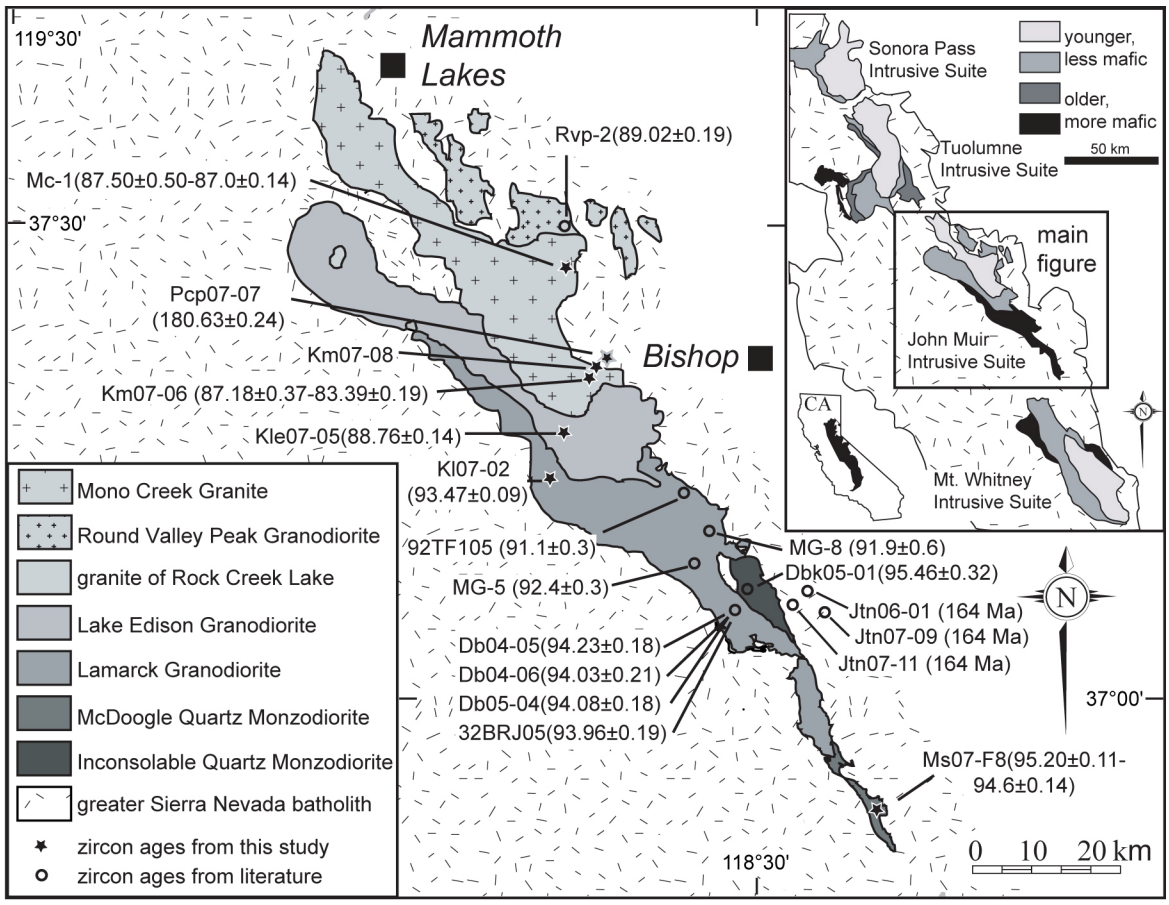

Fig. 3 Simplified geology of the John Muir Intrusive Suite after Bateman (1992). Figure shows sample nomenclature and locations. The Late Cretaceous Muir suite is exposed in Kings Canyon-Sequoia National Park, California. Darker shaded plutons are more mafic. Ages shown are from U-Pb zircon data reported in millions of years and errors are 2-sigma. Lamarck Granodiorite (92TF105, MG-8, MG-5) ages from Coleman et al. (1995). Lamarck Granodiorite (Db04-05, Db04-06, Db05-04, 32BRJ05) and Inconsolable Quartz Monzodiorite (Dbk05-01) ages from Gracely (2006). Round Valley Peak Granodiorite (Rvp-2) age from Gaschnig (2005). Tinemaha Granodiorite (Jtn06-01, Jtn07-09, Jtn07-11) ages are estimated from Chen and Moore (1982).

Muir suite crystallized at depths between 8-12 km (Ague and Brimhall 1988). Within the Muir suite, a dextral shear zone extends along the northeast edge of the suite and crosses through the central region and continues along the southwest margin (Lockwood and Lydon 1975; Tikoff and Teyssier 1992; Tobisch et al. 1995).

The Whitney suite includes the granodiorite of Sugarloaf, granodiorite of Lone Pine Creek, Paradise Granodiorite, and Whitney Granodiorite (Fig. 4; Moore 1978, 1981; du Bray and Moore 1985; Moore and Sisson 1985, 1987; Stone et al. 2000). The Whitney suite is characterized by older, equigranular, relatively mafic marginal units that preserve internal contacts (Hirt 1989, 2007). These marginal units grade into younger, equigranular to porphyritic to megacrystic interior units (Hirt 1989, 2007). Geobarometry data suggest crystallization depths of approximately 4-13 km (Ague and Brimhall 1988; Hirt 1989, 2006). Two dextral fault/shear zones flank the Whitney suite: the Sierra Crest shear zone to the northeast, and the Kern Canyon fault to the southwest.

Both the Muir and Whitney suites intruded Jurassic and early Cretaceous plutonic rocks ranging in composition from quartz diorite to granite (Moore 1981; Bateman 1992). Several of these wall rocks with appropriate mineral assemblages (i.e., titanite ± hornblende ± biotite) were sampled to track their thermal histories during and after Cretaceous magmatism. From north to south, these include the quartz diorite of Pine Lake, the Tinemaha Granodiorite, the Bullfrog Granite, and unnamed mafic intrusive rocks at the northern end of the Whitney suite (Figs. 3 and 4).

The Jurassic quartz diorite of Pine Lake crops out east of the northern Muir suite, is surrounded by Cretaceous intrusions, and was extensively intruded by dikes propagating from the Mono Creek Granite of the Muir suite (Frost and Mattinson 1988; Bateman 1992).

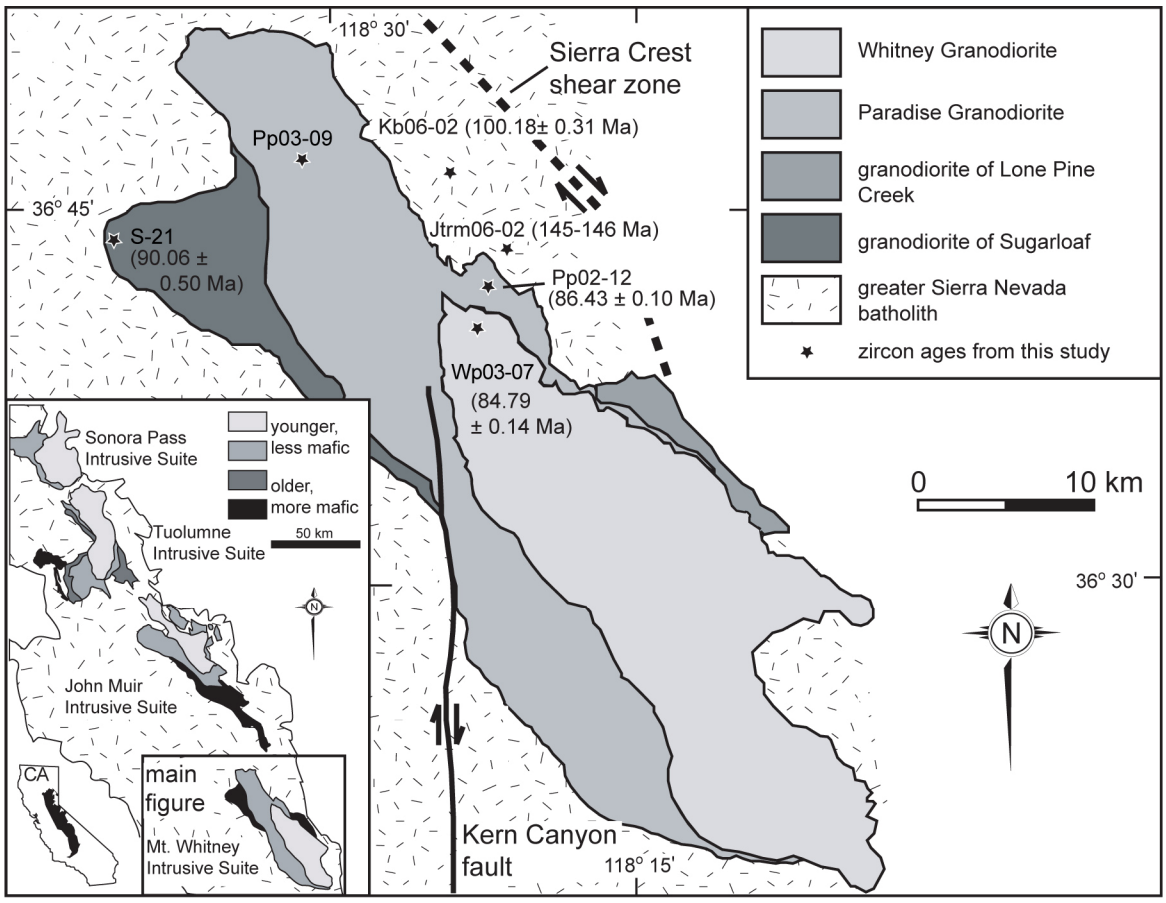

Fig. 4 Simplified geology of the Mount Whitney Intrusive Suite after Hirt (2007). The Late Cretaceous Muir suite is exposed in Kings Canyon-Sequoia National Park, California. Figure shows sample nomenclature and locations. Ages shown are from U-Pb zircon data reported in this study in millions of years and errors are 2-sigma. Darker shaded plutons are more mafic.

The Jurassic Tinemaha Granodiorite crops out east of the southern Muir suite and was intruded by numerous Cretaceous intrusions including the Muir suite's Inconsolable Quartz Monzodiorite and the Lamarck Granodiorite (Bateman 1992). The Bullfrog Granite is the major wall rock unit flanking the northeastern margin of the Whitney suite. Small clusters (approximately 2 km^2) of unnamed mafic plutonic rocks crop out along the Paradise Granodiorite contact and within the southern Bullfrog Granite (Moore 1981). Moore (1981) referred to these rocks simply as mafic plutonic rocks and assigned them a Triassic or Jurassic age.

The extension of the Mesozoic arc from the Sierra Nevada batholith southward into northwestern Mexico is dominated by the Peninsular Ranges batholith (Fig. 1). As in the Sierra Nevada, batholithic rocks in the Peninsular Ranges are predominantly tonalitic to granitic in composition and preserve west-east variations of composition, host rock, and emplacement age (Ortega-Rivera 2003). Plutonism in the Peninsular Ranges batholith migrated from west to east with the western area being intruded between approximately 140-105 Ma and the eastern area between approximately 105-80 Ma (Ortega-Rivera 2003 and references within). In general, emplacement depths in the Peninsular Ranges batholith are estimated to be somewhat deeper than the central Sierra Nevada batholith between 11-23 km (Ague and Brimhall 1988).

The Sierra Nevada and Peninsular Ranges batholiths present ideal locations to explore pluton emplacement and the post-magmatic thermal history of the western margin of the Mesozoic US Cordillera. The zoned Cretaceous intrusive suites of the Sierra Nevada provide an opportunity to examine the magma flux rates and thermal histories of the large zoned suites that are conceptually linked to silicic ignimbrite eruptions (e.g., Hildreth 2004;

Lipman 2007). Together, the Cretaceous intrusions of the Sierra Nevada and Peninsular Ranges batholiths are key to understanding the regional tectonic evolution of the western US Cordilleran margin because the intrusive suites represent the end of magmatic activity in the Sierran arc. Consequently, their post-intrusive thermal histories provide the best opportunity for understanding the post-Cretaceous tectonic evolution of the region. Unlike earlier Cretaceous, Jurassic, and Triassic intrusive rocks, these terminal arc intrusive rocks should preserve thermal histories affected only by post-intrusion cooling and tectonic disturbance of the geothermal gradient.

3. METHODS

U-Pb Analyses

Zircon and titanite separates were obtained by mechanical disaggregation (jaw crusher and disk mill), followed by water table, heavy liquids, and magnetic separator techniques. Zircon grains were thermally annealed and subjected to chemical abrasion to eliminate volumes affected by radiation damage and remove inclusions (Mundil et al. 2004; Mattinson 2005). Zircon and titanite fractions were spiked using ^{205}Pb-^{236}U-^{233}U solution (Parrish and Krogh 1987), and dissolved following a procedure modified after Krogh (1973) and Parrish (1987). Uranium and Pb were isolated using HCl (zircon) and two stage HBr-HCl (titanite) anion exchange procedures modified after Krogh (1973). Isotope ratios of both U and Pb were determined by thermal ionization mass spectrometry (TIMS) on the VG Sector 54 mass spectrometer at the University of North Carolina at Chapel Hill. All data were collected using the Daly detector and peak hopping. Mass fractionation for U was corrected by measuring the ^{233}U/^{236}U ratio (a known constant for the spike), assuming linear fractionation. Isotope ratios for Pb were corrected assuming a linear fractionation of 0.15%/amu. Details regarding corrections for blank and common Pb for zircon and titanite analyses are provided in Appendix 1.

Titanite Common Pb Correction

Titanite fractions have low ratios of radiogenic to common Pb; therefore, titanite dates, when compared to zircon ages, are less precise and more sensitive to the initial

common Pb correction. To help minimize uncertainty in this correction, the composition of the common Pb was determined from leached K-feldspar grains. K-feldspars were separated using the same procedures as for zircon and titanite. Milligram-sized fractions of hand-picked K-feldspar grains were progressively leached following the methods of Schmitz (2010). All leachates were dried and redissolved in HBr for separation of Pb by HBr-HCl anion exchange chemistry. Separated Pb was analyzed by thermal ionization mass spectrometry (TIMS) on the VG Sector 54 mass spectrometer at the University of North Carolina at Chapel Hill in static multicollector mode using faraday detectors (Appendix 1). The least radiogenic leachate was used as the composition of the common Pb in order to calculate titanite dates (e.g., Schmitz and Bowring 2001).

^{40}Ar/ ^{39}Ar Analyses

Hornblende, biotite, and K-feldspar separates were obtained from the same samples that were used for U-Pb geochronology. Mineral separates were washed, weighed, loaded into Cu-foil, and placed into a machined aluminum disk for irradiation. Separates were analyzed by the incremental-heating method using a double-vacuum molybdenum resistance furnace. Isotope ratios were measured on a MAP-215 50 mass spectrometer at the New Mexico Geochronology Research Laboratory, New Mexico Institute of Technology.

It is common in the Ar community to report apparent dates relative to the Fish Canyon sanidine interlaboratory flux monitor (FC-2; 28.02 Ma; Renne et al. 1998) and $^{40}K_{total}$ decay constant of $5.543e^{-10}$ yr^{-1} (Steiger and Jäger 1977). However, Renne et al. (2009) determined a different Fish Canyon sanidine age of 28.293 ± 0.046 Ma as well as different $^{40}K_{\varepsilon}$ and $^{40}K_{\beta}$ decay constants of $5.7926 \pm 0.0066e^{-11}$ yr^{-1} and $4.9647 \pm 0.0109e^{-10}$

yr^{-1}, respectively. In this study, the preferred dates were those calculated using Renne et al. (2009).

In composite hornblende grains, fine-grained mica inclusions or fluid infiltration can disturb Ar concentrations and result in complex K/Ca release patterns and anomalously young ages during low-temperature heating steps (Berger 1975; Sisson and Onstott 1986; Miller et al. 1991; Wartho 1995). Heating steps from hornblende separates displaying these complexities were excluded from plateau and isochron determinations, and only the intermediate and high-temperature heating steps with uniform K/Ca ratios (near 0.1) were used in plateaus and isochrons. Similarly, biotite samples that decrease in K/Ca ratio at the high temperature steps indicate degassing of mineral phases other than biotite (Lo and Onstott 1989), and were excluded from plateau and isochron determinations.

To evaluate the impact of excess ^{40}Ar on all the dates, plateau dates were compared to corresponding inverse isochron dates. Overlap of plateau and inverse isochron dates within 2-sigma error indicates that any excess ^{40}Ar has negligible effect on date determination (e.g., Singer and Pringle 1996).

Thermochronology

Bulk mineral thermochronology was used to determine high-temperature (>300°C) T-t histories by correlating temperatures to ages/dates of coexisting mineral thermochronometers: zircon, titanite, hornblende, and biotite. Titanite, hornblende, and biotite dates indicate timing when samples passed through respective closure temperatures (Dodson 1973). Diffusion experiments were not conducted during this study. Consequently, estimated closure temperatures ranges of 700-660°C for titanite dates (Scott and St-Onge

1995), 580-490°C for hornblende dates (Harrison 1981), and 345-280˚C for biotite dates (Harrison et al. 1985) were used.

K-Feldspar multi-diffusion domain (MDD) modeling

K-feldspar age spectra were interpreted using multi-diffusion domain (MDD) modeling of thermal histories over the temperature range between approximately 350-150°C (Lovera et al. 1989, 1991, 1997, 2002). Thermal modeling was conducted at the New Mexico Geochronology Research Laboratory, New Mexico Tech, following the procedures outlined in Sanders et al. (2006).

The T-t history experienced by a K-feldspar was modeled using the age spectrum data determined during step heating experiments (McDougall and Harrison 1999; but see Parson et al. 1999 for a cautionary view). The age spectrum is a measurement of the natural radiogenic ^{40}Ar ($^{40}Ar^{*}$) concentration distribution within the sample, and the release of ^{39}Ar with increasing temperature is a measure of the K-feldspar closure temperatures. Modeling assumes that the release of Ar was by thermally activated volume diffusion described by an Arrhenius equation. Age spectrum and Arrhenius plot characteristics were assumed to be controlled by the presence of multiple, discrete, diffusion domains within the K-feldspar crystal. Once the diffusion parameters (activation energy and diffusion coefficient) and domain distribution parameters (volume fraction and relative domain size) for a sample were determined, T-t histories were forward modeled to produce a model age spectrum using the algorithms of Lovera et al. (1989, 1991, 1997, 2002). A modeled T-t history results from minimizing the differences between the laboratory generated age spectrum and the modeled age spectrum (Quidelleur et al. 1997).

The MDD algorithm cannot account for excess Ar contamination; however, K-feldspar Ar release spectra commonly show the effects of degassing fluid inclusions at low temperature steps (Harrison et al. 2005). Heating steps that record anomalously old ages were corrected for excess Ar prior to modeling following procedures outlined in Sanders et al. (2006). Similarly, the MDD algorithm only models cooling from an initial high temperature above all possible K-feldspar closure temperatures. Consequently, the high temperature portions of the model were not constrained by data and therefore were not interpreted or shown on figures.

(U-Th)/He Analyses

Zircons chosen for (U-Th)/He analysis were euhedral, clear, and greater than 60 μm long in order to minimize effects of long α-stopping distances (Farley et al. 1996). For each sample, three single grains were loaded into separate Pt foil packages and degassed by heating with a ND-YAG laser. Helium abundances were measured using a quadrupole mass spectrometry system. Degassed grains were unpacked and dissolved, and U and Th concentrations were measured by isotope dissolution using a Fisons/VG Plasma Quad II Inductively Coupled Mass Spectrometer (ICP-MS). All analyses and age corrections for α-ejection followed the procedures utilized at the University of Kansas (U-Th)/He laboratory. Because we did not conduct diffusion experiments, the zircon closure temperature is unknown; however, we estimate it to be between approximately 170-190˚C after Reiners et al. (2004).

Thermal Modeling

Model Algorithms

The motivation for using numerical models was to monitor the heat flow within the crust during pluton assembly, and model conditions within the pluton (e.g., percent melt present) during magma accumulation. I used KWare Heat3D (Wohletz 2008) to model incremental pluton growth in two dimensions. Heat3D is a graphically interfaced application developed for use in transient thermal regimes, and is based on the numerical solution of the heat flow equation using the finite-differencing method. Heat transfer in magmas was conductive and convective. Heat transfer by convection was only calculated when the magma had a thermal Rayleigh number greater than 2000 (Wohletz 2008). Heat transfer in the wall rock was entirely conductive.

Heat3D only conserves thermal energy within the modeled domain and does not conserve mass. Consequently, the model is limited in representing the effects of heat advection as rocks are displaced during incremental magma emplacement. Heat3D approximates heat advection into nearby cells by using the aspect ratio of the intrusion. For example, if the intrusion is vertical and sheet-like, an extensional environment is assumed and heat contained in the rock is displaced to either side of the intrusion. Thus, it ignores any vertical advection of heat – which is unrealistic and limits the applicability of the model during vertical sheeted dike assembly of a magma body. In contrast, if the intrusion is horizontal and sheet-like, heat contained in the rock is displaced upwards (Wohletz 2008).

Initial and Boundary Conditions

The limitations of Heat3D imposed by the fact that the model does not conserve mass require that modeling be limited to stacking horizontal sheets. Except for well-documented evidence for the assembly of the earliest (>92 Ma) parts of the Muir suite as sheeted dikes (Mahan et al. 2003; Gracely 2006; Stearns and Bartley 2010), workers in both the Muir (Hathaway 2002) and Whitney (Moore 1981; Hirt 2007) agree that field evidence supports laccolithic assembly of the suites. This mode of magma accumulation is appropriately modeled with Heat3D.

In order to mimic stacked laccolith assembly, I modeled the growth of the suites as a series of horizontal sheets emplaced directly adjacent to one another antitaxially (Bartley et al. 2008). Dimensions of the model intrusion and rates of magma accumulation were determined by dimensions and fill rates of northern Muir and Whiney suites. Both suites have horizontal dimensions of approximately 30 x 80 km, and thickness is assumed to be 5 km (Hirt 2007). Geochronologic data (see below) indicate assembly times of 6-7 m.y. for both suites, resulting in a long-term accumulation rate of approximately 0.002 km^3y^{-1}. Only a two-dimensional (width and height) half space through the short axis of the intrusive suites was modeled. Because the model cannot reproduce steady-state filling of a chamber, this was approximated by intruding 0.25 km thick x 15 km wide sheets at a rate of approximately 3 sheets per m.y. Modeled intrusions had injection and solidus temperatures of 850°C and 750°C, respectively (Table 1). The first intrusion was emplaced at a depth of 6 km and the last at a depth of 11 km. Model wall rock was allowed to absorb latent heat and melt if temperatures exceed the solidus.

The modeling strategy was to monitor the temperature-time path at various "watch points" in the crust. A watch point corresponds to a material point and thus, could correspond to a sample location. I monitored the T-t history of numerous watch points at numerous depths, both within the intrusions and in adjacent wall rock.

The model domain was a two-layer crustal section 50 km wide and 35 km tall – extending far beyond the intrusion boundaries so as to reduce errors introduced by edge effects. The crustal section consists of an andesitic layer extending from the surface to 8 km depth, and a granodiorite layer extending from a depth of 8-35 km (Table 1). This crustal section is consistent with an oblique column that is exposed in the southern Sierra Nevada batholith that preserves volcanic rocks near the surface and predominantly felsic batholithic rocks extending to depths of about 35 km (Saleeby et al. 2003).

Solutions to the heat flow equation require specification of the initial temperatures throughout the modeled domain and along each boundary. Along the top (surface) boundary, temperature was held constant at 0°C. A steady-state thermal gradient (dT/dt = 0) was maintained along the side and bottom boundaries. Assuming a multi-layer crust, a geothermal gradient defines the initial temperature conditions at depth within the modeled domain using:

$$T(z_i) = -\frac{A_i z_i^2}{2k_i} + \left(\frac{Q_{Di}}{k_i} + \frac{A_i D_i}{k_i}\right) z_i + T_{Di} \qquad \text{Equation 1}$$

where each layer has a thickness of D_i, uniform heat production of A_i, and thermal conductivity of k_i. Q_{Di} is heat flux at the base of each layer, z_i is depth within a layer, T_{Di} is the temperature at the top of each layer (Table 1).

Thermal conductivity is an intrinsic property relating to a material's ability to conduct heat. Robertson (1988) suggested, if the mode of the rock is known, its conductivity can be estimated using:

$k = n_1k_1 + n_2k_2 + n_3k_3 + \ldots$ Equation 2

where n_1, n_2, n_3 are volume fractions of mineral phases 1, 2, 3, and k_1, k_2, k_3 are conductivities of the mineral phases. Average k for quartz, alkali feldspar, plagioclase (oligoclase to andesine) are 7.7, 2.0, 1.9 $W \cdot m^{-1} \cdot K^{-1}$, respectively (Robertson 1988). Average Muir and Whitney suite plutons have modal values of 25, 17, 44% for quartz, alkali feldspar, plagioclase, respectively (Gracely 2006; Hirt 2007). Based on these values, k = 3.1 $W \cdot m^{-1} \cdot K^{-1}$ was assumed for depths between 8-35 km (Table 1). This value is consistent with measured granitic k values (Robertson 1988; Turcotte and Schubert 2002; Whittington et al. 2009) and an average continental crust k value (Spear 1995). For the andesite layer, k = 1.7 $W \cdot m^{-1} \cdot K^{-1}$ was assumed (García et al. 1989). Thermal conductivities of magmas are not as well understood as those for rocks (Stimac et al. 2001). Murase and McBirney (1973) estimated k at 900°C for a rhyolite obsidian to be 2.3 $W \cdot m^{-1} \cdot K^{-1}$ and 1.1 $W \cdot m^{-1} \cdot K^{-1}$ for an andesite. I use the recent estimate of 1.4 $W \cdot m^{-1} \cdot K^{-1}$ that Pertermann et al. (2008) calculated for a $KAlSi_3O_8$ melt because it should best approximate the value for late rhyolite melt in a granodiorite (Table 1). Whittington et al. (2009) showed that thermal conductivity decreases with increasing temperature. This phenomenon reduces heat transfer and magma cooling and is simulated in Heat3D using:

$$k(T,z) = k_0\left(\frac{1+cz}{1+bT}\right)$$ Equation 3

where k_0 is k at 0°C, b is a thermal constant ($1.5e^{-3}$ $°C^{-1}$ for upper crust, $1.0e^{-4}$ $°C^{-1}$ for lower crust), c is crustal depth constant ($1.5e^{-3}$ km^{-1}), z *is* depth (km), and T is temperature (°C) (Table 1).

4. RESULTS

U-Pb Zircon Analyses

Ages[1] for samples having individual zircon fractions that overlap within uncertainty of one another and overlap concordia are reported as concordia ages (Fig. 5; Appendix 1; Ludwig 1998). Concordia ages are reported for samples of the Lamarck Granodiorite (Fig. 5G), Lake Edison Granodiorite (Fig. 5I), granodiorite of Sugarloaf (Fig. 5M), Paradise Granodiorite (Fig. 5N), Whitney Granodiorite (Fig. 5O), and Bullfrog Granite (Fig. 5P) and are interpreted as crystallization ages. In contrast, ages from the McDoogle Quartz Monzodiorite (Fig. 5B), two Mono Creek Granite samples (Fig. 5J, 5K), quartz diorite of Pine Lake (Fig. 5L), and the Jurassic-Triassic mafic rock sample (Fig. 5Q) spread along an interval of concordia; therefore, a concordia age cannot be determined and instead the range of $^{206}Pb/^{238}U$ ages is reported (Fig. 5).

Samples of the two oldest Muir suite units yield indistinguishable ages of 95.46 ± 0.32 Ma for the Inconsolable Quartz Monzodiorite (Fig. 5A; Gracely 2006) and 95.20 ± 0.11 to 94.60 ± 0.14 Ma for the McDoogle Quartz Monzodiorite (Fig. 5B). A new age from the Lamarck Granodiorite is 93.47 ± 0.09 Ma (Fig. 5G). When combined with other geochronologic data the Lamarck Granodiorite assembled over 3 m.y. (Fig. 6A; Coleman et

[1] Throughout the literature, the words “age” and “date” are often used interchangeably. For plutonic rocks, it is generally accepted that the age of a sample indicates the time of crystallization, and a zircon U-Pb analysis best represents this time. A date indicates the timing of some subsequent event in the sample’s history. For example, “date” is used when referring to a time when the sample passed through a particular closure temperature isotherm.

al. 1995; Gracely 2006). Samples collected from the northern Muir suite plutons are the youngest in the suite and are all younger than 90 Ma (Fig. 5H-5K).

Samples from the Whitney suite were all collected from the northern region of the suite (Fig. 4). A sample from the granodiorite of Sugarloaf is 90.59 ± 0.10 Ma (Fig. 5M), which is the oldest reported age for this unit and is over 2 m.y. older than the 88 Ma age for the same granodiorite reported by Chen and Moore (1982). Ages from the Paradise Granodiorite, Whitney Granodiorite, and Bullfrog Granite are 86.43 ± 0.10 Ma (Fig. 5N), 84.79 ± 0.14 Ma (Fig. 5O), and 100.18 ± 0.31 Ma (Fig. 5P), respectively. These results extend the documented intrusive histories of these three plutons to over at least 2 m.y. when combined with previous zircon geochronology (Chen and Moore 1982).

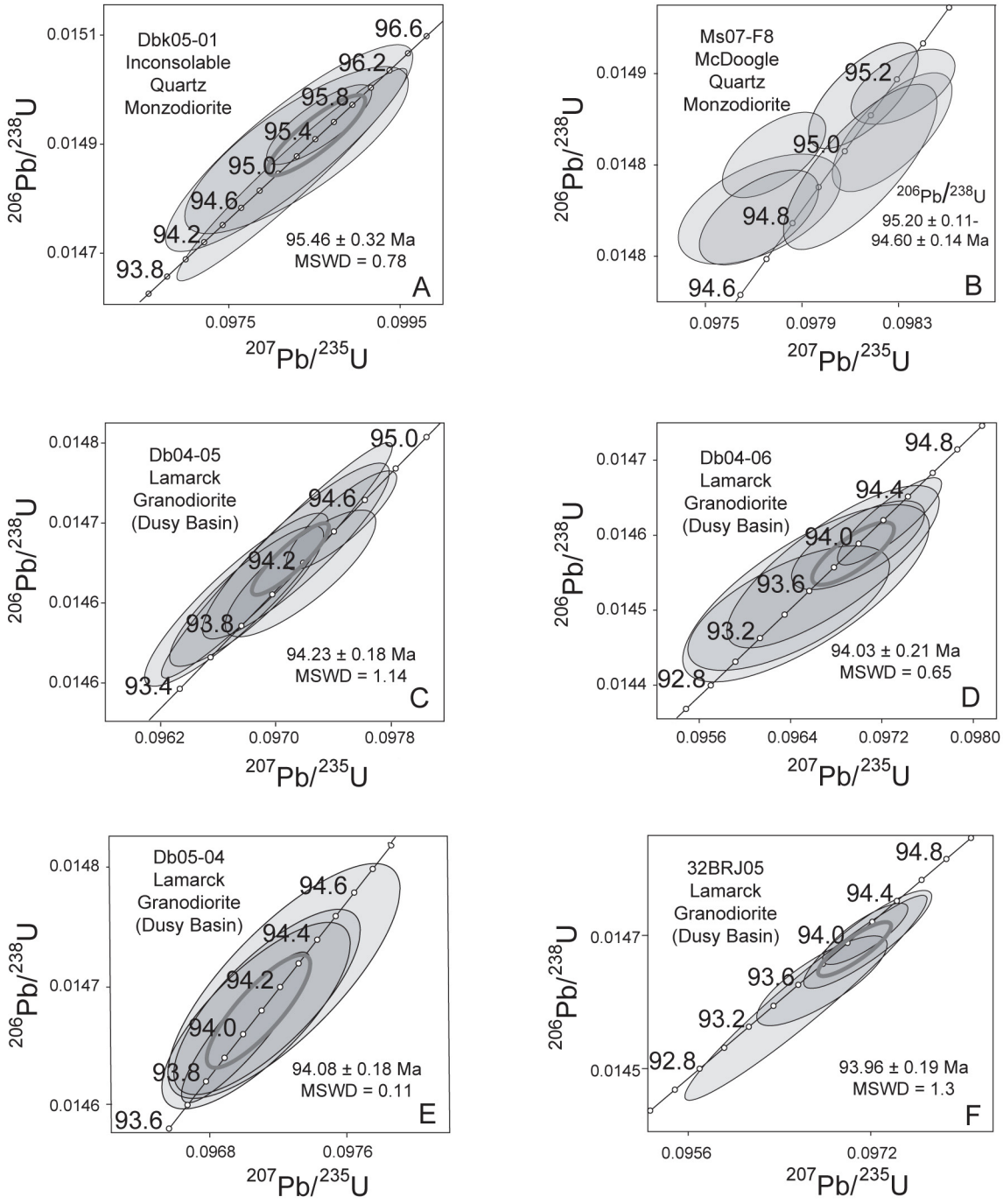
Dbk05-01
Inconsolable
Quartz
Monzodiorite
95.46 ± 0.32 Ma
MSWD = 0.78
A
Ms07-F8
McDoogle
Quartz
Monzodiorite
95.20 ± 0.11-
94.60 ± 0.14 Ma
B
Db04-05
Lamarck
Granodiorite
(Dusy Basin)
94.23 ± 0.18 Ma
MSWD = 1.14
C
Db04-06
Lamarck
Granodiorite
(Dusy Basin)
94.03 ± 0.21 Ma
MSWD = 0.65
D
Db05-04
Lamarck
Granodiorite
(Dusy Basin)
94.08 ± 0.18 Ma
MSWD = 0.11
E
32BRJ05
Lamarck
Granodiorite
(Dusy Basin)
93.96 ± 0.19 Ma
MSWD = 1.3
F
206Pb/238U
207Pb/235U

Fig. 5

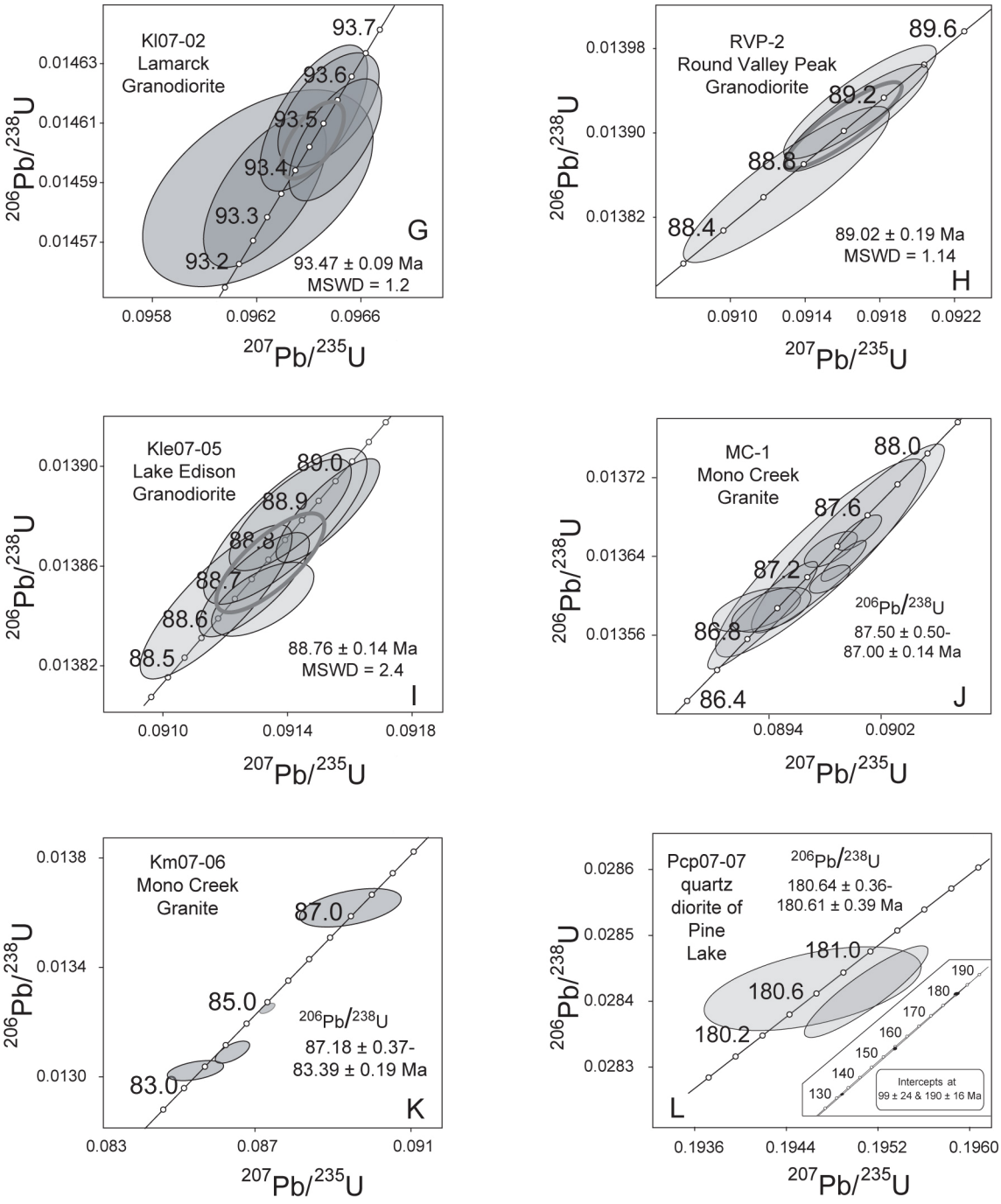
KI07-02
Lamarck
Granodiorite
93.7
93.6
93.5
93.4
93.3
93.2
93.47 ± 0.09 Ma
MSWD = 1.2
G
RVP-2
Round Valley Peak
Granodiorite
89.6
89.2
88.8
88.4
89.02 ± 0.19 Ma
MSWD = 1.14
H
Kle07-05
Lake Edison
Granodiorite
89.0
88.9
88.8
88.7
88.6
88.5
88.76 ± 0.14 Ma
MSWD = 2.4
I
MC-1
Mono Creek
Granite
88.0
87.6
87.2
86.8
86.4
206Pb/238U
87.50 ± 0.50-
87.00 ± 0.14 Ma
J
Km07-06
Mono Creek
Granite
87.0
85.0
83.0
206Pb/238U
87.18 ± 0.37-
83.39 ± 0.19 Ma
K
Pcp07-07
quartz
diorite of
Pine
Lake
206Pb/238U
180.64 ± 0.36-
180.61 ± 0.39 Ma
181.0
180.6
180.2
Intercepts at
99 ± 24 & 190 ± 16 Ma
L
206Pb/238U
207Pb/235U

Fig. 5

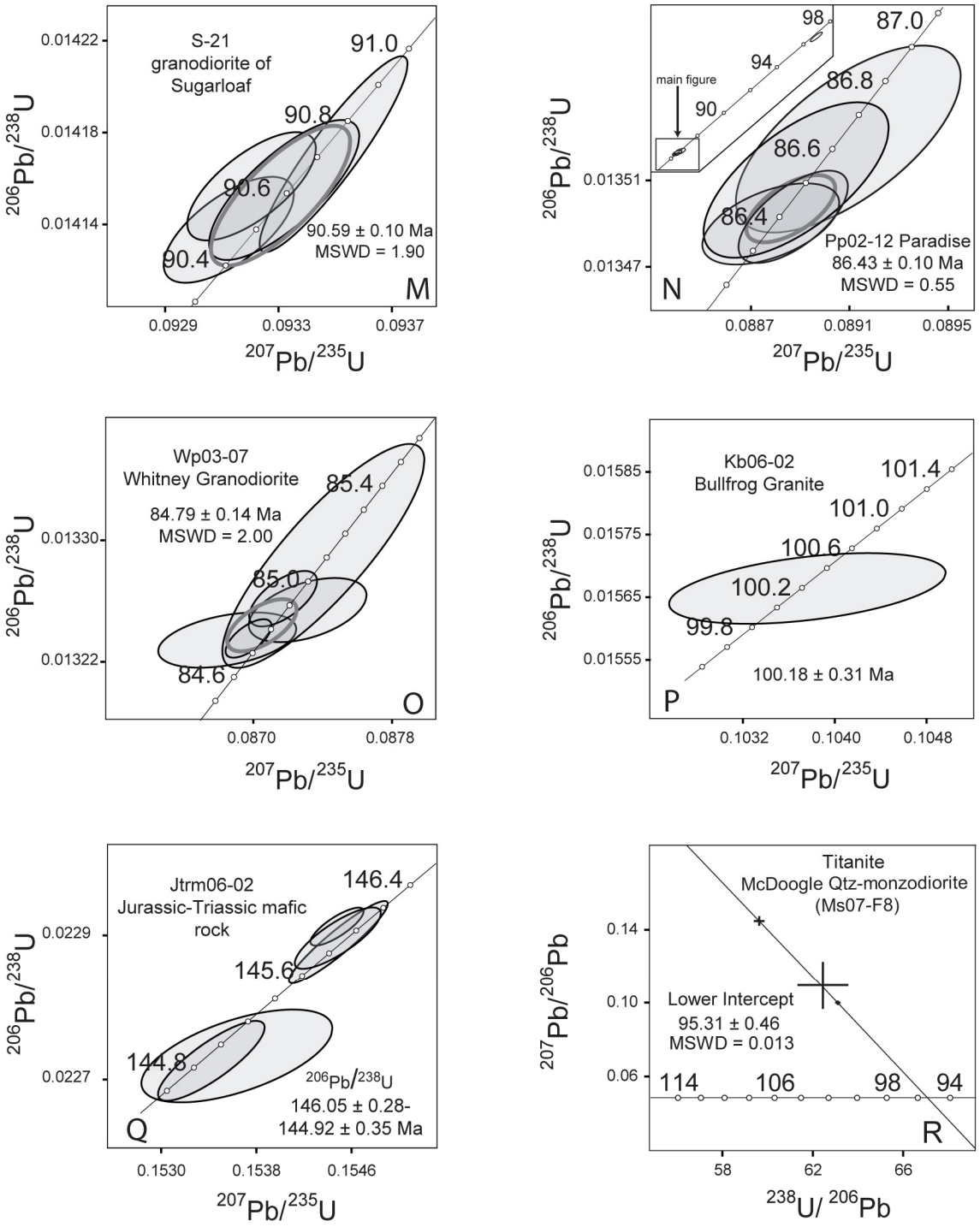
S-21
granodiorite of
Sugarloaf
91.0
90.8
90.6
90.4
90.59 ± 0.10 Ma
MSWD = 1.90
M
0.01422
0.01418
0.01414
0.0929
0.0933
0.0937
206Pb/238U
207Pb/235U
98
94
90
main figure
87.0
86.8
86.6
86.4
Pp02-12 Paradise
86.43 ± 0.10 Ma
MSWD = 0.55
N
0.01351
0.01347
0.0887
0.0891
0.0895
Wp03-07
Whitney Granodiorite
84.79 ± 0.14 Ma
MSWD = 2.00
85.4
85.0
84.6
O
0.01330
0.01322
0.0870
0.0878
Kb06-02
Bullfrog Granite
101.4
101.0
100.6
100.2
99.8
100.18 ± 0.31 Ma
P
0.01585
0.01575
0.01565
0.01555
0.1032
0.1040
0.1048
Jtrm06-02
Jurassic-Triassic mafic
rock
146.4
145.6
144.8
206Pb/238U
146.05 ± 0.28-
144.92 ± 0.35 Ma
Q
0.0229
0.0227
0.1530
0.1538
0.1546
Titanite
McDoogle Qtz-monzodiorite
(Ms07-F8)
Lower Intercept
95.31 ± 0.46
MSWD = 0.013
114
106
98
94
R
0.14
0.10
0.06
58
62
66
207Pb/206Pb
238U/206Pb

Fig. 5

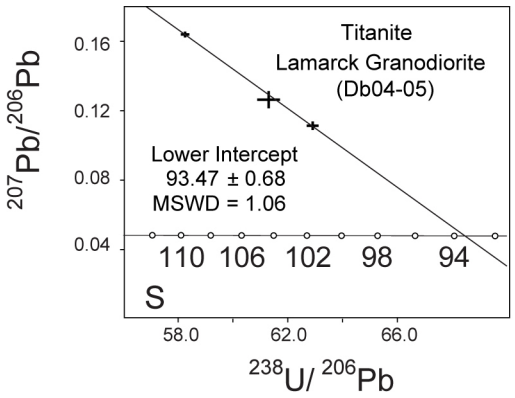

Fig. 5 Concordia diagrams for zircon and titanite fractions from the John Muir and Mount Whitney Intrusive Suites, quartz diorite of Pine Lake (wall rock), Bullfrog Granite (wall rock), and Jurassic-Triassic mafic rock (wall rock). Concordia ages (Ludwig 1998) are reported for samples with zircon fractions that overlap both age and concordia (A, C, D, E, F, G, H, I, M, N, O, P). $^{206}Pb/^{238}U$ weighted mean age spans are reported for samples having individual zircon fraction ages that spread along concordia (B, J, K, L, Q). Tera-Wasserburg concordia diagrams (Tera and Wasserburg 1972) are presented for titanite fractions and lower intercept ages are reported (R, S). Ages are labeled in millions of years. Error ellipse shading increases with overlapping of ellipses. Ellipses and crosses denote 2-sigma error of individual fractions. Bold ellipses represent 2-sigma error of concordia age. All errors include ^{238}U and ^{235}U decay constant and analytical uncertainties. Concordia diagrams generated using Isoplot 3.0 (Ludwig 2003). Ages from the Inconsolable Quartz Monzodiorite (A) and Lamarck Granodiorite (C, D, E, F) are from Gracely (2006) and Round Valley Peak Granodiorite (H) is from Gaschnig (2005). Ages from the literature are included for clarity of discussion and comparison to Ar data.

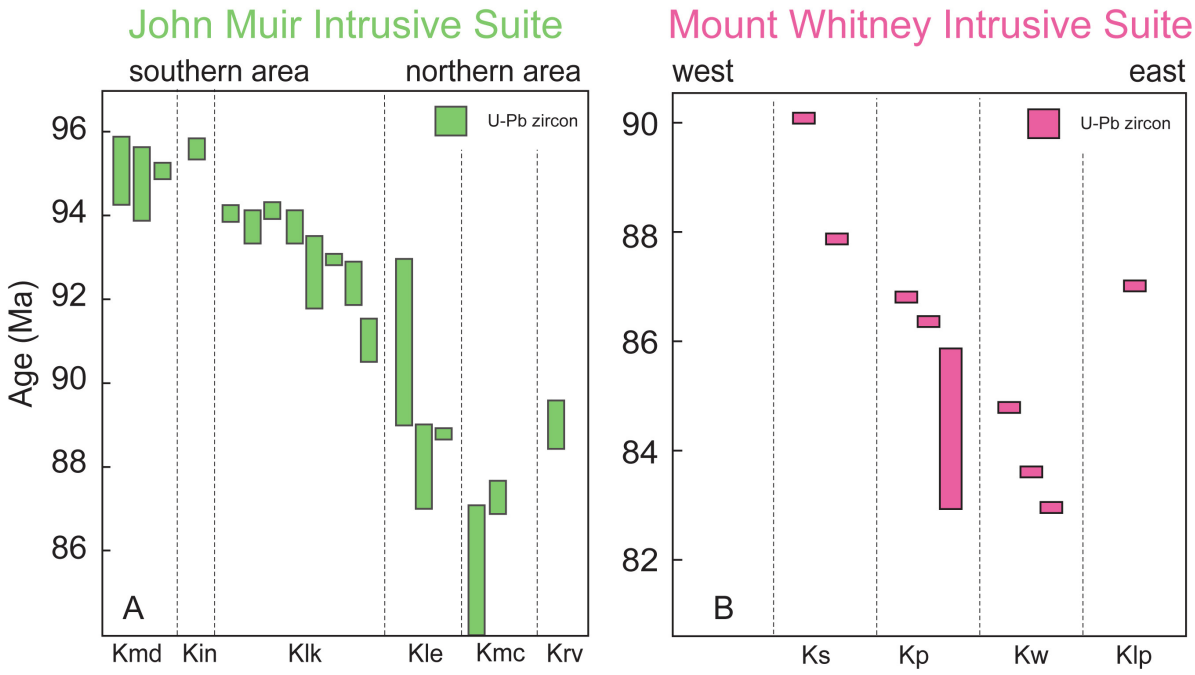

Fig 6A. Summary of U-Pb zircon crystallization ages from the Muir suite indicating an intrusive history over 9 m.y. Kmd, McDoogle Quartz Monzodiorite; Kin, Inconsolable Quartz Monzodiorite; Klk, Lamarck Granodiorite; Kle, Lake Edison Granodiorite; Kmc, Mono Creek Granite; Krv, Round Valley Peak Granodiorite. Ages from this study (Kmd, Klk, Kle, Kmc) and after Gracely (2006; Kin, Klk), Gaschnig (2005; Krv), Mahan et al. (2003; Kmd), Coleman et al. (1995; Klk), and Tobisch et al. (1995; Kle). **Fig 6B**. Summary of U-Pb zircon crystallization ages from the Whitney suite indicating an intrusive history over 7 m.y. Ks, granodiorite of Sugarloaf; Klp, granodiorite of Lone Pine Creek; Kp, Paradise Granodiorite; Kw, Whitney Granodiorite. Ages from this study (Ks, Kp, Kw) and after Mattinson (2005; Kp), Saleeby et al. (1990; Kw), and Chen and Moore (1982; Ks, Klp, Kp, Kw). Note that Chen and Moore (1982) did not report age uncertainties.

U-Pb Titanite Analyses

Individual titanite fractions are dispersed along a line whose lower intercept with the Tera-Wasserburg (1972) projection of the concordia curve defines the titanite date of the sample (Ludwig 1998). Titanite dates from the McDoogle Quartz Monzodiorite and a sample from the Lamarck Granodiorite are 95.31 ± 0.46 Ma (Fig. 5R) and 93.47 ± 0.68 Ma (Fig. 5S), respectively, and overlap within uncertainty to their corresponding zircon ages (Fig. 5B, 5C).

$^{40}Ar/^{39}Ar$ Analyses

Hornblende

Hornblende samples yield age spectra with a variety of complications (Fig. 7; Appendix 2). The Lamarck Granodiorite and Whitney Granodiorite hornblendes yield simple age spectra (Fig. 7B, 7G) and plateaus are assigned from contiguous heating steps that have apparent dates that overlap within 2-sigma. Hornblende samples from the Inconsolable Quartz Monzodiorite, Lake Edison Granodiorite, granodiorite of Sugarloaf, Paradise Granodiorite (two samples), and quartz diorite of Pine Lake all yield age spectra that are characterized by high-temperature heating steps that include very small fractions of the total gas, anomalously young dates, and anomalously high uncertainties (Fig. 7A, 7C, 7D, 7E, 7F, 7H). Hornblende breakdown caused by phase changes during *in vacuo* step heating likely led to high-temperature age spectra complexities encountered these samples (e.g., Wartho et al. 1991). The affected intermediate-temperature heating steps account for less than 8% of the ^{39}Ar released per sample; therefore, noncontiguous heating steps are used when assigning plateaus for these samples (Fig. 7A, 7C, 7D, 7E, 7F, 7H).

Hornblendes from both the Muir and Whitney suites have plateau and inverse isochron dates that overlap, and thus are interpreted to lack significant excess ^{40}Ar. Generally, inverse isochron dates are more robust than plateau dates (Renne 2006). Consequently, inverse isochron dates are used to evaluate T-t histories (Table 3).

The Tinemaha Granodiorite (three samples), Bullfrog Granite, and Jurassic-Triassic mafic rock samples were sampled to evaluate the thermal effects of intrusion of the adjacent Cretaceous intrusive suites. These samples all yield hornblendes with complicated age spectra (Fig. 7I, 7J, 7K, 7L, 7M) that exhibit evidence of partial Ar outgassing during the Cretaceous. Outgassing is indicated by a complex age spectrum that lacks a plateau and does not define an inverse isochron (not shown). Consequently, integrated ages are used to determine T-t histories of these samples (Table 3). With the exception of the three Tinemaha Granodiorite hornblende samples (Fig. 7I, 7J, 7K), all wall rock hornblende dates are Late Cretaceous and range from 90-86 Ma. Tinemaha Granodiorite hornblende dates are Late Jurassic-Early Cretaceous and range from 154-115 Ma. Hornblende dates from the Muir and Whitney suites overlap within uncertainty of their corresponding U-Pb zircon ages (Table 4). Hornblende dates from wall rock samples are significantly younger than their corresponding U-Pb zircon ages (Table 4).

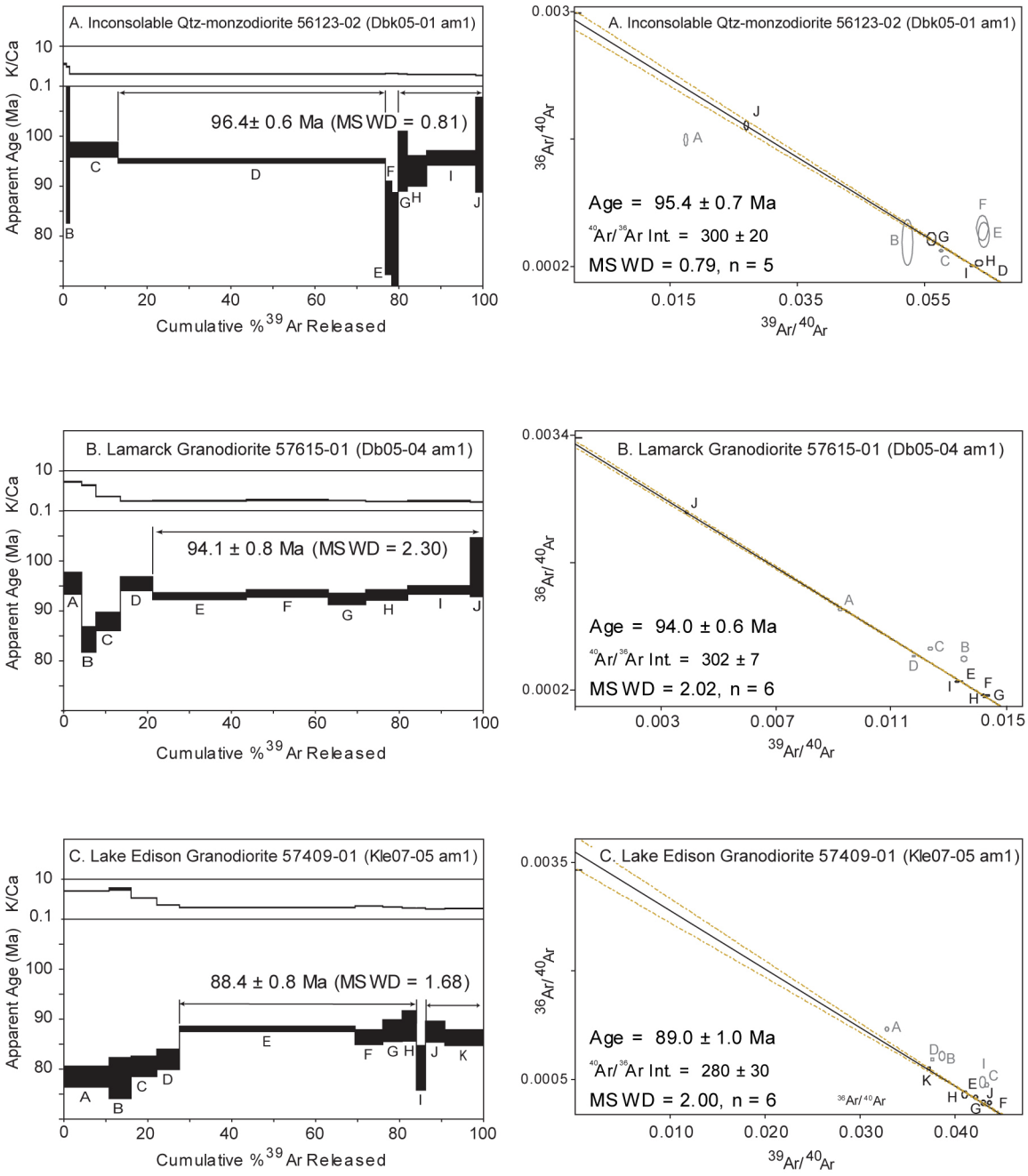
A. Inconsolable Qtz-monzodiorite 56123-02 (Dbk05-01 am1)
K/Ca
Apparent Age (Ma)
96.4± 0.6 Ma (MSWD = 0.81)
Cumulative %39Ar Released
A. Inconsolable Qtz-monzodiorite 56123-02 (Dbk05-01 am1)
36Ar/40Ar
Age = 95.4 ± 0.7 Ma
40Ar/36Ar Int. = 300 ± 20
MSWD = 0.79, n = 5
39Ar/40Ar
B. Lamarck Granodiorite 57615-01 (Db05-04 am1)
94.1 ± 0.8 Ma (MSWD = 2.30)
B. Lamarck Granodiorite 57615-01 (Db05-04 am1)
Age = 94.0 ± 0.6 Ma
40Ar/36Ar Int. = 302 ± 7
MSWD = 2.02, n = 6
C. Lake Edison Granodiorite 57409-01 (Kle07-05 am1)
88.4 ± 0.8 Ma (MSWD = 1.68)
C. Lake Edison Granodiorite 57409-01 (Kle07-05 am1)
Age = 89.0 ± 1.0 Ma
40Ar/36Ar Int. = 280 ± 30
MSWD = 2.00, n = 6

Fig. 7

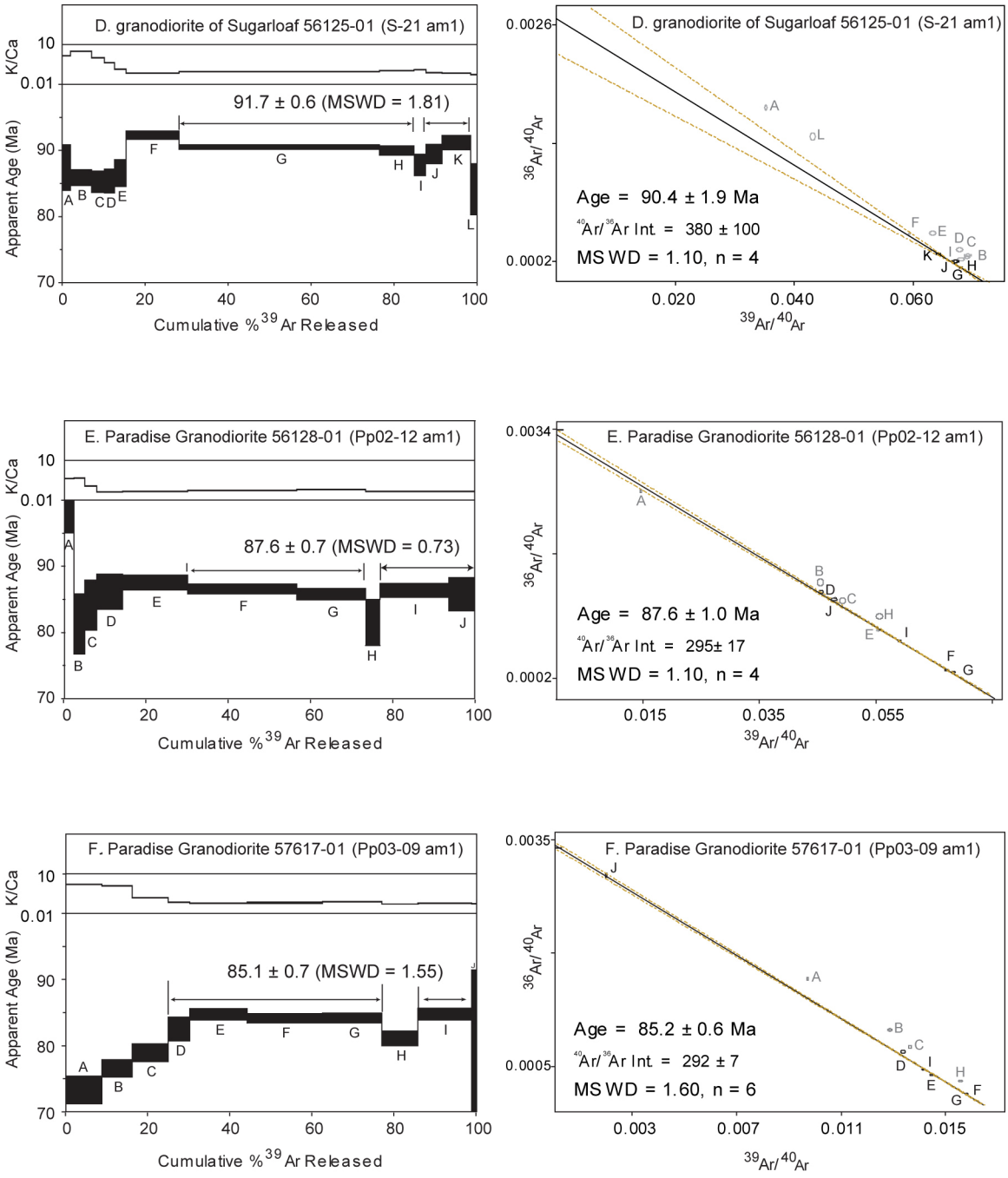
D. granodiorite of Sugarloaf 56125-01 (S-21 am1)
K/Ca
Apparent Age (Ma)
91.7 ± 0.6 (MSWD = 1.81)
Cumulative %39Ar Released
D. granodiorite of Sugarloaf 56125-01 (S-21 am1)
36Ar/40Ar
39Ar/40Ar
Age = 90.4 ± 1.9 Ma
40Ar/36Ar Int. = 380 ± 100
MSWD = 1.10, n = 4
E. Paradise Granodiorite 56128-01 (Pp02-12 am1)
87.6 ± 0.7 (MSWD = 0.73)
Age = 87.6 ± 1.0 Ma
40Ar/36Ar Int. = 295± 17
MSWD = 1.10, n = 4
F. Paradise Granodiorite 57617-01 (Pp03-09 am1)
85.1 ± 0.7 (MSWD = 1.55)
Age = 85.2 ± 0.6 Ma
40Ar/36Ar Int. = 292 ± 7
MSWD = 1.60, n = 6

Fig. 7

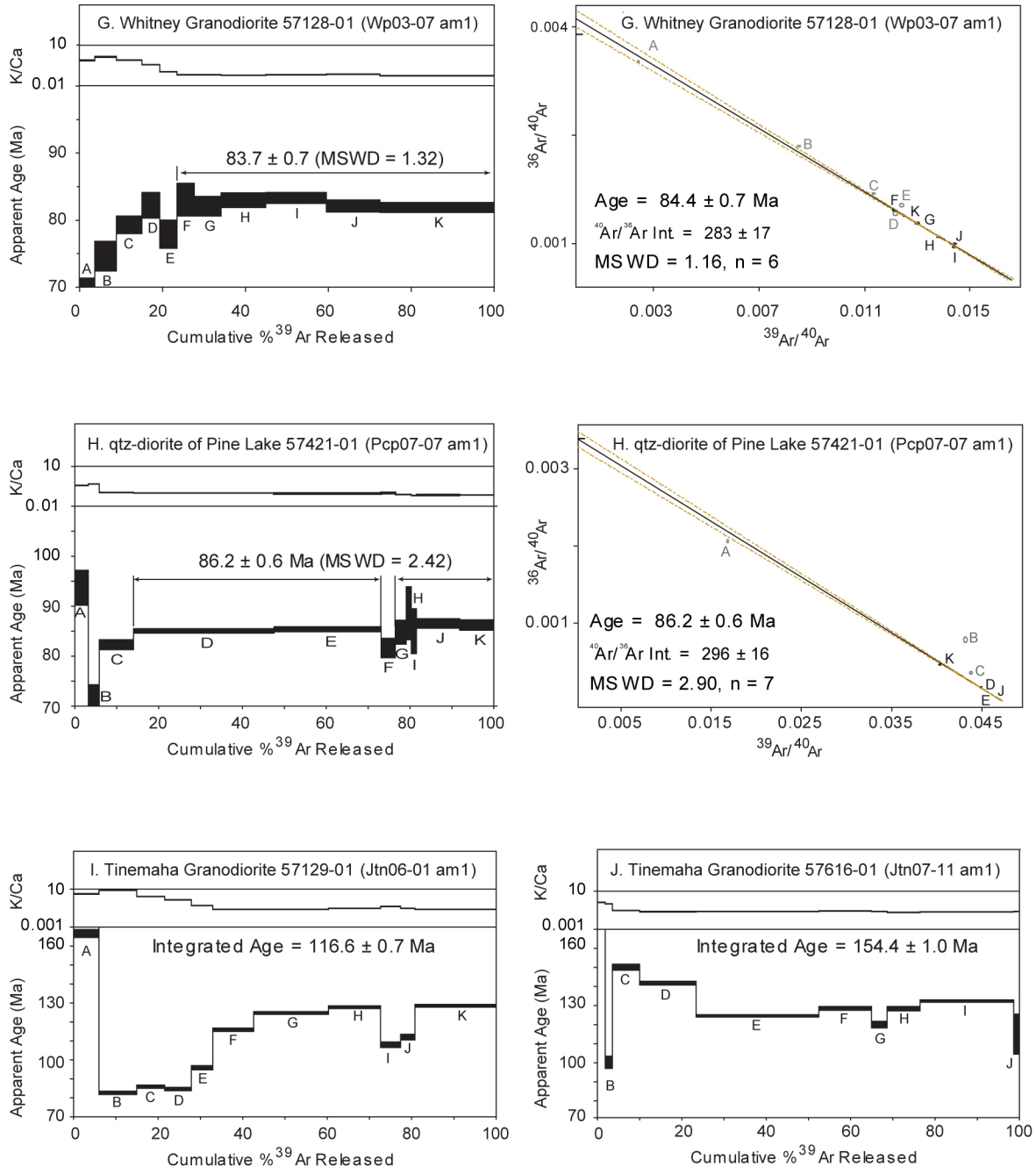
G. Whitney Granodiorite 57128-01 (Wp03-07 am1)
K/Ca
Apparent Age (Ma)
83.7 ± 0.7 (MSWD = 1.32)
Cumulative %39Ar Released
G. Whitney Granodiorite 57128-01 (Wp03-07 am1)
36Ar/40Ar
39Ar/40Ar
Age = 84.4 ± 0.7 Ma
40Ar/36Ar Int. = 283 ± 17
MSWD = 1.16, n = 6
H. qtz-diorite of Pine Lake 57421-01 (Pcp07-07 am1)
86.2 ± 0.6 Ma (MSWD = 2.42)
H. qtz-diorite of Pine Lake 57421-01 (Pcp07-07 am1)
Age = 86.2 ± 0.6 Ma
40Ar/36Ar Int. = 296 ± 16
MSWD = 2.90, n = 7
I. Tinemaha Granodiorite 57129-01 (Jtn06-01 am1)
Integrated Age = 116.6 ± 0.7 Ma
J. Tinemaha Granodiorite 57616-01 (Jtn07-11 am1)
Integrated Age = 154.4 ± 1.0 Ma

Fig. 7

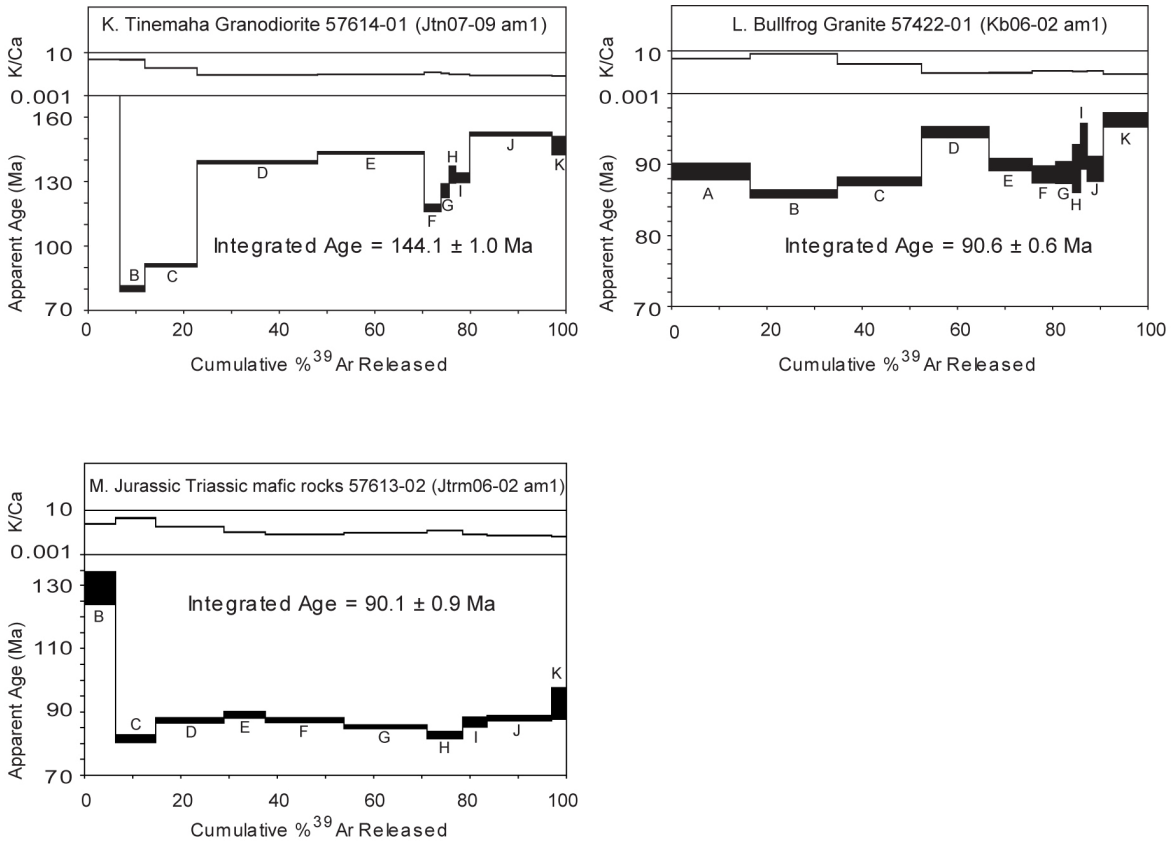

Fig. 7 Hornblende $^{40}Ar/^{39}Ar$ step heating spectra and inverse isochrons from the Muir and Whitney Intrusive Suites and associated wall rocks. Errors reported at 2-sigma confidence interval. Dates and errors are calculated using Fish Canyon flux monitor age and ^{40}K decay constant of Renne et al. (2009). Errors incorporate analytical, J-value, ^{40}K decay constant, and Fish Canyon flux monitor age uncertainties. Gray heating steps on inverse isochron are excluded from regressions and date calculations (see text for discussion). Horizontal line on inverse isochrons indicates $^{40}Ar/^{36}Ar = 295.5$.

Biotite

The Lamarck Granodiorite, Lake Edison Granodiorite, McDoogle Quartz Monzodiorite, Paradise Granodiorite (two samples), Tinemaha Granodiorite (three samples), Bullfrog Granite, and the Jurassic Triassic mafic rock biotites yield simple age spectra (Fig. 8A, 8B, 8C, 8I, 8J, 8M, 8N, 8O, 8P, 8Q; Appendix 2), and plateaus are determined for all contiguous heating steps with dates that overlap within 2-sigma uncertainty. With the exception of one Paradise Granodiorite sample (Fig. 8I), the biotite samples do not indicate excess ^{40}Ar. Therefore (as for hornblende dates), inverse isochron dates are used to evaluate their T-t histories (Table 3). The Paradise Granodiorite biotite (Fig. 8I) has a significant component of non-radiogenic argon and did not yield a valid inverse isochron. Consequently, the plateau date was used to determine a T-t history for this sample (Table 3).

Biotite samples from the Inconsolable Quartz Monzodiorite, Lamarck Granodiorite, granodiorite of Sugarloaf, and the quartz diorite of Pine Lake yield slightly saddle-shaped age spectra (Fig. 8D, 8E, 8H, 8L) thought to be caused by excess ^{40}Ar (e.g., Lanphere and Dalrymple 1976). Two Mono Creek Granite biotite samples and a Whitney Granodiorite biotite samples (Fig. 8F, 8G, 8K) yield slightly hump-shaped age spectra. This pattern suggests that chlorite alteration has affected argon release (Heizler et al. 1988; Sanders et al. 2006). Integrated ages are used to evaluate T-t histories for samples that have saddle or hump-shaped spectra because they lack valid inverse isochrons and do not yield plateaus (Table 3).

Each sample's biotite date postdates its hornblende date and zircon age by several million years with the exception of the Whitney Granodiorite sample which has concordant zircon, hornblende, and biotite data (Table 4).

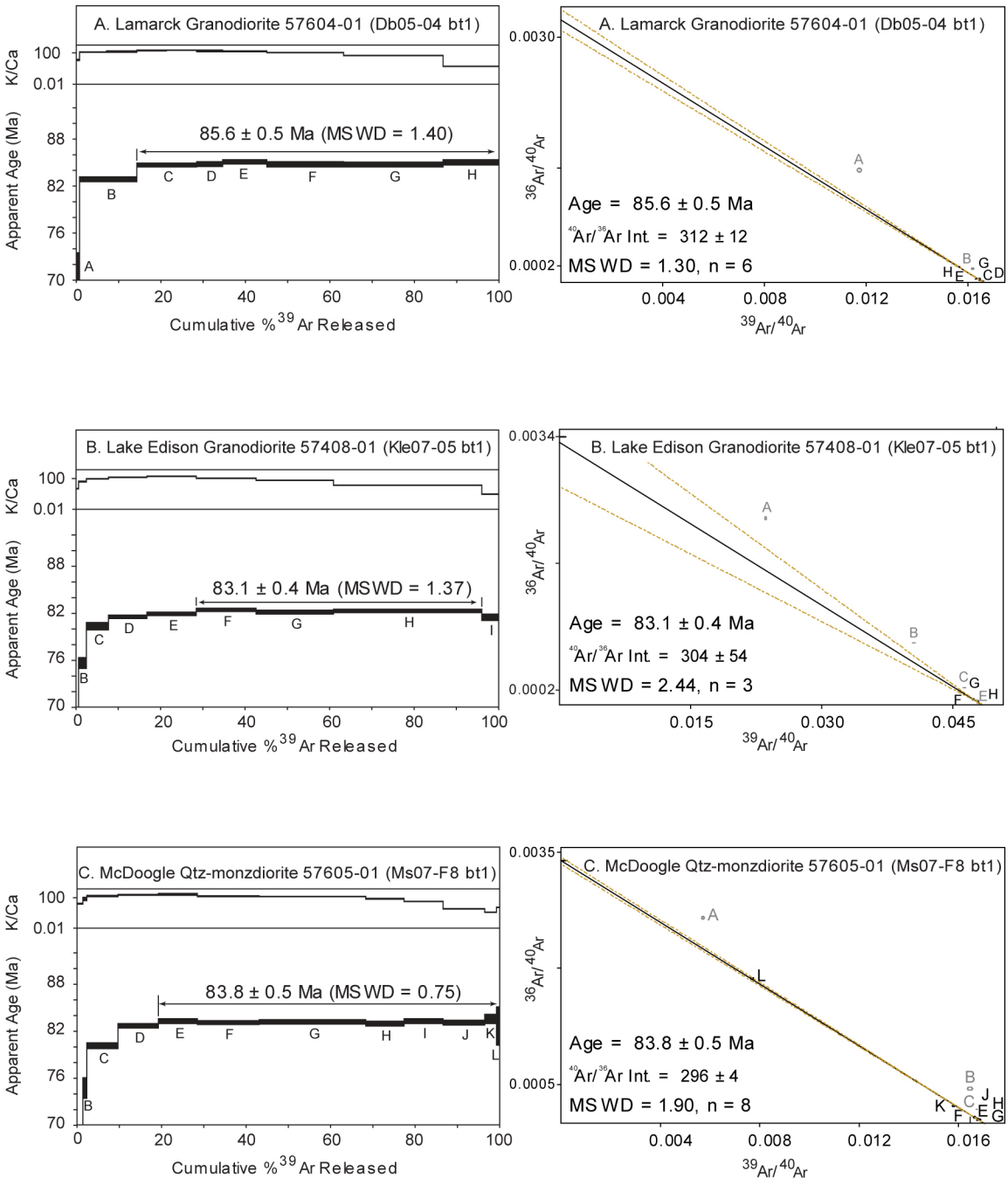
A. Lamarck Granodiorite 57604-01 (Db05-04 bt1)
K/Ca
Apparent Age (Ma)
85.6 ± 0.5 Ma (MSWD = 1.40)
Cumulative %39Ar Released
A. Lamarck Granodiorite 57604-01 (Db05-04 bt1)
36Ar/40Ar
39Ar/40Ar
Age = 85.6 ± 0.5 Ma
40Ar/36Ar Int. = 312 ± 12
MSWD = 1.30, n = 6
B. Lake Edison Granodiorite 57408-01 (Kle07-05 bt1)
83.1 ± 0.4 Ma (MSWD = 1.37)
Age = 83.1 ± 0.4 Ma
40Ar/36Ar Int. = 304 ± 54
MSWD = 2.44, n = 3
C. McDoogle Qtz-monzdiorite 57605-01 (Ms07-F8 bt1)
83.8 ± 0.5 Ma (MSWD = 0.75)
Age = 83.8 ± 0.5 Ma
40Ar/36Ar Int. = 296 ± 4
MSWD = 1.90, n = 8

Fig. 8

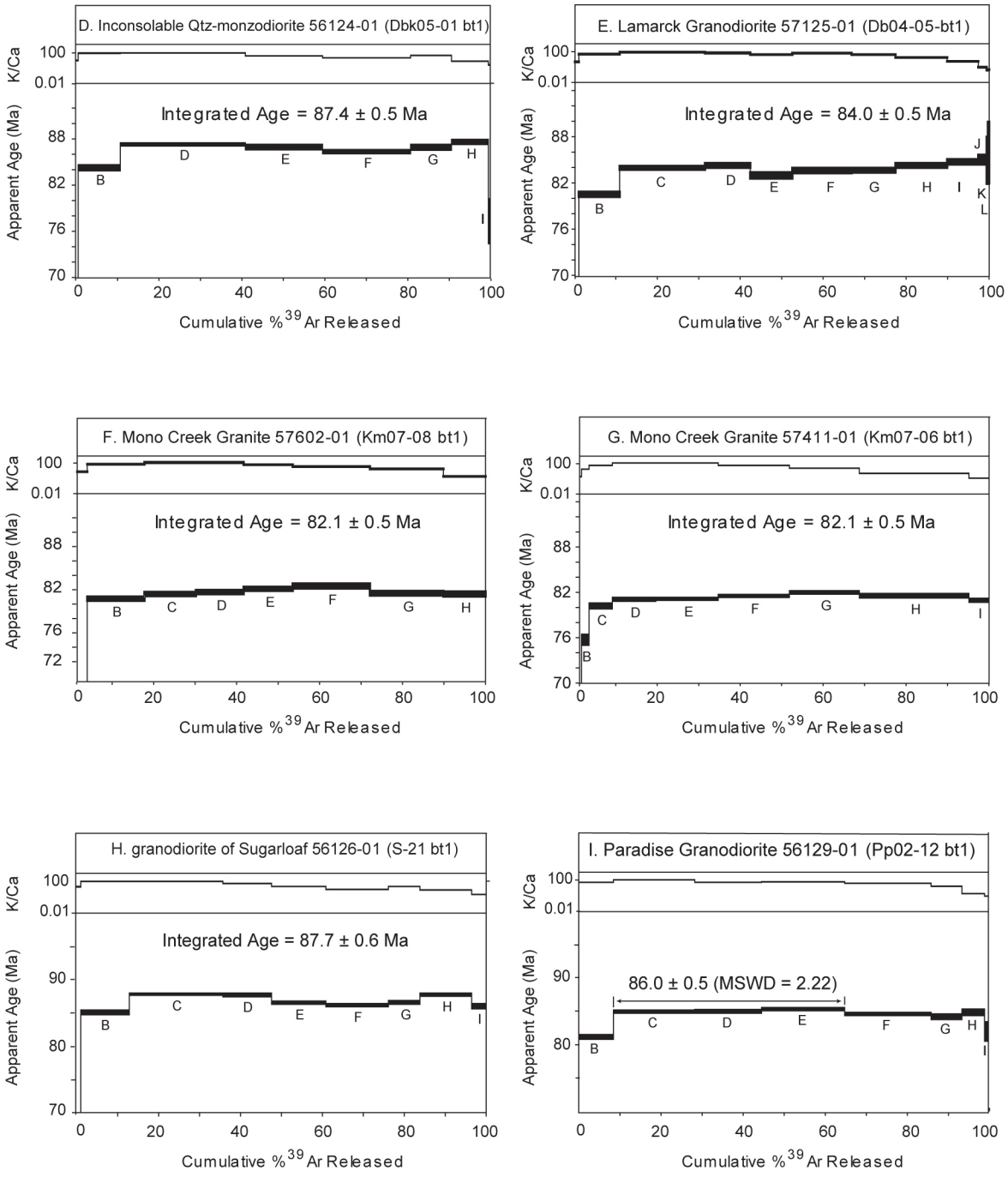
D. Inconsolable Qtz-monzodiorite 56124-01 (Dbk05-01 bt1)
Integrated Age = 87.4 ± 0.5 Ma
E. Lamarck Granodiorite 57125-01 (Db04-05-bt1)
Integrated Age = 84.0 ± 0.5 Ma
F. Mono Creek Granite 57602-01 (Km07-08 bt1)
Integrated Age = 82.1 ± 0.5 Ma
G. Mono Creek Granite 57411-01 (Km07-06 bt1)
Integrated Age = 82.1 ± 0.5 Ma
H. granodiorite of Sugarloaf 56126-01 (S-21 bt1)
Integrated Age = 87.7 ± 0.6 Ma
I. Paradise Granodiorite 56129-01 (Pp02-12 bt1)
86.0 ± 0.5 (MSWD = 2.22)
K/Ca
Apparent Age (Ma)
Cumulative %39Ar Released

Fig. 8

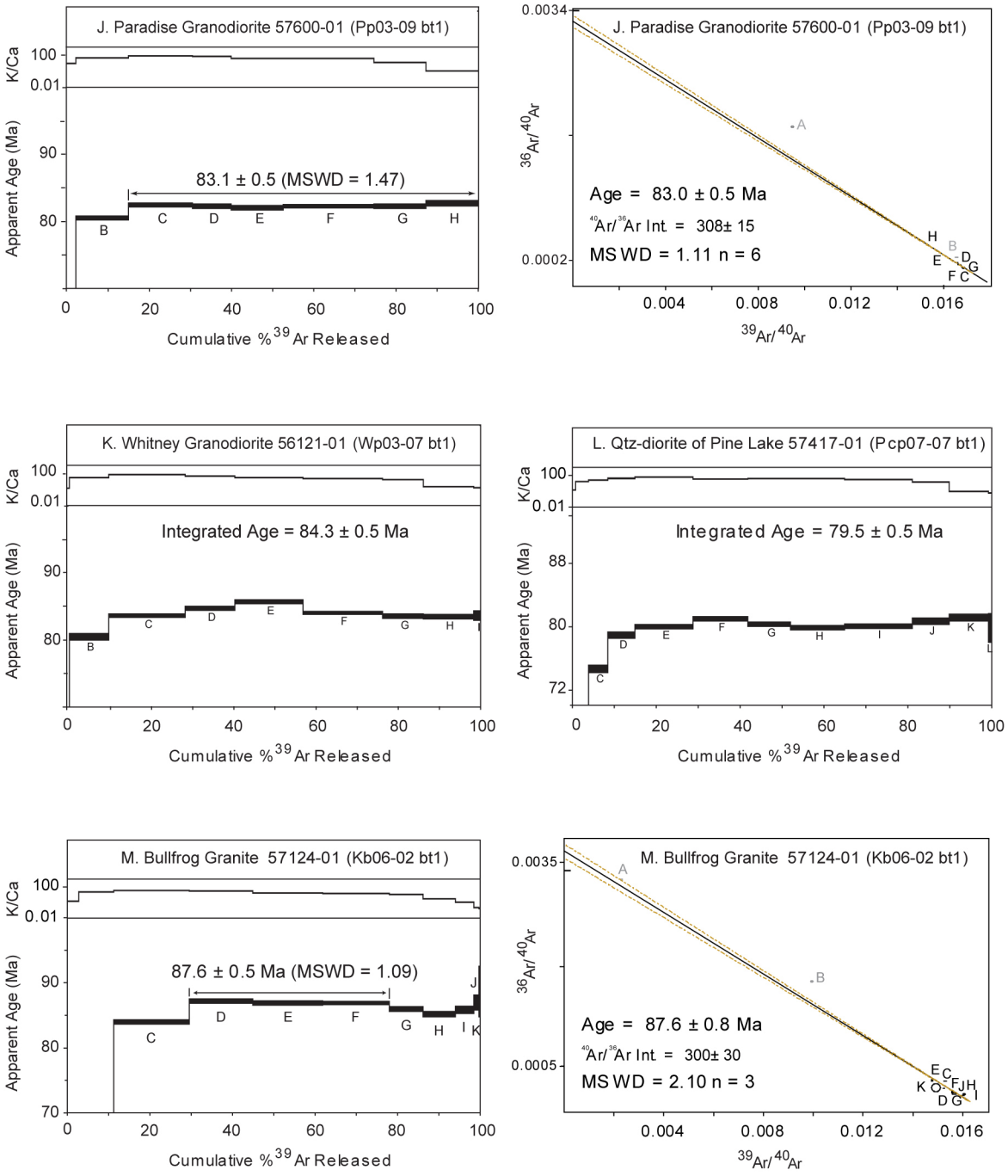
J. Paradise Granodiorite 57600-01 (Pp03-09 bt1)
K/Ca
Apparent Age (Ma)
83.1 ± 0.5 (MSWD = 1.47)
Cumulative %39Ar Released
J. Paradise Granodiorite 57600-01 (Pp03-09 bt1)
36Ar/40Ar
Age = 83.0 ± 0.5 Ma
40Ar/36Ar Int. = 308± 15
MSWD = 1.11 n = 6
39Ar/40Ar
K. Whitney Granodiorite 56121-01 (Wp03-07 bt1)
Integrated Age = 84.3 ± 0.5 Ma
L. Qtz-diorite of Pine Lake 57417-01 (Pcp07-07 bt1)
Integrated Age = 79.5 ± 0.5 Ma
M. Bullfrog Granite 57124-01 (Kb06-02 bt1)
87.6 ± 0.5 Ma (MSWD = 1.09)
M. Bullfrog Granite 57124-01 (Kb06-02 bt1)
Age = 87.6 ± 0.8 Ma
40Ar/36Ar Int. = 300± 30
MSWD = 2.10 n = 3

Fig. 8

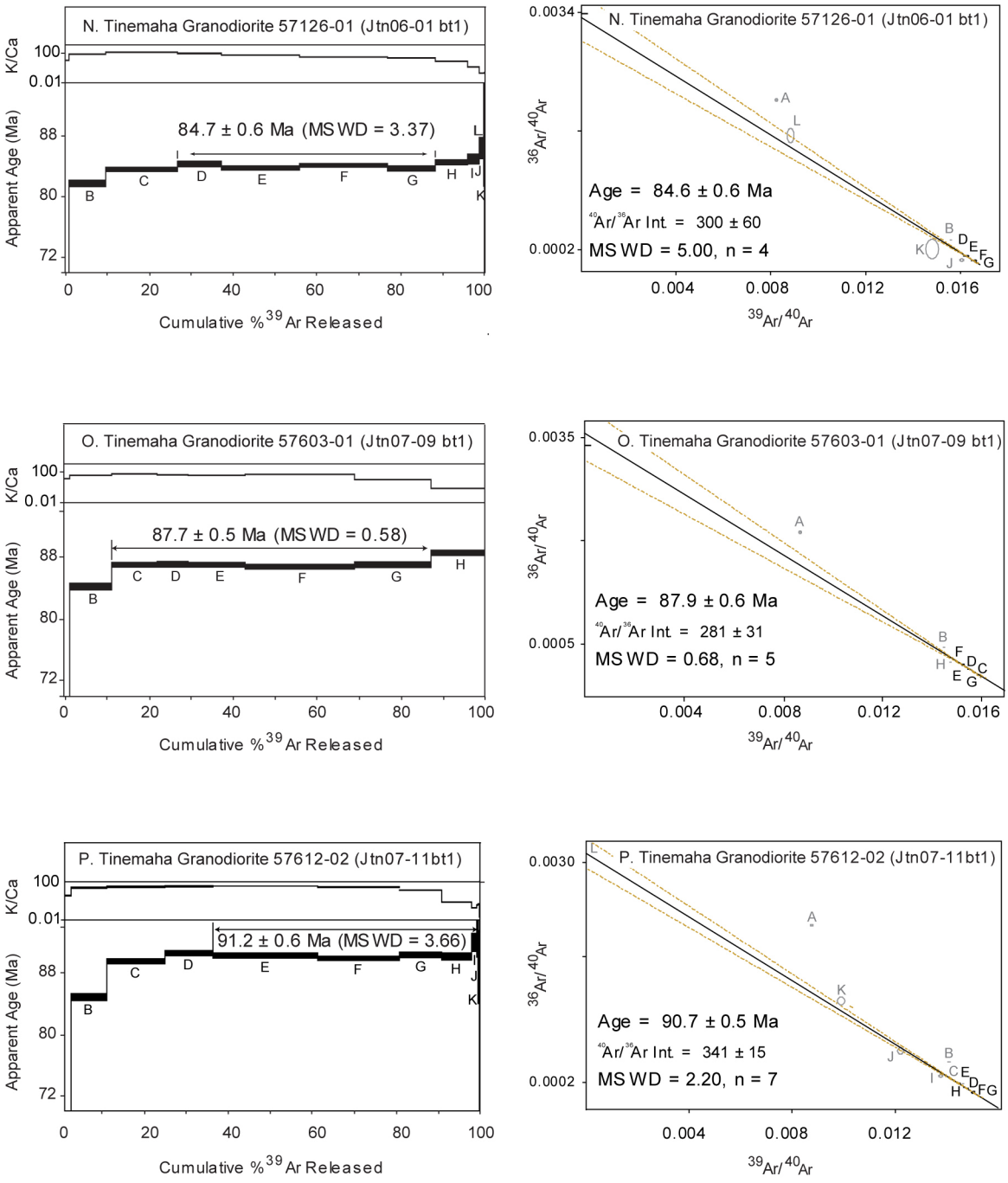
N. Tinemaha Granodiorite 57126-01 (Jtn06-01 bt1)
K/Ca
Apparent Age (Ma)
84.7 ± 0.6 Ma (MSWD = 3.37)
Cumulative %39Ar Released
N. Tinemaha Granodiorite 57126-01 (Jtn06-01 bt1)
36Ar/40Ar
39Ar/40Ar
Age = 84.6 ± 0.6 Ma
40Ar/36Ar Int. = 300 ± 60
MSWD = 5.00, n = 4
O. Tinemaha Granodiorite 57603-01 (Jtn07-09 bt1)
87.7 ± 0.5 Ma (MSWD = 0.58)
O. Tinemaha Granodiorite 57603-01 (Jtn07-09 bt1)
Age = 87.9 ± 0.6 Ma
40Ar/36Ar Int. = 281 ± 31
MSWD = 0.68, n = 5
P. Tinemaha Granodiorite 57612-02 (Jtn07-11bt1)
91.2 ± 0.6 Ma (MSWD = 3.66)
P. Tinemaha Granodiorite 57612-02 (Jtn07-11bt1)
Age = 90.7 ± 0.5 Ma
40Ar/36Ar Int. = 341 ± 15
MSWD = 2.20, n = 7

Fig. 8

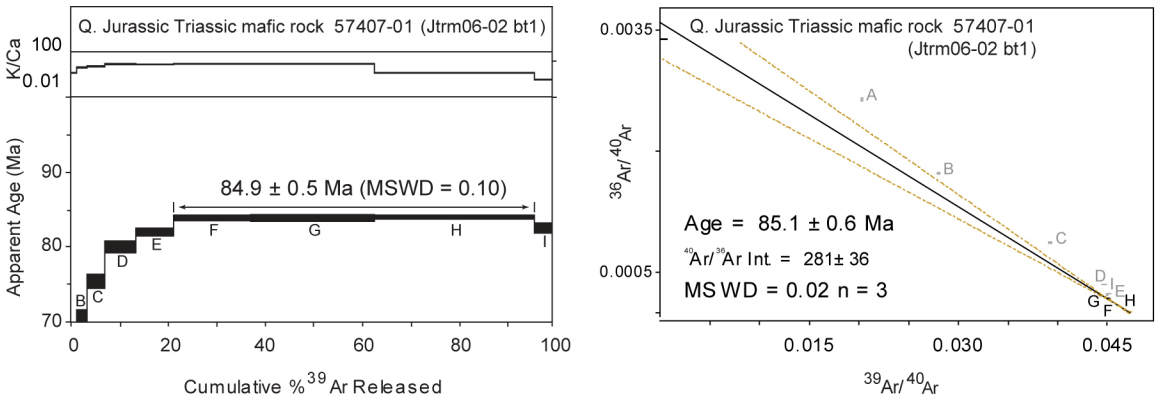

Fig. 8 Biotite $^{40}Ar/^{39}Ar$ step heating spectra and inverse isochrons from John Muir and Mount Whitney Intrusive Suites and associated wall rocks. Errors reported at 2-sigma confidence interval. Dates and errors are calculated using Fish Canyon flux monitor age and ^{40}K decay constant of Renne et al. (2009). Errors incorporate analytical, J-value, ^{40}K decay constant, and Fish Canyon flux monitor age uncertainties. Gray heating steps on inverse isochron are excluded from regressions and date calculations (see text for discussion). Horizontal line on inverse isochrons indicates $^{40}Ar/^{36}Ar = 295.5$.

K-feldspar age spectra

K-feldspar age spectra are determined for samples across two Muir suite transects (Fig. 9; Appendix 2). Anomalously old ages recorded in the initial heating steps for samples from most plutons probably reflect excess Ar released from fluid inclusions (Fig. 10C, 10E, 10G, 10K, 11A, 11C; Harrison et al. 2005). Excluding these steps, K-feldspar age spectra from the Muir suite are characterized by initial steep age gradients that climb to plateaus between 76-80 Ma (transect A; Fig. 10) and 81-88 Ma (transect B; Fig. 11). Age spectra for all samples increase monotonically with temperature and are consistent with Ar release via volume diffusion (Harrison et al. 2005). The samples therefore appear to be well-behaved and record T-t histories.

MDD models

A modeled T-t history from a sample is accepted if the modeled age spectrum (black line overlain on gray release spectrum; Figs. 10 and 11) meets fitting criteria relative to the measured age spectra (Quidelleur et al. 1997). MDD models for K-feldspar from the Muir suite exhibit a tight distribution of acceptable solutions that are reflected by the narrow range of T-t histories (Figs. 10 and 11). The T-t histories are characterized by slow cooling from approximately 82 until 76 Ma, except two Mono Creek Granite samples (Fig. 10H, 10J) that show no evidence for a period of slow cooling. At about 76 Ma, all samples show evidence for a period of accelerated cooling that continued until at least 73-71 Ma. Models for two samples (Fig. 10B, 10J) suggest a return to slow cooling beginning at about 70 Ma.

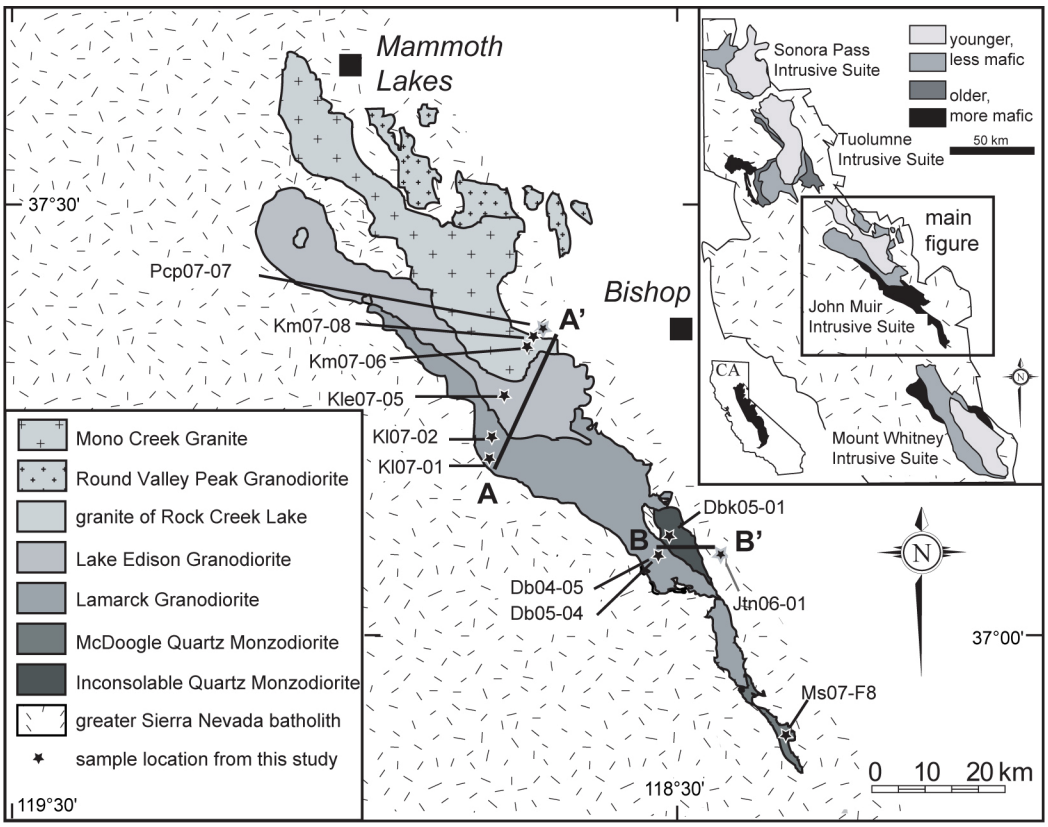

Fig. 9 Simplified geology of the John Muir Intrusive Suite after Bateman (1992). Figure shows sample nomenclature and locations for samples utilized in K-feldspar MDD thermal modeling. Bold black lines mark sample transects.

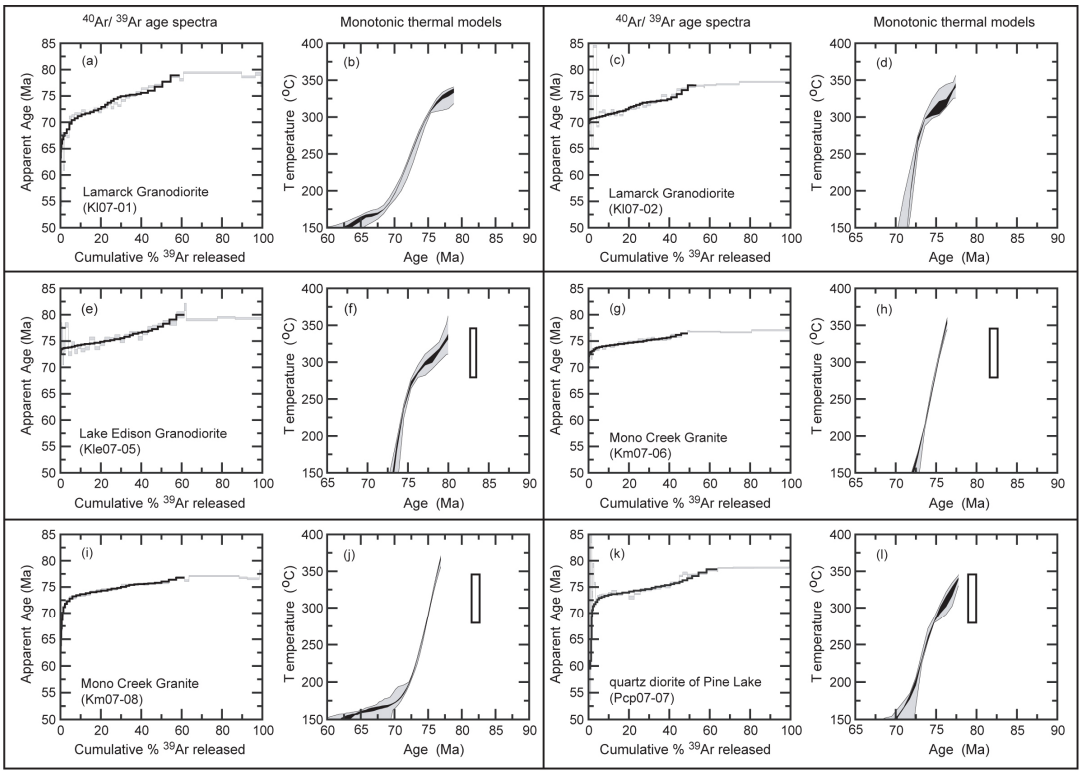

Fig. 10 K-feldspar $^{40}Ar/^{39}Ar$ age spectra and monotonic MDD thermal models generated for the northern John Muir Intrusive Suite transect (A). Gray age spectra are measured; whereas, black lines are modeled age spectra. Gray envelopes in MDD models represent all modeled thermal histories meeting the fitting criteria of Quidelleur et al. (1997); whereas, the black envelopes represent 90% confidence of the mean modeled thermal histories. Black boxes are biotite dates (2-sigma error) using an estimated closure temperature range from 345-280 °C (Harrison et al. 1985).

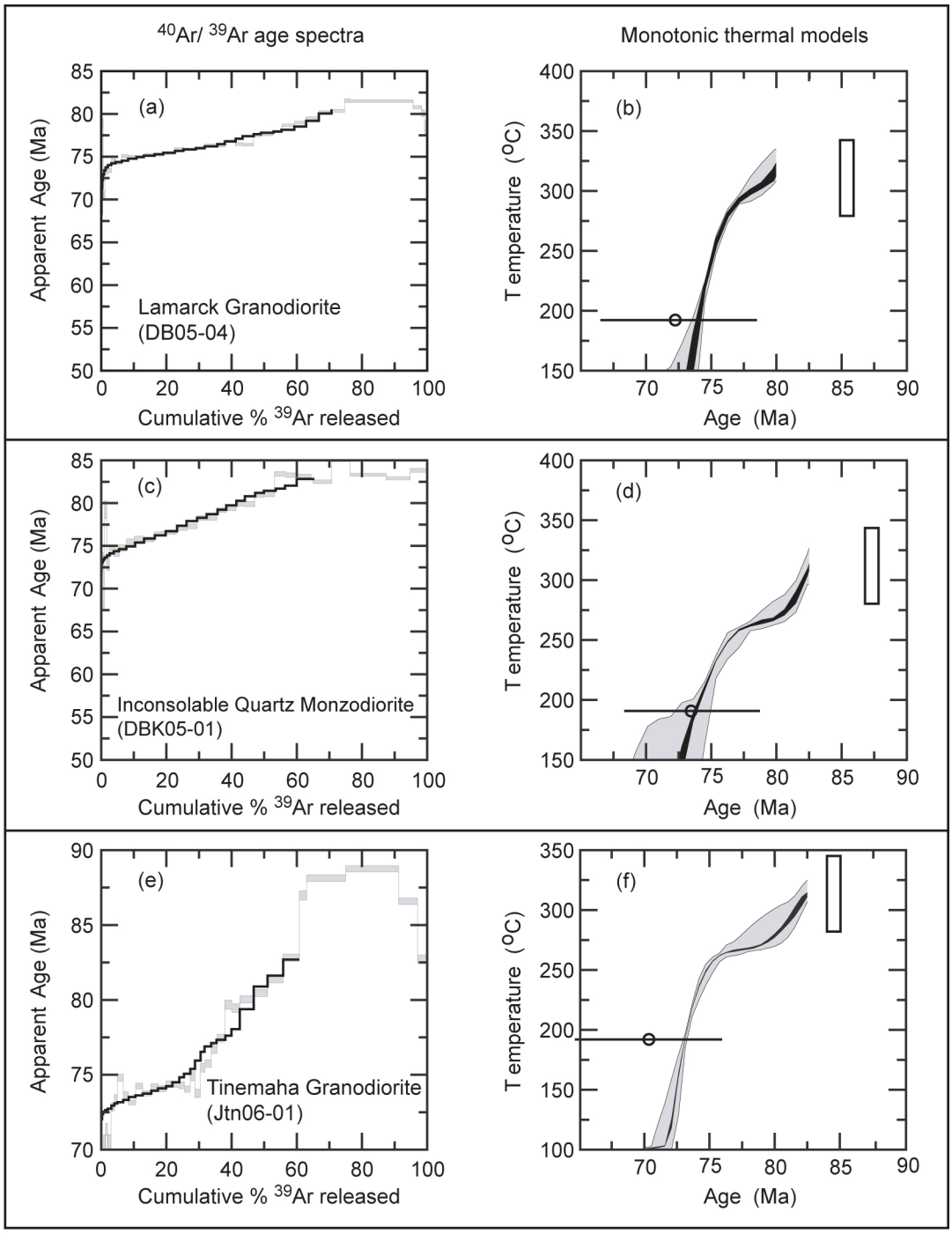

Fig. 11 K-feldspar ^{40}Ar/^{39}Ar age spectra and monotonic MDD thermal models generated for the southern John Muir Intrusive Suite transect (B). Gray age spectra are measured; whereas, black lines are modeled age spectra. Gray envelopes in MDD models represent all modeled thermal histories meeting the fitting criteria of Quidelleur (1997); whereas, black envelopes represent 90% confidence of the mean modeled thermal histories. Open circles are mean zircon (U-Th)/He dates with 2-sigma error bars. Black boxes are biotite dates (2-sigma error) using an estimated closure temperature range from 345-280 °C (Harrison et al. 1985).

(U-Th)/He Analyses

Zircon (U-Th)/He dates range from 83 to 70 Ma and are characterized by large uncertainties (Table 2). For all samples, the (U-Th)/He dates overlap within uncertainty with the low-temperature portions of these MDD models.

Thermal Modeling

Temperature-time histories were monitored at twelve watch points throughout the modeled domain (Fig. 12). All watch points exhibit a characteristic saw-tooth T-t history pattern (Fig. 13). When an intrusive body grows by the incremental emplacement of horizontal sheets, the early increments are emplaced into relatively cool wall rocks and solidify rapidly (Fig. 13; watch points 1, 7). With time, the heat dissipated by new intrusions increases temperatures throughout the system; thus, the later increments are emplaced into hotter environments (Fig. 13; watch points 2, 3, 4, 8, 9, 10). Like the chamber regions intruded by early increments, these regions cool quickly but are maintained at temperatures above the ambient background. In this model, the heat advected by the emplacement of multiple intrusions kept temperatures elevated but did not cause temperatures to be reheated above 450°C. Only when an actual intrusion was emplaced at the level of a watch point did that watch point reach high temperatures. Temperatures in the wall rock above the magma chamber were barely affected by the intrusions (Fig. 13; watch point 5). In contrast, temperatures below the magma chamber were raised significantly above background ambient (Fig. 13; watch point 6).

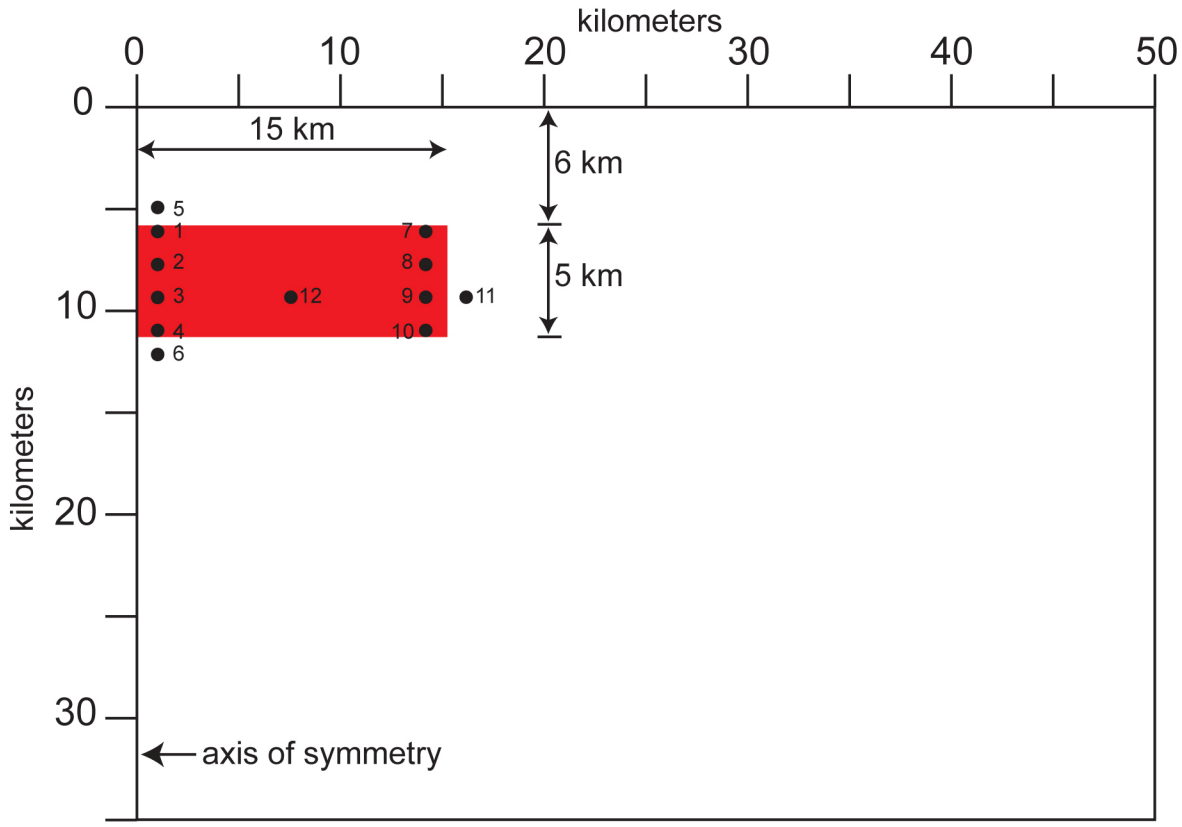

Fig. 12 Domain schematic for 2-D thermal model. Model was run as a half-space with the left boundary acting as an axis of symmetry. Dimensions of the model intrusion and rates of magma accumulation were determined by dimensions and fill rates of northern Muir and Whiney suites. Red box represents the final magma chamber dimensions after stacking 0.25 km thick horizontal sheets, from the top down, for approximately 7 m.y. Black dots and corresponding numbers are watch points. At each watch point the temperature - time path is monitored for the duration of the simulation (see Fig. 13).

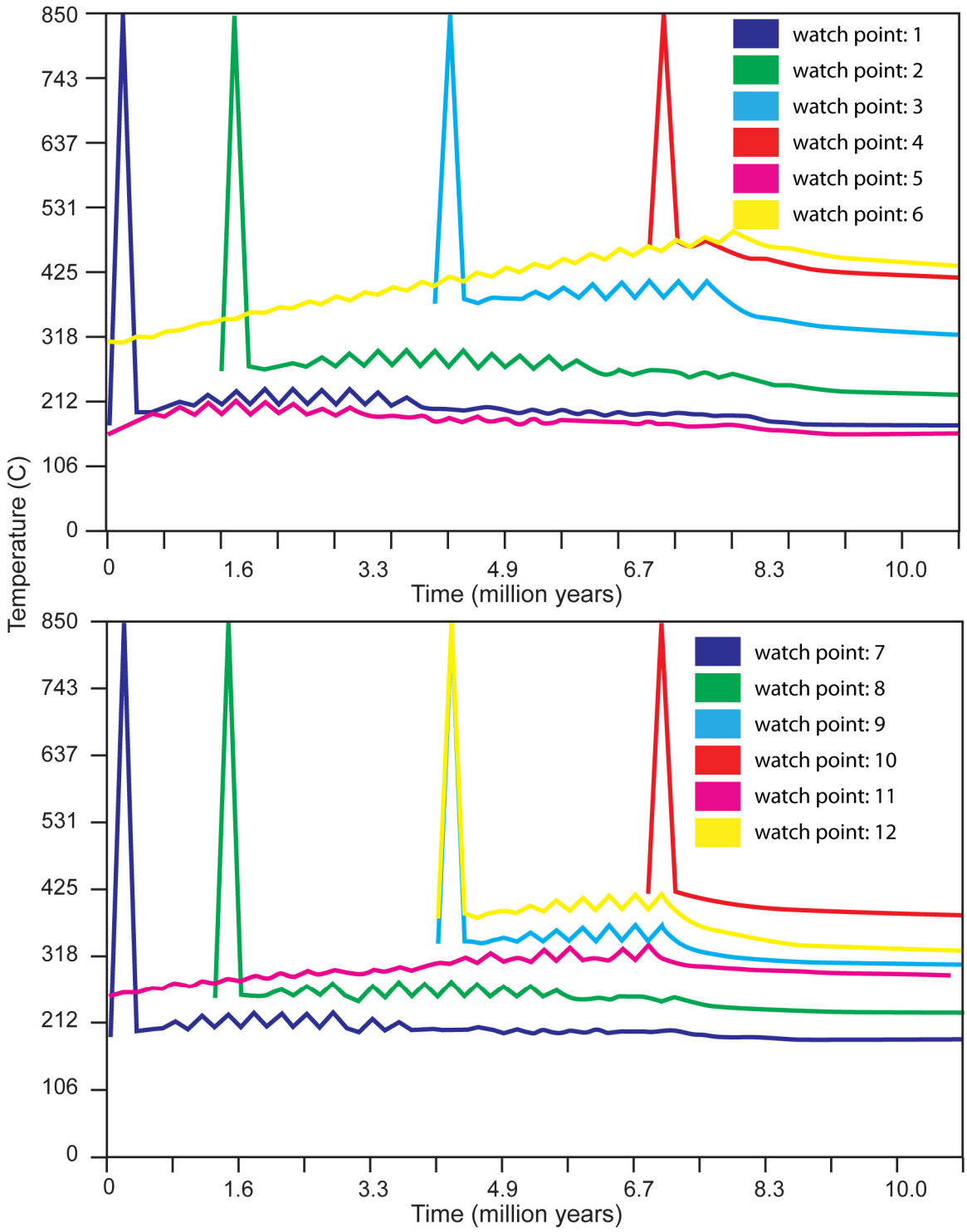

Fig. 13 Watch points from various locations throughout the modeled domain (see Fig. 12). At each watch point the T-t history is monitored for the duration of the simulation. All watch point exhibit a characteristic saw-tooth T-t history pattern which likely indicates temperature oscillation due to the incremental growth of the magma chamber. Early increments are emplaced into relatively cool wall rocks and solidify rapidly (watch points 1, 7). In contrast, the later increments are emplaced into hotter environments (watch points 2, 3, 4, 8, 9, 10, 12).

For the duration of model, a large-volume magma chamber containing melt + crystals did not develop (Fig 14). Although the size of a magma chamber increases during pluton assembly, the percentage of the magma chamber that is above the solidus decreases as the chamber grows. This suggests that during pluton growth the volume of liquid present in the chamber at any point in time is low compared to the overall volume of the chamber.

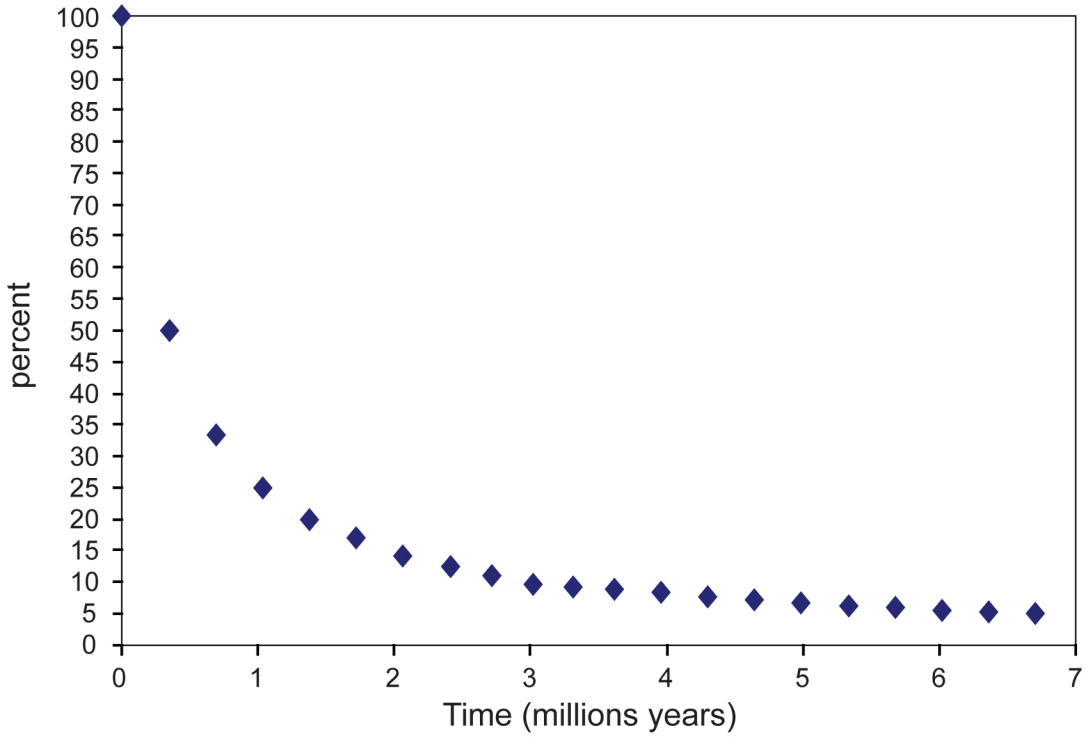

Fig. 14 Percent of magma chamber that is above the solidus during the construction of a chamber built by antitaxially stacking horizontal sheets from the top down over a 7 m.y. period. Note that as the chamber grows the percentage of the chamber above the solidus decreases. This suggests that during pluton growth the volume of liquid present in the chamber at any point in time is low compared to the overall volume of the chamber. These results are consistent with geophysical data (Iyer 1984; Waite and Moran 2009) that fail to locate large volumes of liquid (> 50%) beneath active volcanic regions.

5. DISCUSSION

Zircon U-Pb Crystallization Ages

Most samples from this study yield tightly clustered U-Pb data for which a concordia age can be calculated and those ages are accepted as crystallization ages for the samples. However, several samples yielded data that are either discordant (Fig. 5L, 5N), or concordant, but spread along an interval of concordia, and do not overlap within uncertainty (Fig. 5B, 5J, 5K, 5Q).

The discordant data are likely the result of Pb-loss and inheritance. The quartz diorite of Pine Lake (Fig. 5L) was dated because an earlier study suggested an age (97.5 Ma) similar to the Muir suite (Frost and Mattinson 1988). Zircon fractions from this study for the quartz diorite spread along a discordia line and have $^{206}Pb/^{238}U$ ages ranging from 181-132 Ma (Fig. 5L). Two zircon fractions have indistinguishable $^{206}Pb/^{238}U$ ages of 180.7 Ma that is interpreted as the crystallization age. Discordance in the other fractions is attributed to Pb-loss because the quartz diorite is a small body (3 km^2) that is pervasively intruded by Late Cretaceous granitoids that make up 40% of the outcrop area at Pine Lake, where samples from both studies were collected (Frost and Mattinson 1988). These horizontal sheets of Mono Creek Granite likely contributed enough heat and fluids to disturb zircon systematics. Consequently, the Pine Lake body is interpreted to be Jurassic and the discordant 97.5 Ma age of Frost and Mattinson (1988) to reflect Pb-loss caused by the intrusion of the Muir suite.

The Paradise Granodiorite sample (Fig. 5N) contains one zircon fraction that is significantly older (96.7 Ma) than the cluster of fractions used to determine the concordia age

(84.8 Ma). This fraction is discordant and interpreted to contain an inherited component. Consequently, the concordia age of the clustered data is used to interpret the T-t history of this sample (Table 4).

The observation that zircon data for individual samples are distributed along an interval of concordia, and do not yield ages that overlap within uncertainty is recognized with increasing frequency as the precision of U-Pb data improves (e.g., Miller and Wooden 2004; Miller et al. 2007). The age dispersion along an interval of concordia indicates the potential effects of Pb-loss, grain resorption and regrowth, or extended intervals of zircon crystallization.

Age spread due to Pb-loss is possible in the Jurassic-Triassic mafic rock (Fig. 5Q), the McDoogle Quartz Monzodiorite (Fig. 5B), and the Mono Creek Granite (Fig. 5J, 5K) samples, but is not favored here for several reasons. Zircons from the units are not characterized by anomalously high U and Th which can lead to Pb-loss (Mattinson 2005). In addition, there is nothing unusual about the morphology, zoning, or degree of alteration of zircons from these samples in comparison to other samples from the study (and in some cases, from the same unit). There is also no obvious reason why thermal annealing and chemical abrasion of only these samples from the area would not minimize or eliminate Pb-loss. Finally, in the case of the Jurassic-Triassic mafic rock, Pb-loss during intrusion of the Cretaceous Whitney suite would likely have driven points off concordia along a discordia array as is proposed for the quartz diorite of Pine Lake.

Miller and Wooden (2004) suggest that zircon U-Pb age dispersion along concordia can result from high-temperature fluctuations resulting in zircon resorption and subsequent regrowth in a long-lived magma chamber. Estimated zircon saturation temperatures (Watson

and Harrison 1983) of approximately 755°C are calculated using geochemical data from the Muir and Whitney suite plutons (Frost and Mahood 1987; Hirt 2007); however, the general observation from this study that U-Pb ages and $^{40}Ar/^{39}Ar$ hornblende dates are concordant for all samples suggest reheating by younger intrusions did not re-elevate temperatures above hornblende closure (approximately 550°C). Therefore, it is unlikely that the nearly 4 m.y. age dispersion in data from one of the Mono Creek samples (Fig. 5K) is caused by zircon grain resorption and regrowth. The McDoogle Quartz Monzodiorite (Fig. 5B) and a second sample of the Mono Creek Granite (Fig. 5J) have much a much smaller spread in ages (approximately 0.5 m.y.) which is within the uncertainty of determining concordancy of zircon and hornblende dates. Thus, resorption and regrowth is a plausible explanation for the age dispersion exhibited by these samples. Although, hornblende from the sample of the Jurassic-Triassic mafic rock was reset by the Whitney suite intrusions during in the Late Cretaceous (Fig. 7M), regrowth of zircon in the Cretaceous should have driven those points off concordia (Fig. 5Q).

The large spread in concordant ages for the Jurassic-Triassic mafic rock (Fig. 5Q) and Mono Creek sample (Fig. 5K) are consistent with prolonged or episodic periods of zircon growth. This pattern of zircon growth is most consistent with the presence of antecrysts - grains that crystallized from earlier pulses of magma that were incorporated into younger magma from the same system (e.g., Miller et al. 2007). This interpretation seems particularly likely in the case of the Mono Creek sample, for which there are nearby dated samples spanning the range of zircon ages from the sample. The same interpretation may be valid for both the McDoogle Quartz Monzodiorite (Fig. 5B), and second Mono Creek Granite sample (Fig. 5J), but is not distinguishable from the resorption/regrowth hypothesis.

If dispersion of the data along concordia is the result of resorption/regrowth or the presence of antecrysts, the youngest age for each sample probably best estimates the crystallization age. However, to be conservative, for all data representation, interpretation, and thermal modeling, the entire range in zircon dates for these samples is used to estimate their crystallization age.

Incremental Emplacement

Zircon U-Pb crystallization ages indicate that the Muir suite assembled over about 9 m.y. from 96 to 87 Ma (Fig. 6A). Similarly, ages from this study, combined with zircon data from other studies, indicate that the Whitney suite assembled over about 7 m.y. from 90 to 83 Ma (Fig. 6B; Chen and Moore 1982; Saleeby et al. 1990; Mattinson 2005). Within the suites, individual plutons also record extended age ranges: the Lamarck Granodiorite of the Muir suite was assembled over at least 3 m.y., and data for the Mono Creek (Muir suite), and Sugarloaf, Paradise and Whitney (Whitney suite) plutons all suggest at least 2 m.y. for their assembly. Plutons with crystallization ages spanning millions of years, and intrusive suites with age ranges approaching 10 m.y., cannot be intruded as one (or just a few) pulses of magma, but must have been assembled incrementally (Coleman et al. 2004; Glazner et al. 2004; Matzel et al. 2006). This is consistent with field data from the Muir suite and elsewhere that demands amalgamation of even superficially homogeneous plutons as incrementally assembled sheeted bodies (Mahan et al. 2003; Bartley et al. 2008). Even the relatively rapidly assembled Torres del Paine pluton preserves evidence for incremental assembly (Michel et al. 2008). The growing body of data requiring million year age spans for the crystallization of plutons, supported by a growing body of field evidence for incremental assembly, suggests that incremental pluton growth is the norm and not the exception.

Therefore, caution should be exercised when accepting a single age as representative of any pluton. Also interpretation of the timing of structures by dating deformed or cross cutting plutons must be restricted to samples immediately adjacent to the structure of interest.

Interpretation of Thermal Histories

Muir Suite thermal history

For all samples in this study, zircon crystallization ages are concordant within uncertainty with titanite and hornblende dates, indicating rapid cooling immediately following intrusion. In addition, this indicates that the hornblende dates were not reset by younger intrusions in the suites. Following an initial interval of rapid cooling immediately after intrusion, slow cooling then persisted for millions of years, as indicated by the 5-11 m.y. separation between hornblende and biotite dates (Fig. 15). Together, the data suggest that temperatures remained between hornblende and biotite closure temperatures for millions of years following intrusion.

Two interpretations can account for rapid, followed by slow cooling: exhumation millions of years following emplacement, or cooling complicated by multiple reheating events during the approximately 9 m.y. intrusive history of the rocks.

During the time of emplacement, if ambient temperatures were above biotite closure, the protracted cooling through biotite closure temperatures could reflect cooling during exhumation. In this case, biotite dates would be set once rocks were exhumed through the biotite closure temperature isotherm. In the absence of folding or faulting, biotite dates reflecting regional exhumation cooling should fall in a narrow range (e.g., Renne et al. 1993). The spread of biotite dates throughout the Muir suite is inconsistent with this view (Fig. 15). A spread in biotite ages, like those in this study, could result if deformation

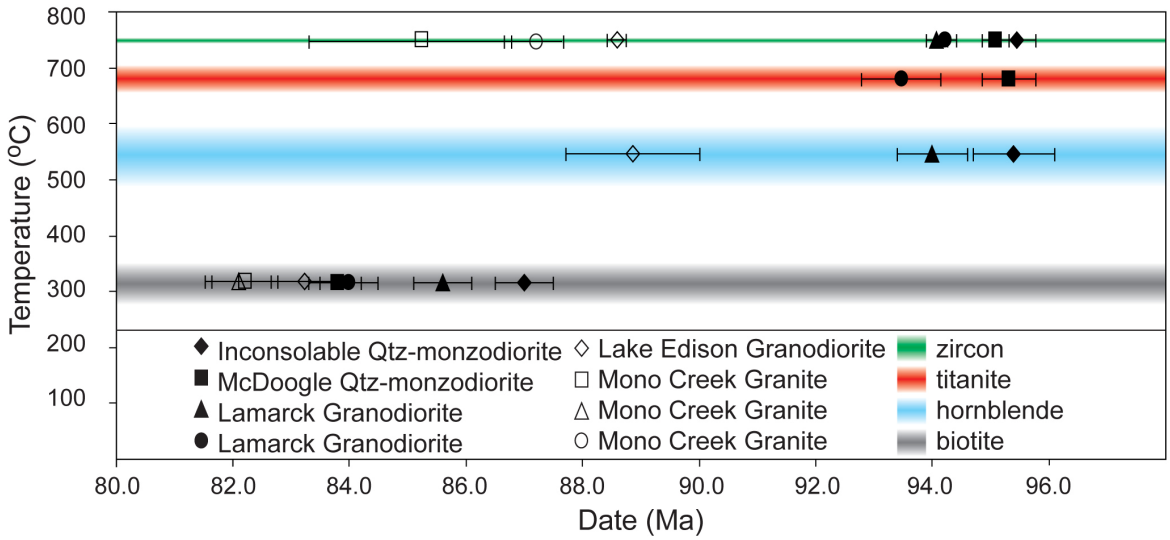

Fig. 15 Temperature-time (T-t) histories for John Muir Intrusive Suite. An estimated zircon saturation temperature (Watson and Harrison 1983) of 750°C is an average of three whole rock samples from the Lamarck Granodiorite (Frost and Mahood 1987). Estimated titanite closure temperatures (700-660°C) after Scott and St-Onge (1995). Estimated hornblende (580-490°C) and biotite (345-280°C) closure temperatures after Harrison (1981) and Harrison et al. (1985), respectively.

resulted in exhumation of some areas prior to others. However, no such deformation is evident in the region that could account for the age spread in biotites. Therefore, exhumation cooling is not favored as a mechanism producing the T-t histories throughout the Muir suite.

Thermal modeling shows that when plutons are assembled incrementally, as demonstrated for the Muir suite here, temperatures oscillate with the intrusion and cooling of each magma pulse, and remain above ambient background for extended time periods (Annen et al. 2006). Thus, the gap between hornblende and biotite dates for the Muir suite could reflect temperature oscillation for millions of years following emplacement. The range of temperature oscillations appears to be limited to being between biotite and hornblende closure because K-feldspar MDD modeling suggests a distinct time gap between biotite closure (estimated to be 345-280˚C) and feldspar cooling (models typically suggest temperatures of approximately 320˚C; Figs. 10 and 11). If temperatures during incremental assembly were dropping significantly below 320˚C, and biotite was getting reset during a subsequent heating event, high-temperature dates for the K-feldspar should be similar to the biotite dates. Instead the data suggest very slow cooling between biotite closure and the onset of high-temperature Ar retention in the K-feldspar.

Throughout the Muir suite, the data indicate that there is a greater time gap between crystallization and subsequent passage through biotite closure for older plutons than for younger plutons (Fig. 16). Older plutons such as the Inconsolable Quartz Monzodiorite, McDoogle Quartz Monzodiorite, and Lamarck Granodiorite record an 11-8 m.y. gap; whereas, younger plutons such as the Lake Edison Granodiorite and Mono Creek Granite record a 6-5 m.y. gap between crystallization and biotite closure. More protracted cooling in

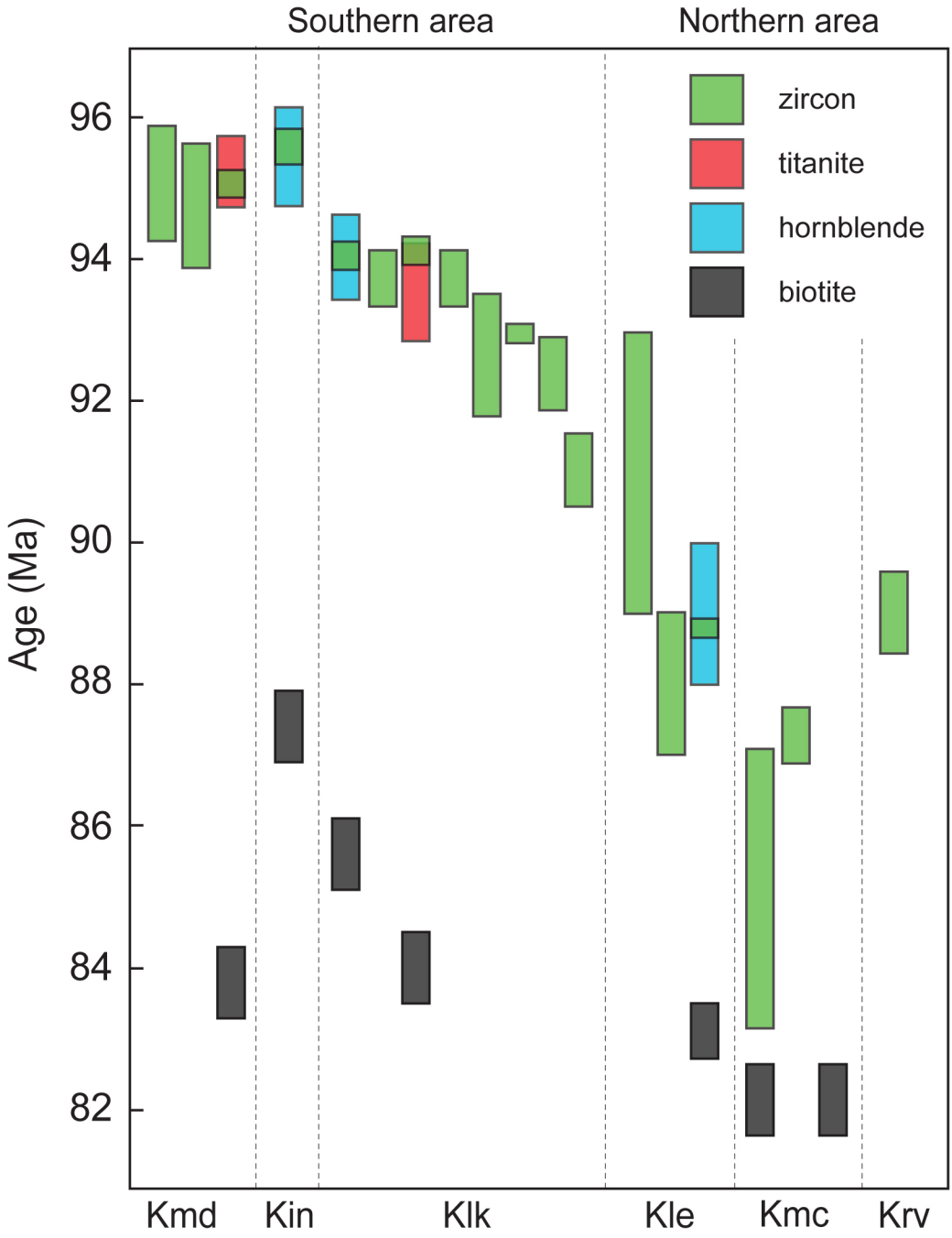

Fig. 16 Summary of geo-thermochronology data from the John Muir Intrusive Suite. As the crystallization ages get younger the cooling time interval between zircon ages and biotite dates decrease. Kmd, McDoogle Quartz Monzodiorite; Kin, Inconsolable Quartz Monzodiorite; Klk, Lamarck Granodiorite; Kle, Lake Edison Granodiorite; Kmc, Mono Creek Granite; Krv, Round Valley Peak Granodiorite. Note that not all zircon ages have corresponding argon dates. Zircon ages from this study (Kmd, Klk, Kle, Kmc) and after Gracely (2006; Kin, Klk), Gaschnig (2005; Krv), Mahan et al. (2003; Kmd), Coleman et al. (1995; Klk), Tobsich et al. (1995; Kle). Hornblende, titanite, and biotite dates from this study. Error bars are 2-sigma.

older plutons is consistent with modeling that shows the thermal anomalies of younger intrusions building across the decaying temperature profiles of older intrusions (e.g., Barton and Hanson 1989; Hanson and Barton 1989). Temperatures in the younger units likely did not stay at elevated temperatures for as long because not long after they intruded the regional magmatic activity waned (e.g., Chen and Moore 1982).

Whitney Suite thermal history

As for the samples from the Muir suite, samples from the Whitney suite yield U-Pb zircon ages and Ar-Ar hornblende dates that overlap within uncertainty consistent with rapid initial cooling after intrusion (Fig. 17). Also like the Muir suite, the older plutons in the Whitney suite took longer to cool below biotite closure temperatures (Fig. 18); however, the pattern is not as clear. The granodiorite of Sugarloaf experienced approximately 3 m.y. of slow cooling following emplacement, and the Paradise Granodiorite experienced about 2 m.y. of slow cooling. Thus, the granodiorite of Sugarloaf and the Paradise Granodiorite are interpreted to have oscillated between hornblende and biotite closure temperatures for 2-3 m.y. In contrast, the sample from the Whitney Granodiorite crystallized and cooled through biotite instantaneously within the uncertainty of the age determinations.

The time gap between hornblende and biotite dates for the Whitney suite is significantly shorter than the Muir suite. One reason for the difference between these two may be that the Whitney suite was assembled at shallower crustal levels than the Muir suite. This would result in more rapid relaxation of the elevated geotherm through biotite closure temperature across the Whitney suite relative to the Muir suite. Also, the Whitney suite is one of the youngest intrusive suites in the Sierras and, coincident with, or shortly after, its emplacement, magmatism in the entire Sierra Nevada shut down (Stern et al. 1981; Chen and

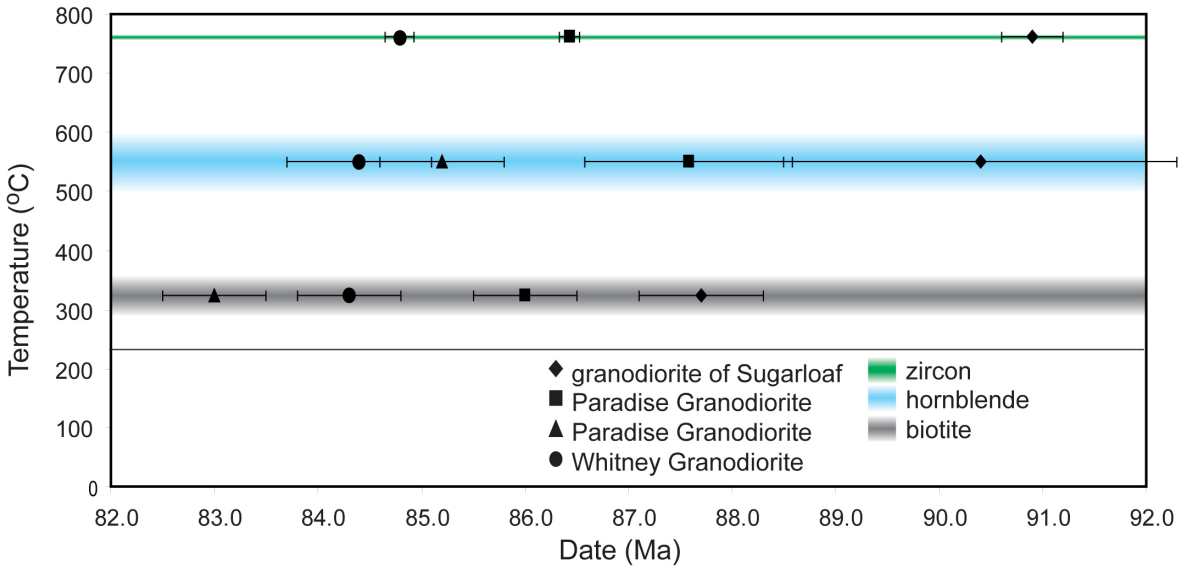

Fig. 17 Temperature-time (T-t) histories for Mount Whitney Intrusive Suite. An estimated zircon saturation temperature (Watson and Harrison 1983) of 760°C is an average determined by using forty-three whole rock samples from the Whitney suite (Hirt 2007). Estimated hornblende (580-490°C) and biotite (345-280°C) closure temperatures after Harrison (1981) and Harrison et al. (1985), respectively.

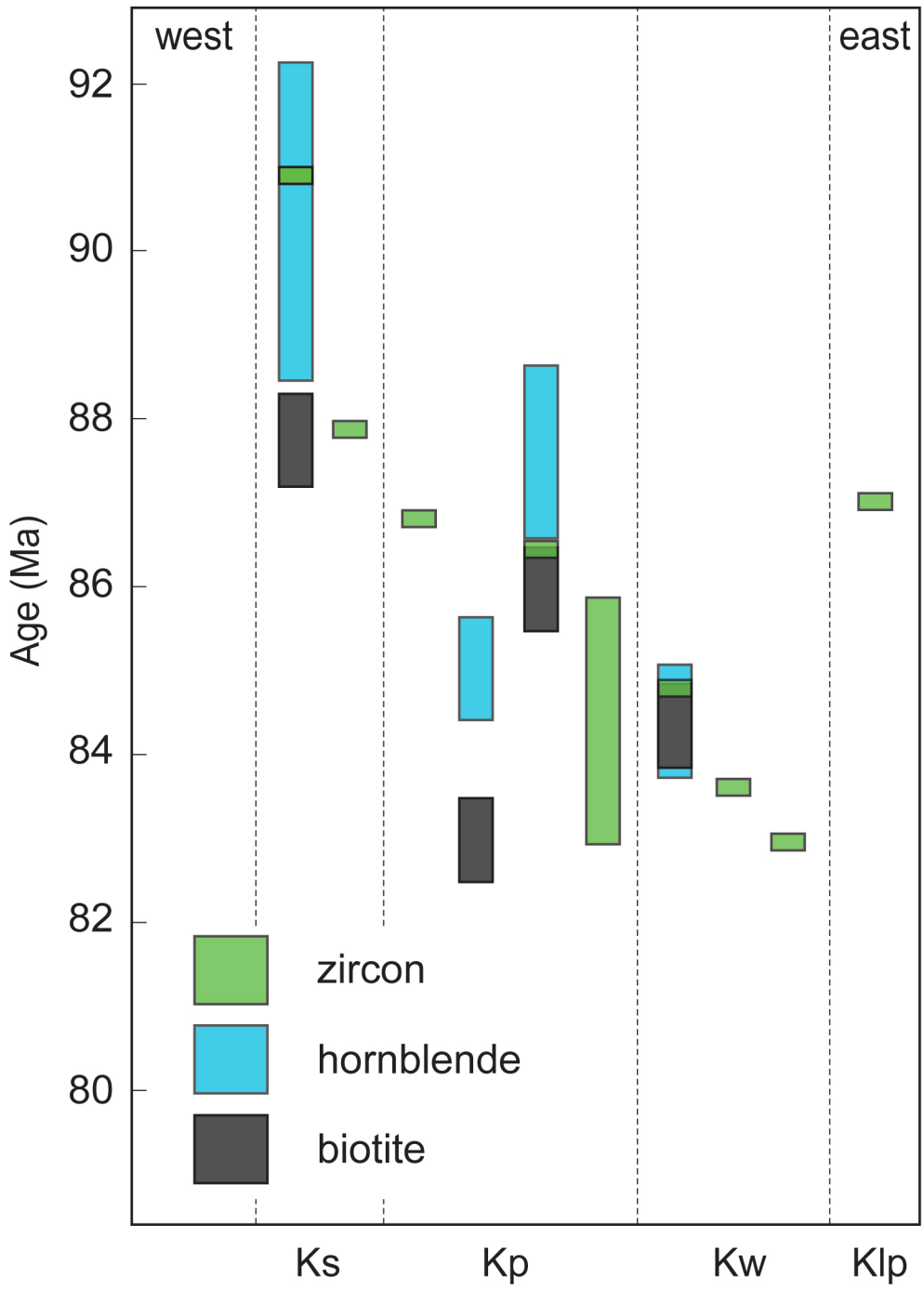

Fig. 18 Summary of geo-thermochronology data from the Mount Whitney Intrusive Suite. Ks, granodiorite of Sugarloaf; Klp, granodiorite of Lone Pine Creek; Kp, Paradise Granodiorite; Kw, Whitney Granodiorite. Zircon ages from this study (Ks, Kp, Kw) and after Chen and Moore (1982; Ks, Klp, Kp, Kw), Saleeby et al. (1990; Kw), Mattinson (2005; Kp). Note that Chen and Moore (1982) did not report age uncertainties. Note that not all zircon ages have corresponding argon dates. Hornblende and biotite dates from this study. Error bars are 2-sigma.

Moore 1982). As the rate of magma intrusion decreased, relaxation of the elevated geotherm and cooling of intrusions was likely accelerated.

Wall rock thermal histories

Hornblendes from wall rock samples adjacent to both the Muir and Whitney suites are significantly younger than the corresponding U-Pb zircon ages, and biotite dates from these same samples are several to tens of millions of years younger than the corresponding hornblende dates (Fig. 19). The thermal histories of wall rocks are placed into two groups: those with dates completely reset and those with dates partially reset. In the Whitney suite area, the Bullfrog Granite, and the Jurassic-Triassic mafic rocks yield statistically identical hornblende dates that cluster around 90.4 Ma (Fig. 7L, 7M). This age is indistinguishable from the age of the granodiorite of Sugarloaf of the Whitney suite (Fig. 5M) and I suggest that intrusion of the Whitney suite locally raised temperatures above hornblende closure and completely reset wall rock dates.

Similarly, the quartz diorite of Pine Lake has a crystallization age of 181 Ma (Fig. 5L) and a hornblende date of 86.2 Ma (Fig. 7H) that is interpreted to reflect complete resetting by the adjacent Muir suite. The quartz diorite is a small body (3 km^2; Frost and Mattinson 1988) that is pervasively intruded by horizontal sheets from the 87 Ma Mono Creek granite (Frost and Mattinson 1988; Bateman 1992). A biotite date of 79.5 Ma (Fig. 8L) suggests that this sample cooled slowly for 5 m.y. – similar to the cooling history of the adjacent Muir suite.

Hornblende dates from the Tinemaha Granodiorite range from 154-116 Ma and there is no correlation between a date and distance of the sample from the Muir suite (Fig. 3). I

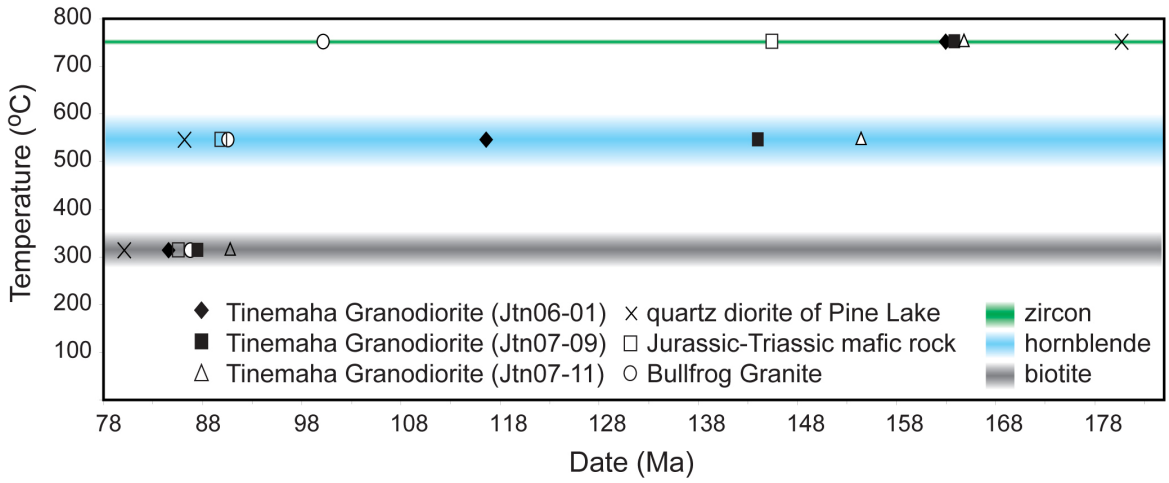

Fig. 19 Temperature-time (T-t) histories for wall rocks adjacent to the John Muir and Mount Whitney Intrusive Suites. Zircon saturation temperatures (Watson and Harrison 1983) were not determined for these samples. Instead, an estimated zircon saturation temperature of 760°C is used. This value is consistent with zircon saturation temperatures determined for both the Muir and Whitney suites. Estimated hornblende (580-490°C) and biotite (345-280°C) closure temperatures after Harrison (1981) and Harrison et al. (1985), respectively. U-Pb zircon ages for Tinemaha Granodiorite (Jtn06-01, Jtn07-09, Jtn07-11) are estimated from Chen and Moore (1982).

suggest these dates reflect partial degassing of Ar during intrusion by numerous Cretaceous plutons in addition to those in the Muir suite (Bateman 1992). Thus, the hornblende dates have no geologic meaning. Biotite dates from the Tinemaha Granodiorite yield simple plateaus and inverse isochrons. These biotites were completely reset by Cretaceous plutonism and indicate the time when samples passed back through closure temperature.

Pluton Emplacement Modeling

Thermal modeling predicts that, during the construction of an incrementally assembled plutonic suite in the shallow crust, it is unlikely that temperatures are maintained significantly higher than background ambient (Fig. 13). Once an intrusion is emplaced, it cools and solidifies rapidly as heat is dissipated into the surrounding area. Subsequent intrusions raise the temperatures of the nearby rocks, yielding the saw-tooth T-t patterns seen in all watch points (Fig. 13). This predicts that rocks from a plutonic suite will experience long time-spans of thermal oscillations during assembly. In addition, at the intrusion rates dictated by the geochronology, raising temperatures high enough to reset the hornblende dates (approximately 550°C) of any early intruded increments is unlikely at depths of less than 10 km (e.g., many Sierran rocks; Ague and Brimhall 1988). The model predicts that after 7 m.y. of magmatic activity the hottest parts of the domain are still less than 500°C (Fig. 13; watch points 4, 6). This is consistent with T-t history determined from individual samples analyzed throughout both the Muir and Whitney intrusive suites (Figs. 15 and 17) which suggest that rock units likely resided at temperatures below hornblende closure for the duration of assembly period.

In addition, thermal modeling reveals that the assembly of plutons results in a persistently low melt fraction that is present in the magma chamber at any one time (Fig. 14).

Figure 14 demonstrates that as an incrementally assembled magma chamber grows the intrusions are not fluxing heat rapidly enough to maintain elevated temperatures necessary for melt-rich chambers to be maintained (e.g., Annen 2009). Together these observations suggest that it is unlikely that the Whitney suite or the Muir suite ever existed as large, high-melt (>50%) fraction magma chambers.

Incremental Emplacement and Volcanic-Plutonic Connections

Detailed geochronology for the Lamarck Granodiorite and field mapping permit the calculation of an average magma flux during pluton growth. Assuming an area of 500 km^2 (Bateman 1992) and estimating a thickness between 5-15 km, a long-term average magma flux between 0.0010-0.0025 $km^3 \cdot yr^{-1}$ (1-2.5x10^6 $m^3 \cdot yr^{-1}$) is needed to construct the Lamarck Granodiorite. Expanding to the entire Muir suite, an estimated area of 1700 km^2 (Bateman 1992) and a thickness between 5-15 km yields essentially the same flux. The Whitney suite has a total outcrop of approximately 1200 km^2 (Hirt 2007). Using the same range of thicknesses estimated for the Muir suite, the same long-term average magma flux is necessary to construct the Whitney suite. These fluxes are consistent with those calculated for other plutons including the Tuolumne Intrusive Suite and the Mount Stuart batholith (e.g., Annen 2009).

A growing body of geochronological data and numerical models shows that the rate of magma emplacement likely determines whether a caldera-forming eruption is possible (e.g., Glazner et al. 2004; Annen 2007, 2009; Crowley et al. 2007; Costa 2008). Caldera-forming eruptions offer evidence that large magma chambers can exist in the upper crust; however, numerical simulations show that magma fluxes greater than 0.1 $km^3 \cdot yr^{-1}$ are necessary to develop and maintain magma chambers voluminous enough to feed the

eruptions (Annen 2009). Rapid magma fluxes are consistent with geochronologic data from ignimbrites that suggest magma residence times less than 1 m.y. and likely less than 500 k.y. prior to eruption (Bachmann et al. 2007; Crowley et al. 2007; Costa 2008; Simon et al. 2008). Several recent papers calculated pluton growth rates on the order of 0.1 to >1 $km^3 \cdot yr^{-1}$ that are necessary to support ignimbrite eruption by assuming rapid assembly times 10^3 to 10^5 years (Petford et al. 2000; de Silva 2007). However, no detailed geochronology supports such rapid assembly rates. In contrast, a growing body of geochronological data indicate that pluton emplacement fluxes are too slow to develop large magma chambers (Annen 2009).

The low magma fluxes during assembly of the Lamarck Granodiorite and the Muir and Whitney suites precluded the development of large, dominantly liquid magma chambers during construction. This interpretation is consistent with the concordance of zircon ages and titanite and hornblende dates, and thermal modeling presented in this study (Fig. 14). Modeling by Annen (2009) also suggests that such low fluxes are capable of maintaining no more than a few percent melt. This conclusion is supported by geophysical data from active volcanic regions that are never consistent with significant melt percentages being present in sub-volcanic magma chambers (Iyer 1984; Moran et al. 1999; Masturyono et al. 2001). If large magma chambers typically do not develop during pluton construction, the genetic relationship hypothesized to exist between zoned plutons and zoned ignimbrites is problematic and must be reevaluated (e.g., Hildreth 2004; Bachmann et al. 2007; Lipman 2007).

Several lines of evidence suggest that the link between plutonic and volcanic rocks may not be through huge ignimbrite eruptions, but rather through “typical” arc volcanism. Data from the Chilean Andes indicates that volcanic centers there record eruptive histories

comparable to the assembly time for zoned intrusive suites (e.g., Aucanquilcha 11 m.y.; Grunder et al. 2008). These centers are also similar in size to the zoned intrusive suites (approximately 3000 km^2), and show similar patterns of compositional evolution through time (Grunder et al. 2008). Finally, although it is difficult to compare time scales, estimates of modern fill rates beneath Andean volcanoes made using InSAR are on the order of 0.05 $km^3 \cdot yr^{-1}$ (Pritchard and Simons 2004). These rates are intermediate between estimates necessary for ignimbrite formation and estimates of pluton filling rates, but it seems likely that this short-term measurement overestimates long-term rates. Taken together, I hypothesize that "Sierran-type" zoned intrusive suites are actively forming beneath modern arc volcanoes, and that suites such as the Muir and the Whitney hold information about "typical" arc magmatism, rather than catastrophic ignimbrite events.

Assembly of the Muir Suite and Regional Tectonics

Slow pluton assembly of the Muir suite over at least 9 m.y. is consistent with passive emplacement mechanisms operating at rates comparable to lithospheric strain rates (Hutton 1988; Tikoff and Teyssier 1992; Menand 2008). If magma intrusion is passive, the sequence, shapes, and timing of the intrusions are controlled by the regional structures and tectonics (Hutton 1988; Tikoff and Teyssier 1992). Therefore, pluton emplacement is fundamentally a tectonic matter because it is controlled by the ability of subduction processes to generate magma, and the lithosphere to make space to accommodate magma.

Assembly of the Muir suite spans a shift in regional tectonics that occurred at the western margin of North America. Between approximately 105-90 Ma, throughout the central Sierra Nevada batholith deformational patterns define tectonic strain regimes that fluctuated between weakly extensional and weakly contractional (Tobisch et al. 1995). This

was followed by a shift to a transpressive and dextral strike-slip tectonic setting that was active between approximately 90-78 Ma (Tikoff and Teyssier 1992; Tobisch et al. 1995; Mahan et al. 2003).

The pre-90 Ma tectonic setting of the central Sierra Nevada batholith is recorded within shear zones by solid state deformation adjacent to and within the Muir suite. Throughout the region, numerous steeply dipping reverse-sense shear zones were active from about 102-91 Ma (Tobisch et al. 1995; Mahan et al. 2003; Stearns and Bartley 2010). Plutons in the Muir suite preserve evidence for passive emplacement during this time interval. For example, the McDoogle Quartz Monzodiorite displays compelling evidence for emplacement as a series of vertical sheets into a steeply dipping reverse-sense shear zone during a period of relaxed horizontal compression or local dilation (Mahan et al. 2003; Bartley et al. 2008; Stearns and Bartley 2010). Similarly, field data suggest that the Lamarck Granodiorite, particularly in Dusy Basin, grew by crack-seal as a series of vertical sheets shortly after the McDoogle Quartz Monzodiorite (Gracely 2006).

Following intrusion of these oldest portions of the Muir suite, by about 90 Ma, a shift in tectonism occurred in the central Sierra Nevada (Tikoff and Teyssier 1992; Tobisch et al. 1995). Tikoff and Teyssier (1992) suggested that plutons in the central Sierra Nevada batholith, specifically the Mono Creek Granite, were emplaced passively into dilational areas during post 90 Ma transpressional deformation. This deformation occurred, in part, along the a shear zone that records dextral shear along the northeast edge of the Mono Creek Granite and crosses through the central Mono Creek Granite, Lake Edison Granodiorite, and the Lamarck Granodiorite (Lockwood and Lydon 1975; Tikoff and Teyssier 1992; Tobisch et al. 1995; Saint Blanquat and Tikoff 1997). Similarly, north of the Muir suite, a segment of a

large unnamed shear zone, that was active prior to and during the emplacement of nearby plutons around 94-91 Ma, records dominant sub-vertical stretching and sub-horizontal shortening (Greene and Schweickert 1995).

There is little direct evidence for a change in the style of pluton assembly in the Muir Suite that may reflect the change in regional tectonics that occurred around 90 Ma. Saint Blanquat and Tikoff (1997) suggested that the presence of sub-horizontal felsic dikes originating from the Mono Creek Granite indicated a regional vertical least compressive stress direction around 87 Ma, consistent with deformation in the shear zones. Additionally, several observations about the younger (post 93 Ma) plutons in eastern part of the Muir suite distinguish them from the older plutons in the west. There are distinct differences in the map patterns of pre- and post-93 Ma plutons of the Muir, including a change from well-documented elongate sheeted dikes (Mahan et al. 2003; Gracely 2006) to more "bulbous", nested units (Fig. 3; Bateman 1992). There are also clearly subhorizontal mafic units in the younger eastern Lamarck Granodiorite (Bateman 1992 in the region around Piute Pass) in contrast to dike-like units in the older western portions (Gracely 2006). Finally, extremely detailed mapping by Hathaway (2002) in the youngest parts of the Lamarck Granodiorite (approximately 92 Ma) indicate that some of the pluton was assembled by laccolith intrusion. Together, these data suggest that an apparent shift in intrusion geometry of Muir suite plutons after 93 Ma could be consistent with, and the result of, a shift in tectonic setting at about 90 Ma.

Post-Magmatic History of the Sierra Nevada-Peninsular Ranges Arc

Late Cretaceous Cooling of the John Muir Intrusive Suite

The combination of U-Pb crystallization ages, $^{40}Ar/^{39}Ar$ hornblende and biotite dates, and K-feldspar MDD thermal modeling enables a detailed evaluation the overall T-t history of the Muir suite (and by inference the central Sierra Nevada batholith). The complete cooling histories of samples from the Muir suite show two distinct inflections, and perhaps a third inflection that is poorly defined: the first is a time-transgressive (dependent on the age of the intrusion) slowing of cooling rates following intrusion, the second is a sudden acceleration of cooling that is reflected in all samples, an the third is a likely return to slow cooling (Fig. 20). The southern Muir suite region began accelerated cooling at about 77 Ma and the northern Muir suite region at about 76 Ma. Generally, thermal models indicate that cooling rates increased from less than $15°C \cdot m.y^{-1}$ to about $50°C \cdot m.y^{-1}$, and samples from both transects (Figs. 10 and 11) resided at temperatures around 150°C by 72 Ma. A compilation of Sierran-wide apatite (U-Th)/He dates from samples collected at elevations similar to those in this study (approximately 2500-3500 m a.s.l.) yields a weighted average date of 63 Ma (House 1997; House et al. 2001; Clark et al. 2005). Together with the MDD modeling, these data indicate the region likely underwent a period of decelerated cooling from 72 Ma to at least 63 Ma.

Explanations for the onset of rapid cooling include cooling from below in response to shallow subduction with (Dumitru 1990; Grove et al. 2003) and without (Cross and Pliger 1982; Gutscher et al. 2000) coincident removal of the subbatholith lithospheric mantle, and cooling from above in response to tectonic and erosional exhumation (Grove et al. 2003; Saleeby et al. 2007; Saleeby et al. 2010).

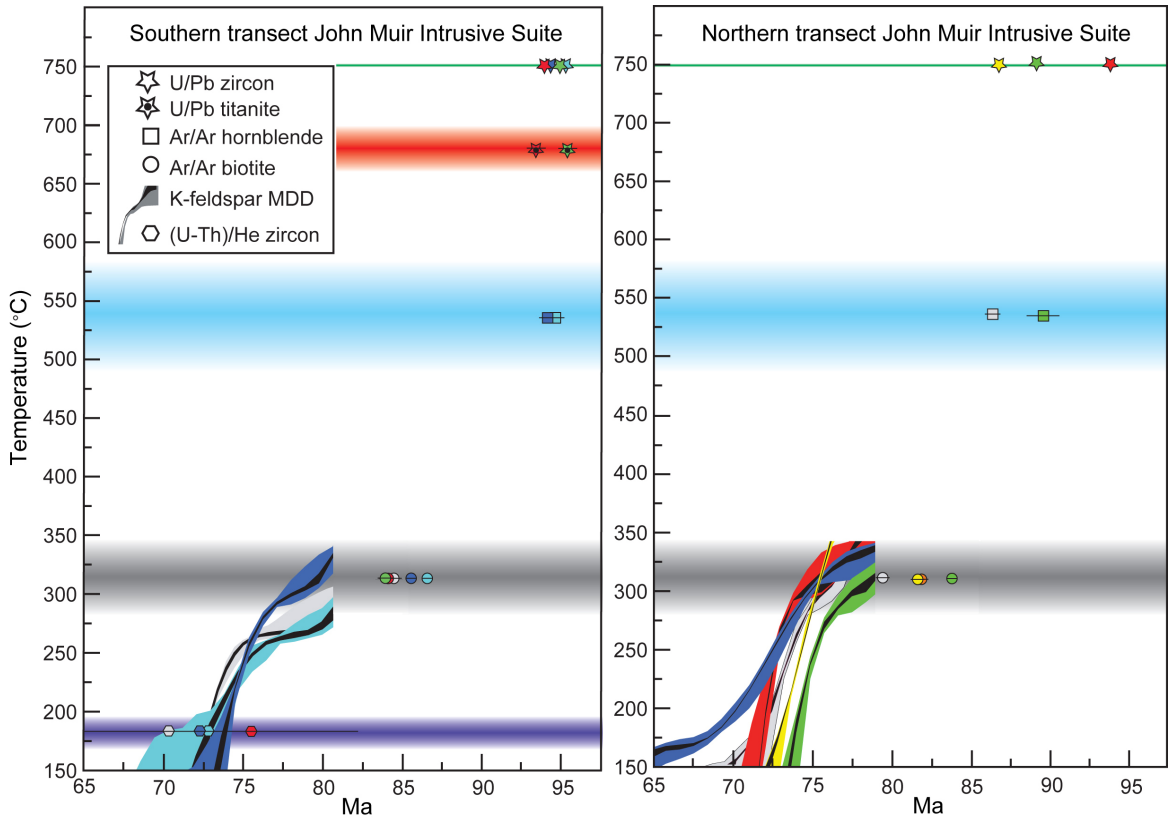

Fig. 20 Compilation of John Muir Intrusive Suite thermal histories. The complete cooling histories for samples show two distinct inflections: the first is a time-transgressive (dependent on the age of the intrusion) slowing of cooling rates following intrusion, and the second a sudden acceleration of cooling that is reflected in all samples at about 76 Ma. Error bars on individual minerals are 2-sigma. Envelopes in MDD models represent all modeled thermal histories meeting the fitting criteria of Quidelleur et al. (1997); whereas, black envelopes represent 90% confidence of the mean modeled thermal histories. Samples are color coordinated. Southern transect: Lamarck Granodiorite Db05-04-blue; Lamarck Granodiorite Db04-05-red; Inconsolable Quartz Monzodiorite Dbk05-01-teal; McDoogle Quartz Monzodiorite Ms07-F8-green; Jurassic Tinemaha Granodiorite Jtn06-01-gray. Northern transect: Lamarck Granodiorite Kl07-01-blue; Lamarck Granodiorite Kl07-02-red; Lake Edison Granodiorite Kle07-05-green; Mono Creek Granite Km07-06-yellow; Mono Creek Granite Km07-08-orange; Jurassic quartz diorite of Pine Lake Pcp07-07-light gray. Estimated zircon saturation temperature (Watson and Harrison 1983) of 750°C is an average calculated from three whole rock compositions from samples of the Lamarck Granodiorite (Frost and Mahood 1987). Estimated titanite closure temperature 700-660°C after Scott and St-Onge (1995). Estimated hornblende closure temperature 580-490°C after Harrison (1981). Estimated biotite closure temperature 345-280°C after Harrison et al. (1985). Estimated zircon (U-Th)/He closure temperature 190-170°C after Reiners et al. (2004).

Thermal modeling of fission-track data suggests the Sierran batholith could have rapidly cooled from below as a cold subducting plate shallowed and removed the overriding lithospheric mantle (Dumitru 1990). However, xenolith data from basalts erupted through the central Sierra Nevada indicate the preservation of a lithospheric mantle (Ducea and Saleeby 1998; Saleeby et al. 2003). Saleeby (2003) argued that only regions in the southern Sierra Nevada batholith and Mojave Desert provide evidence for subbatholith lithosphere removal during Laramide time. Therefore, it seems unlikely that cooling from below in response to subbatholith lithospheric mantle removal is a possible mechanism responsible for the onset of rapid cooling throughout the entire region.

Cross and Pilger (1982) suggested that an increase in the plate convergence rate can cause shallowing of the subducting plate and coeval arc migration. The period of time during and immediately following the cessation of Sierran and Peninsular Ranges magmatism is characterized by an increase in the rate of convergence between the North American and Farallon plates (to rates greater than 100 $mm \cdot yr^{-1}$; Engebretson et al. 1985). The rate increase potentially initiated a period of arc-wide shallow subduction, but not necessarily resulting in the removal of the subbatholith lithosphere. Prolonged shallowing of an oceanic plate can cool and thicken the overriding continental lithosphere (Cross and Pilger 1982; Gutscher et al. 2000). However, the time scale for this thermal perturbation to reach shallow crustal levels is far too long (hundreds of millions of years) to account for the rapid cooling documented in this study.

The inflection points in the Muir suite T-t histories are therefore only consistent with cooling in response to exhumation (e.g., Harrison and Clarke 1979). Thermal modeling predicts that exhumation yields T-t histories characterized by rapid cooling as the sample

approaches the surface (Harrison and Clarke 1979). Thus, it appears that the central Sierra Nevada was characterized by rapid exhumation (cooling rates of up to 50˚C·m.y^{-1}.) immediately following the cessation of magmatism in the Sierran arc.

Late Cretaceous Cooling of the Sierra Nevada-Peninsular Ranges Arc

House et al. (1997) combined helium age-elevation profiles from multiple Sierran and northern Peninsular Ranges transects and concluded that the batholiths had similar low-temperature T-t histories during Late Cretaceous through mid-Cenozoic time. Using titanite and apatite fission track data, Dumitru (1990) determined that the central Sierra Nevada batholith cooled rapidly from above 270°C to below 95°C from 73-67 Ma, largely consistent with K-feldspar MDD modeling from this study. In the east-central Peninsular Ranges batholith, Grove et al. (2003) interpreted biotite dates and K-feldspar MDD modeling and suggested a major cooling event from approximately 78-68 Ma with a maximum average cooling rate of around 30°C·m.y^{-1}. at about 73 Ma. Rocks in the far eastern part of the batholith recorded cooling rates up to 80°C·m.y^{-1}. from about 76-72 Ma (Grove et al. 2003). Together, the data suggest that a Sierran-Peninsular Ranges-wide rapid cooling event commenced at around 76 Ma. In contrast, Saleeby et al. (2007) document a very similar rapid cooling event in the southern Sierra Nevada batholith, but at a significantly earlier time (100˚C·m.y^{-1}. peaking at approximately 95 Ma). These authors also attributed the cooling to a rapid exhumation event.

In support of a rapid exhumation event across the Sierran and Peninsular Ranges arcs, sedimentological data indicate that thick sequences of eroded debris were shed to westward from the Cordilleran arc during the Late Cretaceous. A dramatic increase in the deposition of K-feldspar-rich detritus in the forearc basin led Mansfield (1979) to suggest that significant

erosion of plutonic rocks occurred very late in the Cretaceous. Wakabayashi and Sawyer (2001) inferred that high accumulation rates of sediment shed from the central Sierra Nevada throughout the Late Cretaceous were likely related to accelerated erosion caused by uplift. Finally, regional erosional surfaces throughout the Peninsular Ranges batholith suggest significant exhumation during the Late Cretaceous (Kies and Abbott 1983). Thus, a variety of independent data support Late Cretaceous exhumation as the likely cause of rapid cooling documented in plutonic rocks.

The 20 m.y. difference in the timing of cooling between the southern Sierra Nevada, and the central Sierras and Peninsular Ranges seems significant. Although cooling in the southern Sierras has been attributed to extensional unroofing (Bartley et al. 2007; Saleeby et al. 2007) this same unroofing event cannot entirely account for the cooling in the central Sierras and Peninsular Ranges because the rocks in the southern Sierra are derived from significantly deeper structural levels (8-10 kbar; Saleeby et al. 2007) than the others (typically < 3 kbar). Unroofing alone should have caused cooling in the shallow rocks before the deep rocks, not 20 m.y. later. Consequently, I suggest that a significant component of the rapid cooling in the southern Sierra Nevada is likely to have been driven from below. Unlike the central Sierras and Peninsular Ranges, where there is good evidence for preservation of the lithospheric mantle during flat slab subduction, the occurrence of the Rand Schist adjacent to the southern Sierras strongly supports tectonic erosion of the mantle lithosphere in that region during the late Cretaceous.

6. CONCLUSIONS

Zircon U-Pb geochronology results indicate that the John Muir Intrusive Suite was assembled over at least 9 m.y. from 96 and 87 Ma and the Mount Whitney Intrusive Suite was assembled over at least 7 m.y. from 90 to 83 Ma. Assembly over millions of years favors the development of the intrusive suites, and the individual plutons within them, as a series of incrementally emplaced intrusions. Bulk mineral thermochronology indicate complicated cooling histories that were typically rapid immediately following intrusion, followed by slow cooling as temperatures were maintained between hornblende and biotite closure throughout assembly of the suites. K-feldspar MDD thermal modeling suggests that all of the plutons, and perhaps the entire central Sierra Nevada batholith, then experienced a period of accelerated cooling that began at approximately 76 Ma. This episode of cooling may be related to well-documented rapid cooling elsewhere in the western US Cordillera. Cooling in the central Sierra Nevada and northern Peninsular Ranges likely resulted from rapid exhumation. However, in the southern Sierra Nevada, cooling by exhumation was likely enhanced by cooling from below following tectonic erosion of the lithospheric mantle during an episode of shallow subduction that ultimately led to the Laramide Orogeny.

The high density of U-Pb zircon geochronology for rocks in the Muir and Whitney suites permits reasonable estimates of long-term magma flux during assembly of the suites. Estimated pluton assembly rates for the Muir suite and one of its members, the Lamarck Granodiorite, as well as the Whitney suite, are on the order of 0.0010-0.0025 $km^3 \cdot yr^{-1}$, similar to independent estimates of assembly rates from elsewhere. Thermal modeling

reveals that assembly of plutons at such slow rates results in a persistently low melt fraction present. Therefore, it is unlikely that the Whitney Suite or the Muir suite or the Lamarck Granodiorite ever existed as large, high-melt fraction magma chambers. This result is consistent with geophysical data for magma zones beneath active arcs, but is sharply at odds with petrologic models that place heavy emphasis on processes such as stoping and crystal settling in shallow magma chambers, and the concept that zoned intrusive suites are genetically linked with large silicic ignimbrite eruptions.

TABLES

Table 1 Thermal model input parameters

Parameter	Symbol	Units	Layer1	Layer 2	Magma
Density	ρ	$kg \cdot m^{-1}$	2450	2690	2475
Specific Heat	C_p	$J \cdot kg^{-1} \cdot K^{-1}$	1000	1000	1150
Thermal conductivity	k	$W \cdot m^{-1} \cdot K^{-1}$	1.7	3.1	1.4
Radiogenic heating rate	A	$\mu W \cdot m^{-3}$	1.5	2.0	1.4
Initial geothermal gradient	dT/dz	$°C \cdot km^{-1}$	35	18	-
Grid spacing	Δx	m	250	250	-
Layer thickness	z_i	m	5000	30000	-
Intrusion thickness	-	m	-	-	250
Intrusion temperature	-	°C	-	-	850
Solidus temperature	-	°C	-	-	750

Table 2 Zircon (U-Th)/He thermochronology

Sample	Date [a] [Ma]	± [b] [Ma]	U (ppm)	Th (ppm)	Th/U	He (nmol/g)	mass (μg)	Ft [c]
Lamarck Granodiorite								
Db0405-1	73.6	5.9	321.0	163.3	0.5	117.2	11.9	0.82
Db0405-2	77.4	7.0	260.7	141.8	0.5	98.9	9.7	0.80
Db0405-3	75.7	6.1	240.4	127.6	0.5	86.0	7.6	0.78
Db0405[d]	75.6	6.3	274.0	144.3	0.5	100.7	9.7	0.80
Lamarck Granodiorite								
Db05-04-1	76.2	6.9	340.4	172.7	0.5	112.2	3.4	0.73
Db05-04-2	69.6	5.6	445.6	145.8	0.3	130.8	3.2	0.72
Db05-04-3	71.1	5.7	286.1	156.0	0.5	93.9	5.3	0.76
Db05-04[d]	72.3	6.1	357.3	158.1	0.5	112.3	4.0	0.74
Inconsolable Quartz Diorite								
Dbk0501-1	76.7	6.1	121.6	44.6	0.4	46.5	19.9	0.85
Dbk0501-2	74.7	6.0	189.6	98.2	0.5	67.0	8.0	0.78
Dbk0501-3	69.1	3.9	164.8	151.2	0.9	63.5	13.3	0.82
Dbk0501[d]	73.5	5.3	158.7	98.0	0.6	59.0	13.7	0.81
Tinemaha Granodiorite								
Jtn06-01-1	65.9	5.3	333.9	215.5	0.6	102.5	4.8	0.75
Jtn06-01-2	72.2	5.8	340.9	204.3	0.6	120.7	8.6	0.79
Jtn06-01-3	73.1	5.8	414.4	225.5	0.5	143.0	6.5	0.77
Jtn06-01[d]	70.4	5.6	363.1	215.1	0.6	122.1	6.6	0.77
Whitney Granodiorite								
Wp03-07-1	75.8	6.1	724.0	404.0	0.6	232.0	2.2	0.69
Wp03-07-2	75.0	6.0	597.9	312.8	0.5	188.7	2.2	0.69
Wp03-07-3	73.2	5.9	383.2	252.5	0.7	122.5	2.5	0.70
Wp03-07[d]	74.6	6.0	568.4	323.1	0.6	181.0	2.3	0.69
Paradise Granodiorite								
Pp02-12-1	81.2	6.5	759.7	512.8	0.7	288.9	5.0	0.75
Pp02-12-2	82.4	6.6	422.5	246.6	0.6	165.7	6.4	0.77
Pp02-12-3	87.9	7.0	268.1	168.2	0.6	114.9	7.4	0.78
Pp02-12[d]	83.8	6.7	483.4	309.2	0.6	189.8	6.3	0.77

[a] Ages corrected for alpha-ejection (Farley et al. 1996)
[b] Errors reported at 2-sigma
[c] Ft denotes retained fraction of He (Farley et al. 1996)
[d] Date determined from the mean value of 3 zircon aliquots

Table 3 $^{40}Ar/^{39}Ar$ date comparisons for the John Muir and Mount Whitney Intrusive Suites and associated wall rock

Pluton	Sample ID	Mineral	Date (Ma)[a]	Date (Ma)[b c]
Inconsolable Qtz-monzodiorite	Dbk05-01	hornblende [d]	94.5 ± 0.6	95.4 ± 0.7
		biotite [e]	86.6 ± 0.3	87.4 ± 0.5
Lamarck Granodiorite	Db05-04	hornblende [d]	93.1 ± 0.4	94.0 ± 0.6
		biotite [d]	84.8 ± 0.2	85.6 ± 0.5
Lamarck Granodiorite	Db04-05	biotite [e]	83.2 ± 0.2	84.0 ± 0.5
McDoogle Qtz-monzodiorite	Ms07-F8	biotite [d]	83.0 ± 0.2	83.8 ± 0.5
Lake Edison Granodiorite	Kle07-05	hornblende [d]	88.2 ± 1.0	89.0 ± 1.0
		biotite [d]	82.3 ± 0.4	83.1 ± 0.4
Mono Creek Granite	Km07-06	biotite [e]	81.3 ± 0.2	82.1 ± 0.5
Mono Creek Granite	Km07-08	biotite [e]	81.3 ± 0.2	82.1 ± 0.5
granodiorite of Sugarloaf	S-21	hornblende [d]	89.5 ± 1.8	90.4 ± 1.9
		biotite [e]	86.9 ± 0.4	87.7 ± 0.6
Paradise Granodiorite	Pp02-12	hornblende [d]	86.8 ± 0.8	87.6 ± 1.0
		biotite [f]	85.2 ± 0.2	86.0 ± 0.5
Paradise Granodiorite	Pp03-09	hornblende [d]	84.4 ± 0.4	85.2 ± 0.6
		biotite [d]	82.2 ± 0.2	83.0 ± 0.5
Whitney Granodiorite	Wp03-07	hornblende [d]	83.6 ± 0.6	84.4 ± 0.7
		biotite [e]	83.5 ± 0.2	84.3 ± 0.5
Bullfrog Granite	Kb06-02	hornblende [e]	89.7 ± 0.4	90.6 ± 0.6
		biotite [d]	86.8 ± 0.6	87.6 ± 0.8
Jurassic-Triassic mafics	Jtrm06-02	hornblende [e]	89.2 ± 0.8	90.1 ± 0.9
		biotite [d]	84.3 ± 0.4	85.1 ± 0.6
quartz diorite of Pine Lake	Pcp07-07	hornblende [d]	85.4 ± 0.3	86.2 ± 0.6
		biotite [e]	78.7 ± 0.2	79.5 ± 0.5
Tinemaha Granodiorite	Jtn06-01	hornblende [e]	115.5 ± 0.4	116.6 ± 0.7
		biotite [d]	83.8 ± 0.4	84.6 ± 0.6
Tinemaha Granodiorite	Jtn07-09	hornblende [e]	142.8 ± 0.6	144.1 ± 1.0
		biotite [d]	87.1 ± 0.4	87.9 ± 0.6
Tinemaha Granodiorite	Jtn07-11	hornblende [e]	153.0 ± 0.6	154.4 ± 1.0
		biotite [d]	89.8 ± 0.2	90.7 ± 0.5

Errors reported at 2-sigma

[a] Ar dates calculated using Fish Canyon standard age of 28.02 Ma (Renne et al., 1998) and $\lambda^{40}K_{total} = 5.543e^{-10}yr^{-1}$ (Steiger and Jäger, 1977). Errors incorporate analytical and J-value uncertainties

[b] Ar dates calculated using Fish Canyon standard age of 28.293 ± 0.046 Ma (Renne et al., 2009) and $\lambda^{40}K_{\varepsilon} = 5.7926 \pm 0.0066e^{-11}yr^{-1}$ (Renne et al., 2009) and $\lambda^{40}K_{\beta} = 4.9647 \pm 0.0109e^{-10}yr^{-1}$ (Renne et al., 2009). Errors incorporate analytical, J-value, ^{40}K decay constant, and Fish Canyon flux monitor age uncertainties

[c] Dates recalculated using EARTHTIME Ar tool: http://www.earth-time.org/ar-ar.html

[d] Dates from inverse isochron

[e] Dates from weighted average of all heating steps

[f] Dates from plateau

Table 4 Compilation of U-Pb, K-Ar, and (U-Th)/He data used to determine T-t histories for the John Muir and Mount Whitney Intrusive Suites and associated wall rocks

Pluton	Sample ID	Mineral	Age/Date (Ma) [a]
Inconsolable Qtz-monzodiorite	Dbk05-01	zircon	95.5 ± 0.3
		hornblende [b]	95.4 ± 0.7
		biotite [c]	87.4 ± 0.5
		(U-Th)/He zircon [d]	73.5 ± 5.3
Lamarck Granodiorite	Db05-04	zircon	94.1 ± 0.2
		hornblende [b]	94.0 ± 0.6
		biotite [b]	85.6 ± 0.5
		(U-Th)/He zircon [d]	72.3 ± 6.1
Lamarck Granodiorite	Db04-05	zircon	94.2 ± 0.2
		biotite [c]	84.0 ± 0.5
		(U-Th)/He zircon [d]	75.6 ± 6.3
McDoogle Qtz-monzodiorite	Ms07-F8	zircon	95.2 - 94.6
		titanite	95.3 ± 0.5
		biotite [b]	83.8 ± 0.5
Lake Edison Granodiorite	Kle07-05	zircon	88.8 ± 0.1
		hornblende [b]	89.0 ± 1.0
		biotite [b]	83.1 ± 0.4
Mono Creek Granite	Km07-06	zircon	87.2 – 83.4
		biotite [c]	82.1 ± 0.5
Mono Creek Granite	Km07-08	biotite [c]	82.1 ± 0.5
granodiorite of Sugarloaf	S-21	zircon	90.6 ± 0.1
		hornblende [b]	90.4 ± 1.9
		biotite [c]	87.7 ± 0.6
Paradise Granodiorite	Pp02-12	zircon	86.4 ± 0.1
		hornblende [b]	87.6 ± 1.0
		biotite [e]	86.0 ± 0.5
		(U-Th)/He zircon [d]	83.8 ± 6.7
Paradise Granodiorite	Pp03-09	hornblende [b]	85.2 ± 0.6
		biotite [b]	83.0 ± 0.5
Whitney Granodiorite	Wp03-07	zircon	84.8 ± 0.1
		hornblende [b]	84.4 ± 0.7
		biotite [c]	84.3 ± 0.5
		(U-Th)/He zircon [d]	74.6 ± 6.0
Bullfrog Granite	Kb06-02	zircon	100.2 ± 0.3
		hornblende [c]	90.6 ± 0.6
		biotite [b]	87.6 ± 0.8

Jurassic-Triassic mafics	Jtrm06-02	zircon	146.1 – 144.9
		hornblende [c]	90.1 ± 0.9
		biotite [b]	85.1 ± 0.6
quartz diorite of Pine Lake	Pcp07-07	zircon	180.7 ± 0.3
		hornblende [b]	86.2 ± 0.6
		biotite [c]	79.5 ± 0.5
Tinemaha Granodiorite	Jtn06-01	hornblende [c]	116.6 ± 0.7
		biotite [b]	84.6 ± 0.6
		(U-Th)/He zircon [d]	70.4 ± 5.6
Tinemaha Granodiorite	Jtn07-09	hornblende [c]	144.1 ± 1.0
		biotite [b]	87.9 ± 0.6
Tinemaha Granodiorite	Jtn07-11	hornblende [c]	154.4 ± 1.0
		biotite [b]	90.7 ± 0.5

Errors reported at 2-sigma

[a] Ar dates calculated using Fish Canyon standard age of 28.293 ± 0.046 Ma (Renne et al., 2009) and $\lambda^{40}K_{\varepsilon}$= 5.7926 ± 0.0066$e^{-11}yr^{-1}$ (Renne et al., 2009) and $\lambda^{40}K_{\beta}$ = 4.9647 ± 0.0109$e^{-10}yr^{-1}$ (Renne et al., 2009). Errors incorporate analytical, J-value, ^{40}K decay constant, and Fish Canyon flux monitor age uncertainties

[b] Dates from inverse isochron

[c] Dates from weighted average of all heating steps

[d] Date determined from the mean value of 3 zircon aliquots

[e] Dates from plateau

Appendix 1:

Zircon and titanite U/Pb geochronology from the John Muir Intrusive Suite, Mount Whitney Intrusive Suite, and associated wall rocks

											ages (Ma)				total
fraction (n)	weight (mg)	conc. (ppm) U	Pb*	206 Pb[a] / 204 Pb	206 Pb[b] / 238 U	error (%)	207 Pb[b] / 235 U	error (%)	207 Pb[b] / 206 Pb	error (%)	206 Pb / 238 U	207 Pb / 235 U	207 Pb / 206 Pb	corr. coeff.	Pbc (pg)
Kl07-02 Lamarck Granodiorite (0339408, 4123919)															
z1 (1)	0.006	1857.2	27.47	7015.1	0.01461	(.10)	0.09650	(.16)	0.04792	(.12)	93.47	93.54	95.25	0.65	1.6
z4 (1)	0.004	1536.9	23.64	4414.8	0.01459	(.13)	0.09621	(.21)	0.04783	(.16)	93.37	93.28	90.75	0.63	1.4
z5 (1)	0.005	1475.9	21.88	5699.8	0.01461	(.12)	0.09641	(.18)	0.04786	(.14)	93.51	93.46	92.07	0.67	1.2
z7 (1)	0.004	1104.7	16.54	3652.2	0.01461	(.09)	0.09647	(.17)	0.04788	(.14)	93.53	93.51	93.15	0.58	1.2
z6 (1)	0.001	2706.8	39.80	1563.2	0.01459	(.16)	0.09619	(.39)	0.04781	(.34)	93.38	93.25	89.92	0.49	2.3
z3 (1)	0.005	1698.1	25.71	1050.1	0.01462	(.64)	0.09625	(.72)	0.04776	(.31)	93.53	93.31	87.56	0.90	7.2
Kle07-05 Lake Edison Granodiorite (0342320, 4126001)															
z3 (1)	0.006	1138.1	15.94	7352.0	0.01385	(.18)	0.09117	(.22)	0.04776	(.12)	88.64	88.59	87.29	0.84	0.8
z2 (1)	0.006	1044.9	14.78	3887.5	0.01388	(.13)	0.09141	(.18)	0.04776	(.11)	88.86	88.81	87.45	0.76	1.4
z1 (1)	0.006	848.3	11.87	8406.2	0.01388	(.12)	0.09153	(.15)	0.04782	(.08)	88.88	88.93	90.35	0.82	0.5
z4 (1)	0.006	675.0	9.44	2558.8	0.01388	(.18)	0.09139	(.24)	0.04777	(.15)	88.83	88.80	87.91	0.79	1.4
z5 (1)	0.003	2133.5	29.90	5173.1	0.01385	(.12)	0.09129	(.16)	0.04780	(.10)	88.69	88.71	89.30	0.78	0.9
z6 (1)	0.003	3706.1	52.40	4998.1	0.01385	(.09)	0.09132	(.15)	0.04783	(.12)	88.65	88.73	90.95	0.60	1.8
z8 (1)	0.005	1097.3	15.36	3582.6	0.01387	(.11)	0.09134	(.18)	0.04775	(.14)	88.82	88.75	87.07	0.64	1.4
Mc-1 Mono Creek Granite (0343306, 4142846)															
z4 (2)	0.009	490.2	6.73	4976.7	0.01365	(.11)	0.08983	(.17)	0.04774	(.13)	87.38	87.35	86.36	0.67	0.7
z12 (2)	0.009	744.3	10.28	5749.1	0.01366	(.11)	0.09004	(.14)	0.04779	(.09)	87.49	87.54	88.80	0.76	1.0
z11 (2)	0.011	558.0	7.85	1385.4	0.01366	(.57)	0.08996	(.62)	0.04777	(.23)	87.45	87.46	87.67	0.93	3.8
z2 (2)	0.009	644.6	8.93	1352.2	0.01364	(.60)	0.08976	(.68)	0.04773	(.30)	87.33	87.28	85.91	0.90	3.6
z13 (3)	0.008	1634.7	22.62	10919.8	0.01364	(.12)	0.08992	(.15)	0.04783	(.08)	87.31	87.43	90.75	0.85	1.0
z6 (2)	0.005	418.9	5.85	2682.1	0.01359	(.13)	0.08931	(.29)	0.04767	(.24)	86.99	86.86	83.12	0.53	0.7
z16 (2)	0.011	1047.4	14.51	6897.6	0.01362	(.09)	0.08983	(.13)	0.04784	(.10)	87.19	87.34	91.42	0.671	1.5
z15 (2)	0.005	622.4	8.46	1790.3	0.01359	(.14)	0.08941	(.26)	0.04773	(.21)	86.99	86.96	85.91	0.557	1.5
z5 (2)	0.010	1038.1	14.24	2335.6	0.01358	(.33)	0.08935	(.36)	0.04772	(.14)	86.96	86.90	85.29	0.92	3.8

Ms07-F8 McDoogle Quartz Monzodiorite															
z2 (1)	0.018	447.8	7.17	2605.5	0.01487	(.12)	0.09817	(.18)	0.04789	(.13)	95.14	95.09	93.91	0.69	3.0
z3 (1)	0.020	574.6	9.04	4474.6	0.01485	(.14)	0.09829	(.20)	0.04799	(.14)	95.04	95.19	99.04	0.70	2.5
z8 (2)	0.007	425.8	6.68	4449.0	0.01487	(.09)	0.09833	(.17)	0.04795	(.14)	95.16	95.23	97.02	0.54	0.7
z7 (2)	0.008	445.9	7.20	2120.1	0.01482	(.13)	0.09777	(.27)	0.04784	(.23)	94.84	94.71	91.50	0.52	1.7
z5 (2)	0.004	844.2	13.54	3332.0	0.01484	(.10)	0.09782	(.17)	0.04780	(.14)	94.98	94.77	89.32	0.60	1.0
z1 (1)	0.005	606.4	9.52	2274.7	0.01482	(.11)	0.09776	(.20)	0.04785	(.16)	94.82	94.71	92.05	0.58	1.3
z9 (1)	0.014	292.9	4.73	4103.0	0.01484	(.19)	0.09816	(.25)	0.04798	(.16)	94.95	95.07	98.29	0.768	1.0
Pcp07-07 quartz diorite of Pine Lake (0346512, 4135126)															
z3 (1)	0.013	197.0	6.07	5872.6	0.02842	(.18)	0.19462	(.40)	0.04967	(.34)	180.64	180.57	179.60	0.51	1.6
z2 (1)	0.014	434.9	13.76	8279.4	0.02841	(.20)	0.19509	(.23)	0.04980	(.10)	180.61	180.96	185.59	0.89	1.5
z1 (1)	0.013	271.9	7.24	3502.9	0.02416	(.15)	0.16489	(.26)	0.04951	(.21)	153.86	154.98	172.08	0.58	0.8
z5 (1)	0.009	93.7	2.02	2096.4	0.02063	(.13)	0.13931	(.22)	0.04898	(.17)	131.64	132.43	146.65	0.63	0.6
z6 (1)	0.011	308.9	8.24	5682.2	0.02421	(.08)	0.16482	(.16)	0.04937	(.14)	154.23	154.91	165.32	0.52	0.9
Km07-06 Mono Creek Granite (0345911, 4134385)															
z25 (2)	0.001	273.0	3.54	1109.1	0.01302	(.23)	0.08547	(.70)	0.04761	(.62)	83.39	83.28	80.05	0.46	2.0
z26 (2)	0.012	758.7	9.90	5094.7	0.01325	(.12)	0.08732	(.18)	0.04780	(.14)	84.84	85.00	89.65	0.64	1.5
z28 (2)	0.003	240.8	3.36	504.9	0.01362	(.42)	0.08946	(1.20)	0.04765	(1.07)	87.18	87.00	81.97	0.46	1.2
z27 (3)	0.010	124.0	1.68	1038.5	0.01309	(.25)	0.08642	(.42)	0.04789	(.32)	83.82	84.17	94.00	0.63	1.0
S-21 granodiorite of Sugarloaf															
z5 (1)	0.005	1163.7	16.64	4855.9	0.01414	(.13)	0.09312	(.20)	0.04777	(.15)	90.50	90.41	88.14	0.66	1.1
z4 (1)	0.001	3702.8	54.47	1051.8	0.01417	(.25)	0.09349	(.23)	0.04785	(.17)	90.71	90.75	91.98	0.92	3.2
z6 (1)	0.008	795.4	11.47	3886.8	0.01416	(.14)	0.09320	(.20)	0.04775	(.14)	90.62	90.48	86.97	0.69	1.4
z8 (1)	0.005	1065.3	15.26	5173.1	0.01415	(.18)	0.09332	(.23)	0.04782	(.15)	90.61	90.59	90.15	0.76	0.9
Pp02-12 Paradise Granodiorite (0377401, 4061611)															
z2 (1)	0.006	632.6	10.28	6084.3	0.015105	(.36)	0.100191	(.40)	0.048106	(.17)	96.65	96.95	104.48	0.90	0.6
z3 (1)	0.006	621.9	8.97	4173.8	0.013489	(.11)	0.088779	(.26)	0.047733	(.22)	86.38	86.37	86.07	0.51	0.8
z4 (1)	0.006	830.9	11.93	5031.9	0.013493	(.13)	0.088870	(.21)	0.047771	(.16)	86.40	86.45	87.95	0.65	0.9
z5 (1)	0.006	409.9	5.80	1322.2	0.013510	(.22)	0.088882	(.35)	0.047716	(.26)	86.51	86.46	85.22	0.66	1.7
z6 (1)	0.005	680.3	9.88	894.6	0.013529	(.26)	0.089094	(.42)	0.047763	(.31)	86.63	86.66	87.50	0.67	3.4

Wp03-07 Whitney Granodiorite (0376397, 4059761)															
z8 (2)	0.004	604.9	8.50	2508.84	0.013234	(.11)	0.086852	(.37)	0.047598	(.34)	84.75	84.57	79.34	0.40	0.9
z7 (2)	0.008	425.5	5.87	5096.30	0.013254	(.13)	0.087313	(.32)	0.047779	(.28)	84.88	85.00	88.37	0.46	0.5
z6 (2)	0.010	539.5	7.52	7672.79	0.013261	(.11)	0.087172	(.18)	0.047675	(.14)	84.93	84.87	83.22	0.63	0.6
z5 (2)	0.011	678.6	9.29	6354.04	0.013235	(.08)	0.086972	(.12)	0.047660	(.09)	84.76	84.68	82.44	0.65	1.0
z4 (3)	0.004	1772.0	26.99	577.30	0.013289	(.45)	0.087403	(.54)	0.047700	(.28)	85.11	85.08	84.38	0.85	11.3
Jtrm06-02 Jurassic-Triassic Mafics (0377690, 4064286)															
z2 (1)	0.027	134.1	3.27	4617.8	0.022725	(.20)	0.153422	(.24)	0.048965	(.13)	144.85	144.93	146.22	0.83	1.1
z3 (1)	0.027	75.2	1.81	1218.5	0.022731	(.23)	0.153637	(.43)	0.049019	(.35)	144.90	145.12	148.74	0.59	2.4
z1 (1)	0.035	180.4	4.46	7047.9	0.022889	(.21)	0.154493	(.22)	0.048952	(.08)	145.89	145.87	145.52	0.93	1.3
z5 (1)	0.034	188.4	4.80	7358.5	0.022911	(.09)	0.154481	(.12)	0.048902	(.07)	146.03	145.86	143.14	0.81	1.3
z7 (1)	0.025	76.4	2.04	2569.4	0.022895	(.15)	0.154487	(.19)	0.048938	(.11)	145.93	145.87	144.84	0.81	1.1
Kb06-02 Bullfrog Granite (0374987, 4068632)															
z4 (1)	0.003	446.6	7.49	734.8	0.015663	(.30)	0.103757	(.95)	0.048046	(.86)	100.18	100.24	101.50	0.44	1.9
Titanite [c] Ms07-F8 McDoogle Quartz Monzodiorite															
t1 (1)	0.055	160.9	6.16	146.3	0.01471	(.32)	0.09729	(.69)	0.04798	(.58)	94.12	94.27	98.27	0.54	65.4
t5 (1)	0.027	1217.0	29.20	278.2	0.01480	(.12)	0.09802	(.53)	0.04803	(.49)	94.72	94.95	100.84	0.43	121.1
t6 (1)	0.115	14.0	0.41	173.0	0.01477	(1.73)	0.09813	(1.78)	0.04820	(.42)	94.49	95.05	109.15	0.97	9.9
Titanite [d] Db04-05 Lamarck Granodiorite (0361988, 4106523)															
t2 (1)	0.200	89.4	3.40	125.1	0.01463	(.19)	0.09678	(.73)	0.04799	(.68)	93.61	93.80	98.59	0.40	157.8
t6 (1)	0.055	204.9	5.70	220.2	0.01461	(.28)	0.09661	(.50)	0.04796	(.39)	93.50	93.64	97.29	0.61	52.4
t5 (1)	0.128	35.3	1.32	169.9	0.01468	(.61)	0.09704	(.73)	0.04794	(.40)	93.95	94.04	96.47	0.84	28.2

Analysis accomplished with a VG Sector 54 thermal ionization mass spectrometer at the University of North Carolina-Chapel Hill. Decay constants used are $^{238}U = 0.155125 \times 10^{-9} \pm 0.16598 \times 10^{-14}$ a^{-1}, and $^{235}U = 0.98485 \times 10^{-9} \pm 0.13394 \times 10^{-13}$ a^{-1} (Steiger and Jäger, 1977). Weights are estimated using a video camera and scale, and are known to within 10%. Data reduction and error analysis was accomplished using PbMacDat-2 by D.S. Coleman and Isoplot 3.00 (Ludwig, 2003) using the algorithms of Ludwig (1989). All errors are reported in percent at the 2σ confidence interval. All locations reported as UTM zone 11N coordinates using NAD 83.

[*] Radiogenic Pb

[a] Measured ratio corrected for fractionation only. All U/Pb isotope ratios were measured using the Daly detector, and are corrected for mass fractionation using 0.15%/a.m.u.

[b] Corrected for fractionation, spike, blank, and initial common Pb. After subtraction of blank Pb (<3.0 pg), common Pb corrections were unnecessary for most fractions. For fractions with total common Pb in excess of 3.0 pg, corrections were made using Stacey and Kramers (1975) initial Pb.

[c] Initial Pb values determined from K-feldspar separates: $^{206}Pb/^{204}Pb = 18.7551$; $^{207}Pb/^{204}Pb = 15.6540$; $^{208}Pb/^{204}Pb = 38.7860$

[d] Initial Pb values determined from K-feldspar separates: $^{206}Pb/^{204}Pb = 18.8128$; $^{207}Pb/^{204}Pb = 15.6419$; $^{208}Pb/^{204}Pb = 38.6906$

Appendix 2:

$^{40}Ar/^{39}Ar$ analytical data

ID	Temp (°C)	$^{40}Ar/^{39}Ar$	$^{37}Ar/^{39}Ar$	$^{36}Ar/^{39}Ar$ (x 10^{-3})	$^{39}Ar_K$ (x 10^{-15} mol)	K/Ca	$^{40}Ar^*$ (%)	^{39}Ar (%)	Age (Ma)	±1s (Ma)
Dbk05-01 am1, Amphibole, 3.59 mg, J=0.0036114±0.09%, D=1.002±0.001, NM-194C, Lab#=56123-02										
A	800	57.06	1.093	100.611	0.212	0.467	48.1	0.9	170.5	8.4
B	900	19.16	1.840	9.871	0.166	0.277	85.6	1.6	103.9	10.2
C	1000	17.36	6.440	8.573	2.678	0.079	88.6	13.1	97.9	0.7
D	1030	15.53	6.199	3.637	14.824	0.082	96.5	76.8	95.4	0.2
E	1050	15.55	5.660	10.705	0.382	0.090	82.8	78.4	82.2	4.6
F	1070	15.62	5.779	12.168	0.360	0.088	80.2	80.0	80.0	4.6
G	1090	17.83	6.203	11.320	0.497	0.082	84.2	82.1	95.6	3.0
H	1120	15.74	6.742	5.605	1.057	0.076	93.2	86.7	93.5	1.5
I	1300	16.01	6.589	5.049	2.734	0.077	94.2	98.4	96.1	0.7
J	1700	36.94	8.421	73.846	0.375	0.061	42.8	100.0	100.8	4.7
Integrated			n=10				K2O=0.69%		95.9	0.3
Plateau		steps D, G-J	n=5	MSWD=0.81					95.5	0.2
Isochron		steps D, G-J	n=5	MSWD=0.79		$^{40}Ar/^{36}Ar$=	300±20		94.5	0.3
Db05-04 am1, Amphibole, 1120 mg, J=0.0007864±0.06%, D=1.004±0.001, NM-215C, Lab#=57615-01										
A	800	108.13	0.354	132.278	0.711	1.442	63.9	4.5	95.5	1.1
B	900	73.70	0.638	44.088	0.520	0.800	82.4	7.7	84.2	1.3
C	1000	80.49	4.507	59.646	0.930	0.113	78.6	13.5	87.8	0.9
D	1020	84.12	9.968	55.521	1.229	0.051	81.5	21.2	95.3	0.7
E	1040	73.68	9.344	26.083	3.569	0.055	90.6	43.6	92.9	0.3
F	1060	69.41	8.550	9.912	3.122	0.060	96.8	63.2	93.4	0.4
G	1120	69.09	8.779	11.810	1.426	0.058	96.0	72.1	92.3	0.6
H	1180	69.87	10.621	13.221	1.599	0.048	95.7	82.1	93.1	0.5
I	1250	74.45	9.943	25.894	2.369	0.051	90.8	97.0	94.1	0.4
J	1650	254.77	11.583	625.414	0.480	0.044	27.8	100.0	98.7	2.9
Integrated			n=10				K2O=0.01%		93.0	0.3
Plateau		steps E-J	n=6	MSWD=2.30					93.2	0.3
Isochron		steps E-J	n=6	MSWD=2.00		$^{40}Ar/^{36}Ar$=	302±7		93.1	0.2

ID	Temp (°C)	$^{40}Ar/^{39}Ar$	$^{37}Ar/^{39}Ar$	$^{36}Ar/^{39}Ar$ (x 10^{-3})	$^{39}Ar_K$ (x 10^{-15} mol)	K/Ca	$^{40}Ar^*$ (%)	^{39}Ar (%)	Age (Ma)	±1s (Ma)
Kle07-05 am1, Amphibole, 5.4 mg, J=0.00225±0.06%, D=1.002±0.001, NM-212A, Lab#=57409-01										
A	800	30.38	0.415	36.091	4.743	1.229	65.0	10.9	78.5	1.1
B	900	25.84	0.277	20.929	2.250	1.844	76.1	16.0	78.1	2.0
C	1000	23.02	1.370	9.694	2.723	0.372	88.0	22.2	80.5	1.0
D	1050	26.50	4.457	21.242	2.360	0.114	77.7	27.6	81.9	1.0
E	1080	23.81	7.231	7.768	18.255	0.071	92.9	69.4	88.0	0.3
F	1100	22.80	5.168	5.153	2.875	0.099	95.2	76.0	86.3	0.7
G	1120	23.14	6.464	5.546	2.070	0.079	95.2	80.8	87.7	1.1
H	1140	24.21	7.310	8.821	1.429	0.070	91.9	84.0	88.5	1.5
I	1160	23.17	7.626	12.572	0.935	0.067	86.7	86.2	80.2	2.2
J	1220	23.54	8.725	7.888	2.022	0.058	93.2	90.8	87.4	1.0
K	1650	26.65	7.772	19.129	4.018	0.066	81.2	100.0	86.2	0.8
Integrated			n=11				K2O=1.38%		85.2	0.3
Plateau	steps E-H, J-K		n=6	MSWD=1.70					87.6	0.3
Isochron	steps E-H, J-K		n=6	MSWD=2.00		$^{40}Ar/^{36}Ar$=	280±30		88.2	0.5
Db04-05 bt1, Biotite, 6.93 mg, J=0.0007983±0.07%, D=1.004±0.001, NM-208A, Lab#=57125-01										
A	650	128.63	0.127	312.206	0.445	4.012	28.3	1.0	51.7	1.2
B	750	64.83	0.012	26.073	4.345	43.368	88.1	10.9	80.5	0.2
C	850	61.04	0.007	4.790	9.064	76.049	97.7	31.5	83.9	0.1
D	920	61.69	0.008	6.239	4.796	60.391	97.0	42.4	84.2	0.2
E	1000	63.40	0.014	15.264	4.455	37.734	92.9	52.5	82.9	0.2
F	1075	62.46	0.009	10.462	6.319	54.170	95.1	66.8	83.5	0.2
G	1110	61.17	0.014	6.058	4.673	36.673	97.1	77.5	83.6	0.2
H	1180	61.66	0.030	6.137	5.490	17.046	97.1	89.9	84.2	0.2
I	1210	61.30	0.097	3.817	3.306	5.250	98.2	97.4	84.7	0.2
J	1250	61.88	0.538	5.291	0.907	0.948	97.5	99.5	84.9	0.3
K	1300	68.82	1.290	29.327	0.120	0.396	87.6	99.8	84.8	1.5
L	1700	86.02	1.214	85.353	0.098	0.420	70.8	100.0	85.7	2.0
Integrated			n=12				K2O=3.06%		83.2	0.1

ID	Temp (°C)	$^{40}Ar/^{39}Ar$	$^{37}Ar/^{39}Ar$	$^{36}Ar/^{39}Ar$ (x 10^{-3})	$^{39}Ar_K$ (x 10^{-15} mol)	K/Ca	$^{40}Ar^*$ (%)	^{39}Ar (%)	Age (Ma)	±1s (Ma)
Kle07-05 bt1, Biotite, 7.3 mg, J=0.0022504±0.06%, D=1.003±0.0011, NM-212A, Lab#=57408-01										
A	625	42.45	0.136	99.240	6.470	3.754	30.9	0.7	52.5	1.0
B	700	24.73	0.017	19.049	17.646	29.872	77.2	2.6	75.9	0.4
C	750	21.62	0.007	4.588	47.743	68.215	93.7	7.8	80.4	0.2
D	800	21.01	0.005	1.498	83.901	106.361	97.9	16.9	81.6	0.1
E	875	20.95	0.004	0.970	107.860	132.410	98.6	28.6	82.0	0.1
F	975	21.17	0.006	1.305	130.256	82.004	98.2	42.7	82.4	0.1
G	1075	21.08	0.012	1.211	168.239	43.798	98.3	61.0	82.2	0.1
H	1250	20.93	0.050	0.600	324.198	10.174	99.2	96.1	82.3	0.1
I	1700	21.20	0.672	2.382	35.694	0.759	96.9	100.0	81.6	0.2
Integrated			n=9				K2O=21.56%		81.7	0.1
Plateau		steps F-H	n=3	MSWD=1.37					82.3	0.1
Isochron		steps F-H	n=3	MSWD=2.44		$^{40}Ar/^{36}Ar$=	304±54		82.3	0.2
Km07-06 bt1, Biotite, 6.9 mg, J=0.0022529±0.07%, D=1.003±0.0011, NM-212A, Lab#=57411-01										
A	625	53.07	0.266	144.116	3.452	1.919	19.8	0.5	42.2	1.7
B	700	27.61	0.029	28.600	14.142	17.582	69.4	2.5	76.2	0.4
C	750	21.78	0.009	5.197	40.705	58.699	93.0	8.1	80.4	0.2
D	800	20.88	0.004	1.413	75.586	117.006	98.0	18.7	81.3	0.1
E	875	20.74	0.004	0.876	109.824	118.854	98.8	34.0	81.3	0.1
F	975	20.83	0.008	0.905	124.189	63.196	98.7	51.3	81.7	0.1
G	1075	21.00	0.019	1.043	123.022	26.216	98.5	68.4	82.2	0.1
H	1250	20.73	0.091	0.548	192.174	5.582	99.3	95.2	81.7	0.1
I	1700	20.78	0.441	1.334	34.717	1.157	98.3	100.0	81.1	0.1
Integrated			n=9				K2O=17.74%		81.3	0.1
Km07-08 bt1, Biotite, 8.8 mg, J=0.0007963±0.10%, D=1.0032±0.0012, NM-215A, Lab#=57602-01										
A	625	69.09	0.062	87.318	4.052	8.241	62.7	2.5	61.1	0.4
B	700	58.68	0.007	3.478	22.330	78.358	98.2	16.6	81.0	0.1
C	750	58.27	0.004	0.537	20.107	127.024	99.7	29.2	81.6	0.1
D	800	58.70	0.004	1.271	18.387	128.476	99.4	40.8	81.9	0.1
E	875	59.30	0.008	2.284	19.268	66.091	98.9	52.9	82.3	0.1
F	975	59.44	0.015	1.874	30.046	35.169	99.1	71.8	82.7	0.2
G	1075	58.87	0.027	2.271	28.529	18.631	98.9	89.7	81.7	0.2
H	1250	64.02	0.253	20.048	16.386	2.015	90.8	100.0	81.6	0.2
Integrated			n=8				K2O=8.72%		81.3	0.1

ID	Temp (°C)	$^{40}Ar/^{39}Ar$	$^{37}Ar/^{39}Ar$	$^{36}Ar/^{39}Ar$ (x 10^{-3})	$^{39}Ar_K$ (x 10^{-15} mol)	K/Ca	$^{40}Ar^*$ (%)	^{39}Ar (%)	Age (Ma)	±1s (Ma)
Db05-04 bt1, Biotite, 7.1 mg, J=0.0007992±0.08%, D=1.0032±0.0012, NM-215A, Lab#=57604-01										
A	625	85.09	0.043	116.660	1.552	11.930	59.5	0.8	71.5	1.0
B	700	61.73	0.004	9.883	25.131	116.291	95.3	14.4	82.9	0.2
C	750	60.31	0.003	0.690	26.267	189.907	99.7	28.5	84.6	0.1
D	800	60.64	0.003	1.454	11.572	163.753	99.3	34.8	84.8	0.2
E	875	61.09	0.004	2.260	19.358	139.480	98.9	45.2	85.1	0.1
F	975	60.92	0.005	2.474	33.731	94.517	98.8	63.4	84.8	0.2
G	1075	60.76	0.012	2.085	43.719	44.190	99.0	86.9	84.7	0.2
H	1250	63.94	0.257	12.217	24.278	1.983	94.4	100.0	85.0	0.2
Integrated			n=8				K2O=12.56%		84.4	0.1
Plateau		steps C-H	n=6	MSWD=1.40					84.8	0.1
Isochron		steps C-H	n=6	MSWD=1.30		$^{40}Ar/^{36}Ar$=	312±12		84.8	0.1
Ms07-F8 bt1, Biotite, 6.6 mg, J=0.0008012±0.10%, D=1.0032±0.0012, NM-215A, Lab#=57605-01										
A	625	174.22	0.040	461.920	2.524	12.871	21.7	1.5	53.7	1.4
B	625	60.67	0.009	26.846	1.587	56.676	86.9	2.4	74.7	0.7
C	700	59.74	0.004	10.552	12.327	118.674	94.8	9.7	80.0	0.2
D	750	58.98	0.003	1.818	16.330	163.611	99.1	19.3	82.6	0.2
E	800	60.00	0.002	3.820	15.645	205.810	98.1	28.6	83.2	0.2
F	875	60.03	0.005	4.426	24.628	108.051	97.8	43.1	83.0	0.1
G	975	59.64	0.005	2.800	42.786	93.920	98.6	68.3	83.1	0.1
H	1025	59.30	0.010	2.190	15.448	53.617	98.9	77.4	82.9	0.2
I	1075	59.48	0.020	2.037	15.670	25.196	99.0	86.7	83.2	0.2
J	1150	59.56	0.163	2.838	16.689	3.128	98.6	96.5	83.0	0.2
K	1200	63.19	0.472	14.085	4.666	1.081	93.5	99.3	83.4	0.3
L	1300	129.75	0.126	241.418	1.224	4.047	45.0	100.0	82.5	1.2
Integrated			n=12				K2O=12.31%		82.3	0.2
Plateau		steps E-L	n=8	MSWD=0.75					83.0	0.1
Isochron		steps E-L	n=8	MSWD=1.90		$^{40}Ar/^{36}Ar$=	296±4		83.0	0.1

ID	Temp (°C)	$^{40}Ar/^{39}Ar$	$^{37}Ar/^{39}Ar$	$^{36}Ar/^{39}Ar$ (x 10^{-3})	$^{39}Ar_K$ (x 10^{-15} mol)	K/Ca	$^{40}Ar^*$ (%)	^{39}Ar (%)	Age (Ma)	±1s (Ma)
Dbk05-01, Biotite, 3.16 mg, J=0.0036195±0.09%, D=1.002±0.001, NM-194C, Lab#=56124-01										
A	650	22.90	0.0612	55.54	2.26	8.3	28.3	0.7	41.8	1.5
B	750	14.62	0.0071	4.574	31.8	72.1	90.8	10.8	84.6	0.2
D	920	14.19	0.0066	1.538	95.1	77.4	96.8	41.0	87.5	0.1
E	1000	14.42	0.0157	2.479	58.5	32.6	94.9	59.6	87.2	0.2
F	1075	13.98	0.0270	1.338	66.9	18.9	97.2	80.8	86.6	0.2
G	1110	14.00	0.0141	1.116	31.2	36.2	97.7	90.7	87.1	0.2
H	1180	13.99	0.0727	0.6939	28.2	7.0	98.6	99.7	87.8	0.2
I	1210	14.60	0.2206	8.249	1.05	2.3	83.4	100.0	77.8	1.5
Integrated			n=8				K2O=10.58%		86.6	0.1
Wp03-07 bt1, Biotite, 4.47 mg, J=0.0036036±0.05%, D=1.002±0.001, NM-194C, Lab#=56121-01										
A	650	40.44	0.3859	120.0	1.72	1.3	12.4	0.3	32.2	1.7
B	750	16.08	0.0174	11.58	25.7	29.4	78.7	5.4	80.4	0.2
C	850	13.68	0.0073	1.751	49.7	70.1	96.2	16.7	83.6	0.1
D	920	13.63	0.0111	0.9596	32.4	46.0	97.9	25.5	84.7	0.2
E	1000	14.01	0.0178	1.732	44.5	28.6	96.4	40.1	85.6	0.1
F	1075	13.50	0.0244	0.9109	51.5	20.9	98.0	61.7	84.0	0.1
G	1110	13.48	0.0306	1.128	26.5	16.7	97.5	75.7	83.5	0.2
H	1180	13.35	0.2496	0.7661	32.9	2.0	98.5	96.9	83.4	0.2
I	1210	13.36	0.3383	0.7672	4.30	1.5	98.5	100.0	83.5	0.4
Integrated			n=9				K2O=6.42%		83.5	0.1
S-21 bt1, Biotite, 5.67 mg, J=0.0036311±0.12%, D=1.002±0.001, NM-194C, Lab#=56126-01										
A	650	41.33	0.0270	107.5	7.38	18.9	23.1	1.3	61.5	1.1
B	750	15.81	0.0060	8.199	67.1	85.2	84.7	13.2	85.6	0.2
C	850	14.01	0.0059	0.7366	128.2	86.7	98.5	35.9	88.1	0.1
D	920	14.06	0.0097	0.9469	67.4	52.4	98.0	47.8	88.0	0.1
E	1000	14.09	0.0221	1.668	74.8	23.1	96.5	61.0	86.9	0.1
F	1075	13.91	0.0524	1.298	85.7	9.7	97.3	76.2	86.5	0.1
G	1110	14.01	0.0248	1.385	43.7	20.5	97.1	83.9	86.9	0.2
H	1180	13.94	0.0614	0.5547	71.3	8.3	98.9	96.6	88.0	0.1
I	1210	13.96	0.2241	1.612	19.5	2.3	96.7	100.0	86.3	0.2
Integrated			n=9				K2O=10.54%		86.9	0.2

ID	Temp (°C)	$^{40}Ar/^{39}Ar$	$^{37}Ar/^{39}Ar$	$^{36}Ar/^{39}Ar$ (x 10^{-3})	$^{39}Ar_K$ (x 10^{-15} mol)	K/Ca	$^{40}Ar^*$ (%)	^{39}Ar (%)	Age (Ma)	±1s (Ma)
Pp02-12 bt1, Biotite, 4.66 mg, J=0.0036152±0.07%, D=1.002±0.001, NM-194C, Lab#=56129-01										
A	0	-47.3748	8.220	-453.7827	0.004	0.062	-184.5	0.0	497.8	316.2
B	750	14.32	0.0105	5.262	33.9	48.5	89.1	8.5	81.3	0.2
C	850	13.53	0.0050	0.5542	79.1	102.6	98.8	28.5	85.1	0.1
D	920	13.50	0.0099	0.4602	64.4	51.7	99.0	44.7	85.1	0.2
E	1000	13.61	0.0094	0.6449	80.7	54.4	98.6	65.0	85.4	0.1
F	1075	13.46	0.0138	0.5302	83.8	36.9	98.8	86.1	84.7	0.1
G	1110	13.48	0.0301	0.8424	29.8	17.0	98.2	93.6	84.3	0.2
H	1180	13.44	0.2689	0.4184	22.0	1.9	99.2	99.1	84.9	0.3
I	1210	13.71	0.5695	2.973	3.50	0.90	93.9	100.0	82.1	0.7
Integrated			n=9				K2O=9.05%		84.6	0.1
Plateau		steps C-E	n=3	MSWD=2.22					85.2	0.1
S-21 am1, Amphibole, 11.77 mg, J=0.0036269±0.11%, D=1.002±0.001, NM-194C, Lab#=56125-01										
A	750	28.52	0.3571	49.32	1.81	1.4	49.0	2.1	89.2	1.7
B	850	14.54	0.1647	3.488	4.42	3.1	93.0	7.1	86.3	0.6
C	920	14.51	0.5154	3.856	2.67	0.99	92.4	10.2	85.7	0.8
D	970	14.81	1.182	5.003	2.26	0.43	90.7	12.8	85.8	0.9
E	1000	15.84	3.611	8.554	2.38	0.14	85.9	15.5	87.1	1.0
F	1030	16.86	7.016	9.945	11.1	0.073	86.1	28.2	92.9	0.3
G	1060	14.98	5.656	4.246	42.3	0.090	94.8	76.5	90.9	0.2
H	1090	14.72	4.729	3.361	7.25	0.11	96.0	84.8	90.4	0.3
I	1120	14.72	3.932	4.308	2.62	0.13	93.6	87.8	88.2	0.8
J	1150	14.89	6.850	4.871	3.29	0.074	94.2	91.6	89.9	0.7
K	1300	15.56	7.621	6.420	6.15	0.067	91.9	98.6	91.6	0.5
L	1700	23.17	9.279	36.01	1.21	0.055	57.4	100.0	85.5	1.9
Integrated			n=12				K2O=0.79%		90.2	0.2
Plateau		steps G-H,J-K	n=4	MSWD=1.81					90.8	0.2
Isochron		steps G-H,J-K	n=4	MSWD=1.10		$^{40}Ar/^{36}Ar$=	380±100		89.5	0.9

ID	Temp (°C)	$^{40}Ar/^{39}Ar$	$^{37}Ar/^{39}Ar$	$^{36}Ar/^{39}Ar$ (x 10^{-3})	$^{39}Ar_K$ (x 10^{-15} mol)	K/Ca	$^{40}Ar^*$ (%)	^{39}Ar (%)	Age (Ma)	±1s (Ma)
Pp02-12 am1, Amphibole, 8 mg, J=0.0036233±0.10%, D=1.002±0.001, NM-194C, Lab#=56128-01										
A	800	69.08	1.270	176.8	0.775	0.40	24.5	2.4	107.6	3.4
B	900	22.11	1.105	31.44	0.892	0.46	58.4	5.1	82.5	2.3
C	970	20.33	4.602	25.06	0.956	0.11	65.4	8.0	85.1	1.9
D	1000	21.86	12.14	31.38	2.03	0.042	62.1	14.2	87.3	1.3
E	1030	18.01	11.32	17.59	5.21	0.045	76.3	30.0	88.3	0.6
F	1050	14.88	9.208	7.036	8.75	0.055	91.1	56.7	87.0	0.4
G	1070	14.63	8.064	6.267	5.53	0.063	91.9	73.5	86.2	0.4
H	1090	17.95	10.94	20.48	1.15	0.047	71.3	77.0	82.3	1.7
I	1300	16.87	11.16	14.39	5.50	0.046	80.2	93.8	87.0	0.5
J	1700	20.84	11.07	27.86	2.05	0.046	64.9	100.0	86.8	1.3
Integrated			n=10				K2O=0.44%		87.2	0.3
Plateau		steps F-G,I-J	n=4	MSWD=0.73					86.8	0.3
Isochron		steps F-G,I-J	n=4	MSWD=1.10		$^{40}Ar/^{36}Ar$=	295±17		86.8	0.5
Kb06-02 bt1, Biotite, 5.61 mg, J=0.0007971±0.07%, D=1.004±0.001, NM-208A, Lab#=57124-01										
A	650	428.2	0.3816	1396.3	0.899	1.3	3.6	2.8	22.3	2.6
B	750	100.3	0.0258	176.4	2.76	19.8	48.0	11.3	67.9	0.4
C	850	65.23	0.0161	18.81	5.92	31.8	91.5	29.6	83.8	0.2
D	920	65.49	0.0179	11.72	5.02	28.6	94.7	45.1	87.1	0.2
E	1000	67.63	0.0309	19.73	5.44	16.5	91.4	61.9	86.7	0.2
F	1075	64.04	0.0392	7.567	5.25	13.0	96.5	78.1	86.8	0.1
G	1110	62.52	0.0497	4.738	2.62	10.3	97.8	86.2	85.8	0.2
H	1180	62.18	0.1773	5.489	2.56	2.9	97.4	94.1	85.1	0.2
I	1210	62.35	0.4533	4.543	1.42	1.1	97.9	98.5	85.7	0.3
J	1250	63.62	2.463	7.011	0.394	0.21	97.1	99.7	86.8	0.6
K	1300	66.72	3.307	13.61	0.091	0.15	94.4	100.0	88.5	2.0
Integrated			n=11				K2O=2.78%		82.7	0.2
Plateau		steps D-F	n=3	MSWD=1.09					86.8	0.1
Isochron		steps D-F	n=3	MSWD=2.10		$^{40}Ar/^{36}Ar$=	300±30		86.8	0.3

ID	Temp (°C)	$^{40}Ar/^{39}Ar$	$^{37}Ar/^{39}Ar$	$^{36}Ar/^{39}Ar$ (x 10^{-3})	$^{39}Ar_K$ (x 10^{-15} mol)	K/Ca	$^{40}Ar^*$ (%)	^{39}Ar (%)	Age (Ma)	±1s (Ma)
Jtn06-01 bt1, Biotite, 4.39 mg, J=0.0008008±0.10%, D=1.004±0.001, NM-208B, Lab#=57126-01										
A	650	121.1	0.0581	269.2	0.344	8.8	34.3	1.0	59.0	1.2
B	750	64.04	0.0091	21.15	2.95	56.4	90.2	9.8	81.6	0.2
C	850	61.16	0.0048	6.923	5.79	105.8	96.7	26.9	83.5	0.1
D	920	61.62	0.0075	6.653	3.53	68.2	96.8	37.4	84.2	0.2
E	1000	61.19	0.0119	6.531	6.27	42.7	96.8	55.9	83.6	0.1
F	1075	60.41	0.0201	2.955	7.06	25.3	98.6	76.9	84.0	0.1
G	1110	60.01	0.0293	2.669	3.86	17.4	98.7	88.3	83.6	0.2
H	1180	60.66	0.0717	2.872	2.57	7.1	98.6	95.9	84.4	0.2
I	1210	60.91	0.4019	2.783	0.961	1.3	98.7	98.8	84.9	0.3
J	1250	62.06	2.528	4.050	0.330	0.20	98.4	99.7	86.3	0.7
K	1300	67.32	2.803	14.57	0.046	0.18	94.0	99.9	89.3	4.1
L	1700	112.8	2.328	197.4	0.040	0.22	48.5	100.0	77.5	4.8
Integrated			n=12				K2O=3.69%		83.4	0.1
Plateau		steps D-G	n=4	MSWD=3.37					83.9	0.2
Isochron		steps D-G	n=4	MSWD=5.00		$^{40}Ar/^{36}Ar$=	300±60		83.8	0.2
Wp03-07 am1, Amphibole, 9.71 mg, J=0.0007977±0.08%, D=1.0068±0.0015, NM-208B, Lab#=57128-01										
A	800	413.7	0.7267	1231.4	0.202	0.70	12.0	3.8	70.4	4.1
B	900	116.1	0.3768	211.1	0.278	1.4	46.3	9.0	75.7	1.2
C	1000	87.07	0.6945	102.8	0.329	0.73	65.2	15.1	79.9	0.7
D	1050	81.29	1.475	76.65	0.235	0.35	72.3	19.5	82.7	1.0
E	1080	79.34	4.671	81.89	0.218	0.11	70.0	23.6	78.4	1.1
F	1100	80.79	7.807	75.55	0.226	0.065	73.2	27.8	83.6	1.2
G	1120	75.51	8.311	60.54	0.341	0.061	77.2	34.2	82.5	0.7
H	1140	71.21	8.404	43.95	0.583	0.061	82.7	45.1	83.3	0.6
I	1160	68.08	8.259	32.63	0.781	0.062	86.8	59.7	83.6	0.4
J	1220	68.12	7.582	35.41	0.691	0.067	85.6	72.6	82.4	0.5
K	1650	78.59	9.519	71.80	1.47	0.054	74.0	100.0	82.3	0.4
Integrated			n=11				K2O=0.27%		81.6	0.4
Plateau		steps F-K	n=6	MSWD=1.32					82.9	0.3
Isochron		steps F-K	n=6	MSWD=1.16		$^{40}Ar/^{36}Ar$=	283±17		83.6	0.3

ID	Temp (°C)	$^{40}Ar/^{39}Ar$	$^{37}Ar/^{39}Ar$	$^{36}Ar/^{39}Ar$ (x 10^{-3})	$^{39}Ar_K$ (x 10^{-15} mol)	K/Ca	$^{40}Ar^*$ (%)	^{39}Ar (%)	Age (Ma)	±1s (Ma)
Jtn06-01 am1, Amphibole, 9.02 mg, J=0.0007956±0.09%, D=1.0044±0.001, NM-208B, Lab#=57129-01										
A	800	196.6	0.1782	257.5	0.545	2.9	61.3	6.1	165.2	0.9
B	900	72.16	0.0624	46.15	0.797	8.2	81.1	15.0	82.1	0.4
C	1000	67.11	0.3337	20.83	0.598	1.5	90.9	21.6	85.5	0.4
D	1050	65.79	0.7437	19.87	0.568	0.69	91.2	28.0	84.1	0.4
E	1080	81.11	2.891	44.82	0.451	0.18	84.0	33.0	95.4	0.5
F	1100	96.57	6.827	49.37	0.875	0.075	85.5	42.7	115.3	0.4
G	1120	96.96	6.691	28.12	1.58	0.076	92.0	60.4	124.2	0.3
H	1140	96.24	5.228	17.67	1.10	0.098	95.0	72.7	127.1	0.3
I	1160	82.69	3.496	20.36	0.424	0.15	93.1	77.4	107.5	0.8
J	1220	89.64	5.816	34.94	0.305	0.088	89.0	80.8	111.5	0.7
K	1650	103.5	6.622	41.05	1.72	0.077	88.8	100.0	128.0	0.3
Integrated			n=11				K2O=0.48%		115.5	0.2
JTrm 06-02 bt1, Biotite, 5.9 mg, J=0.002252±0.05%, D=1.003±0.0011, NM-212A, Lab#=57407-01										
A	625	49.40	0.1281	129.0	2.93	4.0	22.9	1.3	45.3	1.6
B	700	35.77	0.0304	60.93	4.63	16.8	49.7	3.4	70.7	0.9
C	750	25.53	0.0221	21.87	8.22	23.1	74.7	7.1	75.8	0.5
D	800	22.46	0.0131	7.625	14.7	38.9	90.0	13.7	80.3	0.4
E	875	22.18	0.0145	5.005	17.5	35.2	93.3	21.5	82.2	0.3
F	975	22.16	0.0125	3.303	35.5	40.9	95.6	37.5	84.1	0.2
G	1075	22.24	0.0122	3.543	57.1	42.0	95.3	63.1	84.1	0.2
H	1250	21.80	0.1185	2.022	74.1	4.3	97.3	96.4	84.1	0.1
I	1700	22.31	0.6607	5.178	8.04	0.77	93.4	100.0	82.7	0.3
Integrated			n=9				K2O=6.44%		82.6	0.2
Plateau		steps F-H	n=3	MSWD=0.10					84.1	0.1
Isochron		steps F-H	n=3	MSWD=0.02		$^{40}Ar/^{36}Ar$=	281±36		84.3	0.2

ID	Temp (°C)	$^{40}Ar/^{39}Ar$	$^{37}Ar/^{39}Ar$	$^{36}Ar/^{39}Ar$ (x 10^{-3})	$^{39}Ar_K$ (x 10^{-15} mol)	K/Ca	$^{40}Ar^*$ (%)	^{39}Ar (%)	Age (Ma)	±1s (Ma)
Pcp07-07 bt1, Biotite, 6.03 mg, J=0.0022697±0.07%, D=1.002±0.001, NM-212B, Lab#=57417-01										
A	625	42.78	0.3733	125.7	4.35	1.4	13.3	0.9	23.1	1.3
B	700	26.97	0.0329	40.63	15.1	15.5	55.5	4.0	60.3	0.4
C	750	23.36	0.0213	16.18	22.6	23.9	79.5	8.6	74.5	0.2
D	800	21.78	0.0130	7.162	31.7	39.2	90.3	15.0	78.8	0.2
E	875	21.01	0.0088	3.605	67.6	58.2	94.9	28.8	79.8	0.1
F	975	21.41	0.0151	4.111	64.2	33.8	94.3	41.9	80.8	0.1
G	1025	21.59	0.0146	5.303	49.6	34.9	92.7	52.0	80.1	0.1
H	1075	21.43	0.0138	5.143	63.7	37.0	92.9	65.0	79.7	0.1
I	1150	21.04	0.0168	3.671	79.3	30.3	94.9	81.1	79.9	0.1
J	1200	21.01	0.0345	3.046	43.3	14.8	95.7	90.0	80.5	0.2
K	1300	20.88	0.5335	2.374	46.0	0.96	96.9	99.3	81.0	0.2
L	1700	31.90	0.8197	40.92	3.20	0.62	62.3	100.0	79.6	0.9
Integrated			n=12				K2O=13.77%		78.7	0.1
Pcp07-07 am1, Amphibole, 9.2 mg, J=0.0022835±0.10%, D=1.002±0.001, NM-212C, Lab#=57421-01										
A	800	59.30	1.410	122.4	2.32	0.36	39.3	3.2	93.6	1.8
B	900	23.16	1.103	18.34	1.97	0.46	77.0	6.0	72.0	1.1
C	1000	22.77	4.659	9.429	5.81	0.11	89.5	14.1	82.3	0.5
D	1050	22.19	5.596	5.454	24.0	0.091	94.9	47.6	85.0	0.2
E	1080	21.24	5.759	1.993	18.3	0.089	99.5	73.2	85.4	0.3
F	1100	18.24	5.363	-5.0943	2.41	0.095	110.7	76.6	81.6	1.0
G	1120	18.04	6.541	-7.9812	1.90	0.078	116.3	79.2	84.7	1.2
H	1140	12.22	7.095	-30.7082	0.811	0.072	179.4	80.4	88.5	2.7
I	1160	13.25	7.907	-23.9811	0.919	0.065	158.6	81.6	84.9	2.3
J	1220	21.22	7.663	1.572	7.40	0.067	100.8	92.0	86.5	0.5
K	1650	24.65	7.269	13.30	5.74	0.070	86.5	100.0	86.2	0.5
Integrated			n=11				K2O=1.31%		84.9	0.2
Plateau	steps D-E,G-K		n=7	MSWD=2.42					85.4	0.2
Isochron	steps D-E,G-K		n=7	MSWD=2.90		$^{40}Ar/^{36}Ar$=	296±16		85.4	0.2

ID	Temp (°C)	$^{40}Ar/^{39}Ar$	$^{37}Ar/^{39}Ar$	$^{36}Ar/^{39}Ar$ (x 10^{-3})	$^{39}Ar_K$ (x 10^{-15} mol)	K/Ca	$^{40}Ar^*$ (%)	^{39}Ar (%)	Age (Ma)	±1s (Ma)
Kb06-02 am1, Amphibole, 6.6 mg, J=0.002285±0.10%, D=1.002±0.001, NM-212C, Lab#=57422-01										
A	800	40.02	0.2876	60.65	13.6	1.8	55.3	16.5	89.0	0.6
B	900	24.46	0.0995	10.62	15.1	5.1	87.2	34.8	85.8	0.3
C	1000	24.43	0.8624	9.256	14.6	0.59	89.1	52.6	87.6	0.3
D	1050	27.77	6.467	16.46	11.6	0.079	84.4	66.7	94.5	0.4
E	1080	24.09	6.222	7.866	7.48	0.082	92.5	75.8	89.9	0.4
F	1100	23.64	4.071	6.819	4.07	0.13	92.9	80.7	88.6	0.6
G	1120	24.22	4.035	8.527	2.91	0.13	91.0	84.3	88.8	0.8
H	1140	25.21	4.608	11.78	1.38	0.11	87.9	85.9	89.3	1.7
I	1160	25.32	4.392	9.197	1.18	0.12	90.7	87.4	92.5	1.6
J	1220	24.68	3.879	9.592	2.68	0.13	89.8	90.6	89.3	0.9
K	1650	29.32	8.247	20.78	7.72	0.062	81.4	100.0	96.3	0.5
Integrated			n=11				K2O=2.10%		89.7	0.2
Pp03-09 bt1, Biotite, 5.8 mg, J=0.0008008±0.11%, D=1.0032±0.0012, NM-215A, Lab#=57600-01										
A	625	105.5	0.0589	198.1	2.93	8.7	44.5	2.4	66.6	0.8
B	700	60.37	0.0118	11.59	15.8	43.1	94.3	15.1	80.5	0.2
C	750	59.28	0.0069	3.091	19.2	73.7	98.5	30.6	82.4	0.1
D	800	59.97	0.0078	5.892	11.7	65.4	97.1	40.1	82.2	0.2
E	875	60.36	0.0141	7.685	15.6	36.2	96.2	52.7	82.0	0.2
F	975	59.83	0.0138	5.383	27.1	36.9	97.3	74.6	82.2	0.1
G	1075	59.37	0.0431	3.826	15.7	11.8	98.1	87.3	82.2	0.2
H	1250	66.04	0.4595	25.51	15.7	1.1	88.6	100.0	82.7	0.2
Integrated			n=8				K2O=10.23%		81.7	0.2
Plateau		steps C-H	n=6	MSWD=1.47					82.3	0.1
Isochron		steps C-H	n=6	MSWD=1.11		$^{40}Ar/^{36}Ar$=	308±15		82.2	0.1
Jtn07-09 bt1, Biotite, 8.5 mg, J=0.0007968±0.10%, D=1.0032±0.0012, NM-215A, Lab#=57603-01										
A	625	114.8	0.0447	243.5	2.62	11.4	37.3	1.5	60.6	0.9
B	700	69.00	0.0155	30.63	17.6	33.0	86.9	11.4	84.2	0.2
C	750	64.62	0.0108	8.939	19.0	47.4	95.9	22.2	87.0	0.2
D	800	65.58	0.0138	11.99	13.0	37.0	94.6	29.5	87.0	0.2
E	875	65.67	0.0166	12.50	24.0	30.7	94.4	43.1	87.0	0.2
F	975	65.46	0.0123	12.42	46.1	41.6	94.4	69.2	86.7	0.2
G	1075	64.46	0.0566	8.409	31.9	9.0	96.2	87.3	87.0	0.2
H	1250	67.73	0.7695	15.92	22.5	0.66	93.1	100.0	88.5	0.2
Integrated			n=8				K2O=10.03%		86.4	0.2
Plateau		steps C-G	n=5	MSWD=0.58					86.9	0.1
Isochron		steps C-G	n=5	MSWD=0.68		$^{40}Ar/^{36}Ar$=	281±31		87.1	0.2

ID	Temp (°C)	$^{40}Ar/^{39}Ar$	$^{37}Ar/^{39}Ar$	$^{36}Ar/^{39}Ar$ (x 10^{-3})	$^{39}Ar_K$ (x 10^{-15} mol)	K/Ca	$^{40}Ar^*$ (%)	^{39}Ar (%)	Age (Ma)	±1s (Ma)
Jtn07-09 am1, Amphibole, 10.8 mg, J=0.0007844±0.07%, D=1.004±0.001, NM-215C, Lab#=57614-01										
A	800	297.0	0.2295	279.9	1.74	2.2	72.2	6.7	280.4	1.5
B	900	74.91	0.2347	58.01	1.33	2.2	77.1	11.9	80.0	0.6
C	1000	76.59	1.383	36.83	2.84	0.37	85.9	22.9	90.9	0.3
D	1050	108.3	6.728	24.68	6.54	0.076	93.8	48.1	138.9	0.3
E	1080	106.1	5.193	5.110	5.78	0.098	99.0	70.4	143.3	0.3
F	1100	82.42	3.539	-9.8363	0.908	0.14	103.9	73.9	117.5	0.9
G	1120	84.23	4.694	-23.6224	0.440	0.11	108.7	75.6	125.6	1.6
H	1140	84.91	5.454	-40.1864	0.358	0.094	114.5	77.0	133.1	2.0
I	1160	92.10	5.748	-12.0226	0.741	0.089	104.4	79.9	131.7	1.1
J	1220	113.2	7.124	7.701	4.49	0.072	98.5	97.2	152.0	0.4
K	1650	228.9	7.522	413.4	0.717	0.068	46.9	100.0	146.6	2.1
Integrated			n=11				K2O=1.17%		142.8	0.3
Pp09-09 am1, Amphibole, 13.4 mg, J=0.000788±0.07%, D=1.004±0.001, NM-215C, Lab#=57617-01										
A	800	103.0	0.3485	170.8	1.51	1.5	51.0	8.9	73.3	1.0
B	900	77.57	0.4281	76.54	1.26	1.2	70.9	16.3	76.5	0.7
C	1000	73.10	3.409	56.80	1.49	0.15	77.4	25.0	78.9	0.7
D	1020	74.27	7.695	53.66	0.868	0.066	79.5	30.1	82.5	0.9
E	1040	68.67	8.727	29.59	2.38	0.058	88.3	44.1	84.7	0.4
F	1060	62.95	8.270	11.13	3.14	0.062	95.9	62.6	84.3	0.4
G	1120	62.89	6.806	10.63	2.46	0.075	95.9	77.1	84.1	0.4
H	1180	63.70	9.768	22.22	1.47	0.052	91.0	85.7	81.1	0.6
I	1250	70.24	9.053	34.95	2.22	0.056	86.4	98.8	84.7	0.5
J	1650	504.3	9.841	1526.1	0.207	0.052	10.7	100.0	76.0	7.7
Integrated			n=10				K2O=0.62%		81.9	0.3
Plateau	steps D-G,I-J		n=6	MSWD=1.55					84.3	0.3
Isochron	steps D-G,I-J		n=6	MSWD=1.60		$^{40}Ar/^{36}Ar$=	292±7		84.4	0.2
Jtn07-11 am1, Amphibole, 11.2 mg, J=0.0007881±0.05%, D=1.004±0.001, NM-215C, Lab#=57616-01										
A	800	1164.2	0.7837	552.8	0.426	0.65	86.0	1.9	1049.6	8.2
B	900	84.25	1.105	40.41	0.391	0.46	85.9	3.6	100.2	1.6
C	1000	128.8	5.708	66.58	1.43	0.089	85.1	10.0	150.0	0.8
D	1020	113.1	7.729	35.90	3.04	0.066	91.2	23.5	141.7	0.5
E	1040	93.72	7.154	13.75	6.52	0.071	96.3	52.5	124.5	0.3
F	1060	95.97	6.329	11.20	2.82	0.081	97.1	65.0	128.4	0.5
G	1120	88.27	6.923	6.966	0.809	0.074	98.3	68.6	119.9	0.9
H	1180	96.55	8.612	14.39	1.77	0.059	96.3	76.5	128.3	0.6
I	1250	101.2	8.332	20.16	5.01	0.061	94.8	98.8	132.2	0.4
J	1650	407.1	7.236	1099.0	0.277	0.071	20.4	100.0	114.8	5.2
Integrated			n=10				K2O=0.98%		153.0	0.3

ID	Temp (°C)	$^{40}Ar/^{39}Ar$	$^{37}Ar/^{39}Ar$	$^{36}Ar/^{39}Ar$ (x 10^{-3})	$^{39}Ar_K$ (x 10^{-15} mol)	K/Ca	$^{40}Ar^*$ (%)	^{39}Ar (%)	Age (Ma)	±1s (Ma)
Jtrm06-02 am1, Amphibole, 12.7 mg, J=0.0007843±0.06%, D=1.004±0.001, NM-215C, Lab#=57613-02										
A	800	426.7	0.8833	1124.3	1.42	0.58	22.2	6.5	129.1	2.7
B	900	107.9	1.005	240.6	0.009	0.51	34.2	6.6	51.5	54.7
C	900	85.87	0.2785	91.33	1.82	1.8	68.6	14.9	81.5	0.6
D	1000	80.93	1.607	60.96	3.08	0.32	77.9	29.0	87.2	0.4
E	1020	82.51	5.106	63.17	1.88	0.100	77.9	37.6	89.0	0.6
F	1040	71.83	7.523	32.26	3.57	0.068	87.6	54.0	87.3	0.4
G	1080	67.12	5.173	20.64	3.74	0.099	91.6	71.1	85.2	0.3
H	1120	67.87	3.323	28.92	1.62	0.15	87.8	78.5	82.6	0.6
I	1180	66.21	7.641	14.94	1.11	0.067	94.3	83.6	86.7	0.8
J	1250	71.54	9.376	30.55	2.92	0.054	88.5	97.0	87.9	0.4
K	1700	276.4	12.76	714.0	0.662	0.040	24.1	100.0	92.5	2.5
Integrated			n=11				K2O=0.84%		89.2	0.4
Jtn07-11 bt1, Biotite, 6 mg, J=0.0007859±0.06%, D=1.004±0.001, NM-215C, Lab#=57612-02										
A	650	114.0	0.1551	249.6	1.53	3.3	35.3	1.6	56.3	0.9
B	750	70.85	0.0221	32.39	8.31	23.1	86.5	10.2	84.9	0.2
C	850	68.30	0.0179	12.04	13.6	28.4	94.8	24.2	89.5	0.2
D	920	68.06	0.0153	8.495	11.1	33.3	96.3	35.7	90.6	0.2
E	1000	68.86	0.0132	11.95	24.6	38.7	94.9	61.0	90.3	0.2
F	1075	66.35	0.0200	4.431	19.1	25.5	98.0	80.7	89.9	0.1
G	1110	66.54	0.0395	3.848	9.77	12.9	98.3	90.8	90.4	0.2
H	1180	67.58	0.6666	8.211	7.06	0.77	96.5	98.1	90.2	0.2
I	1210	72.41	2.855	20.90	1.17	0.18	91.8	99.3	92.0	0.6
J	1250	81.72	1.508	49.11	0.382	0.34	82.4	99.7	93.1	1.5
K	1300	100.7	1.127	124.0	0.270	0.45	63.7	100.0	88.8	2.4
Integrated			n=12				K2O=7.89%		89.2	0.1
Plateau		steps D-J	n=7	MSWD=3.66					90.3	0.2
Isochron		steps D-J	n=7	MSWD=2.20		$^{40}Ar/^{36}Ar$=	341±15		89.8	0.1

ID	Temp (°C)	$^{40}Ar/^{39}Ar$	$^{37}Ar/^{39}Ar$	$^{36}Ar/^{39}Ar$ (x 10^{-3})	$^{39}Ar_K$ (x 10^{-15} mol)	K/Ca	$^{40}Ar^*$ (%)	^{39}Ar (%)	Age (Ma)	±1s (Ma)
Dbk05-01 k1, K-Feldspar, 2.62 mg, J=0.003605±0.07%, D=1.002±0.001, NM-194C, Lab#=56122-01										
B	460	95.43	0.5263	270.7	0.262	0.97	16.2	0.1	98.0	8.9
C	460	36.14	0.7752	84.41	0.119	0.66	31.1	0.2	71.8	14.8
D	510	18.40	0.3411	23.38	0.240	1.5	62.6	0.3	73.4	7.3
E	510	13.72	0.3964	12.54	0.287	1.3	73.2	0.4	64.1	6.3
F	560	13.21	0.2391	6.898	0.602	2.1	84.7	0.6	71.3	2.9
G	560	11.72	0.1744	2.418	0.711	2.9	94.0	0.9	70.2	2.5
H	610	13.81	0.0934	4.570	1.86	5.5	90.3	1.7	79.2	1.0
I	610	11.90	0.1102	1.449	1.85	4.6	96.5	2.5	73.1	1.0
J	660	11.88	0.0823	0.6490	3.44	6.2	98.4	4.0	74.5	0.5
K	660	11.86	0.0863	0.7110	3.73	5.9	98.3	5.5	74.2	0.5
L	710	11.98	0.0869	0.8278	5.26	5.9	98.0	7.8	74.8	0.4
M	710	11.92	0.0739	0.2127	5.72	6.9	99.5	10.2	75.5	0.3
N	760	11.99	0.0781	0.2375	7.36	6.5	99.5	13.3	75.9	0.3
O	760	12.05	0.0722	0.4947	7.18	7.1	98.8	16.3	75.8	0.3
P	810	12.11	0.0789	0.3412	8.49	6.5	99.2	19.9	76.4	0.2
Q	810	12.15	0.0771	0.3729	7.58	6.6	99.1	23.1	76.6	0.3
R	860	12.19	0.0673	0.2767	7.56	7.6	99.4	26.3	77.1	0.3
S	860	12.28	0.0627	0.4630	7.20	8.1	98.9	29.3	77.3	0.3
T	910	12.41	0.0684	0.3557	7.40	7.5	99.2	32.5	78.3	0.3
U	910	12.44	0.0520	0.4631	7.08	9.8	98.9	35.5	78.3	0.3
V	960	12.58	0.0442	0.4145	7.04	11.5	99.1	38.4	79.2	0.3
W	960	12.68	0.0355	0.6400	7.01	14.4	98.5	41.4	79.4	0.3
X	1010	12.73	0.0330	0.5206	6.76	15.5	98.8	44.2	79.9	0.3
Y	1010	12.81	0.0357	0.8359	6.75	14.3	98.1	47.1	79.9	0.3
Z	1060	12.97	0.0452	0.7587	6.97	11.3	98.3	50.0	81.0	0.3
AA	1060	13.04	0.0300	0.9859	7.39	17.0	97.8	53.2	81.0	0.3
AB	1110	13.61	0.0526	1.631	8.19	9.7	96.5	56.6	83.4	0.3
AC	1110	13.45	0.0409	1.171	7.95	12.5	97.5	60.0	83.3	0.3
AD	1110	13.58	0.0355	1.635	11.8	14.4	96.5	65.0	83.2	0.2
AE	1110	13.75	0.0361	2.589	13.5	14.1	94.5	70.7	82.5	0.2
AF	1210	13.90	0.0272	1.686	13.3	18.8	96.4	76.3	85.1	0.2
AG	1260	13.71	0.0301	2.003	26.3	17.0	95.7	87.4	83.3	0.2
AH	1360	13.75	0.0821	2.388	17.6	6.2	94.9	94.8	82.9	0.2
AI	1700	14.28	0.0889	3.678	12.2	5.7	92.4	100.0	83.8	0.2
Integrated			n=34		236.7	8.9	K2O=9.63%		80.3	0.1

ID	Temp (°C)	$^{40}Ar/^{39}Ar$	$^{37}Ar/^{39}Ar$	$^{36}Ar/^{39}Ar$ (x 10^{-3})	$^{39}Ar_K$ (x 10^{-15} mol)	K/Ca	$^{40}Ar^*$ (%)	^{39}Ar (%)	Age (Ma)	±1s (Ma)
Jtn06-01 k1, K-Feldspar, 8.38 mg, J=0.0007956±0.08%, D=1.0068±0.0015, NM-208A, Lab#=57122-01										
A	520	621.8	0.0365	845.6	0.337	14.0	59.8	0.3	467.6	3.2
B	520	63.82	0.0502	50.18	0.392	10.2	76.8	0.7	69.0	0.6
C	570	78.54	0.0268	40.93	0.625	19.0	84.6	1.3	92.9	0.5
D	570	55.23	0.0170	15.27	0.612	30.0	91.8	1.9	71.4	0.4
E	620	83.55	0.0185	45.85	1.13	27.5	83.8	3.0	97.8	0.4
F	620	54.50	0.0153	9.160	1.02	33.3	95.0	4.0	72.8	0.3
G	670	55.06	0.0070	9.794	0.972	73.3	94.7	5.0	73.4	0.3
H	670	56.13	0.0061	9.838	1.86	83.7	94.8	6.8	74.8	0.2
I	720	53.88	0.0074	5.202	1.54	69.1	97.1	8.3	73.6	0.3
J	720	53.01	0.0040	3.361	2.27	126.4	98.1	10.5	73.2	0.2
K	770	54.49	0.0083	5.694	2.27	61.5	96.9	12.8	74.2	0.2
L	770	53.33	0.0085	2.981	2.58	60.0	98.3	15.3	73.8	0.2
M	820	54.15	0.0077	4.659	2.26	66.1	97.5	17.5	74.2	0.2
N	820	53.56	0.0083	2.963	2.45	61.2	98.4	19.9	74.1	0.2
O	870	54.77	0.0103	6.359	1.98	49.4	96.6	21.8	74.4	0.2
P	870	54.27	0.0064	4.699	2.09	79.7	97.4	23.9	74.4	0.2
Q	920	55.42	0.0064	8.717	1.67	79.2	95.4	25.5	74.3	0.2
R	920	54.58	0.0088	6.525	1.82	57.9	96.5	27.3	74.0	0.2
S	970	58.47	0.0102	17.53	1.48	50.2	91.1	28.7	74.9	0.3
T	970	56.04	0.0114	12.14	1.68	44.7	93.6	30.4	73.8	0.3
U	1020	61.65	0.0147	26.95	1.46	34.7	87.1	31.8	75.5	0.3
V	1020	60.32	0.0066	21.71	1.99	77.6	89.4	33.8	75.8	0.3
W	1070	65.63	0.0090	37.27	1.81	56.9	83.2	35.5	76.7	0.3
X	1070	64.30	0.0116	31.03	2.39	43.9	85.7	37.9	77.4	0.3
Y	1120	69.33	0.0086	42.55	2.23	59.0	81.9	40.1	79.7	0.3
Z	1170	68.15	0.0153	39.12	2.54	33.4	83.0	42.5	79.5	0.3
AA	1170	65.96	0.0147	30.26	4.27	34.7	86.4	46.7	80.0	0.2
AB	1170	64.71	0.0106	25.01	4.46	48.0	88.6	51.1	80.5	0.2
AC	1170	65.03	0.0125	23.88	4.82	40.7	89.2	55.8	81.3	0.2
AD	1170	66.27	0.0079	24.39	5.07	64.2	89.1	60.8	82.8	0.2
AE	1270	72.77	0.0155	36.20	2.35	32.8	85.3	63.1	87.0	0.3
AF	1320	70.30	0.0030	24.95	12.1	168.2	89.5	75.0	88.1	0.2
AG	1370	68.69	0.0015	17.95	16.6	346.2	92.3	91.2	88.8	0.2
AH	1570	67.49	0.0045	19.26	5.90	112.3	91.6	97.0	86.6	0.2
AI	1720	67.80	0.0046	29.87	3.05	110.3	87.0	100.0	82.7	0.3
Integrated			n=35		102.1	65.6	K2O=5.88%		82.9	0.2

ID	Temp (°C)	$^{40}Ar/^{39}Ar$	$^{37}Ar/^{39}Ar$	$^{36}Ar/^{39}Ar$ (x 10^{-3})	$^{39}Ar_K$ (x 10^{-15} mol)	K/Ca	$^{40}Ar^*$ (%)	^{39}Ar (%)	Age (Ma)	±1s (Ma)
Kle07-05 k1, K-Feldspar, 15.2 mg, J=0.0022532±0.06%, D=1.002±0.001, NM-212A, Lab#=57406-01										
A	500	76.20	0.4074	160.6	1.36	1.3	37.8	0.4	113.4	2.4
B	500	30.37	0.1933	38.04	0.961	2.6	63.0	0.7	76.2	2.3
C	550	21.92	0.2723	9.299	1.57	1.9	87.6	1.2	76.4	1.3
D	550	20.70	0.0583	9.185	1.75	8.8	86.9	1.7	71.6	1.2
E	600	19.80	0.0493	4.152	2.07	10.4	93.8	2.3	73.9	1.1
F	600	21.84	0.0362	7.498	5.26	14.1	89.9	3.9	78.1	0.5
G	650	19.23	0.0493	3.388	5.73	10.3	94.8	5.6	72.6	0.4
H	650	19.37	0.0467	2.263	4.96	10.9	96.6	7.1	74.4	0.4
I	700	18.91	0.0774	1.942	4.84	6.6	97.0	8.5	73.0	0.4
J	700	19.27	0.0465	2.340	5.66	11.0	96.4	10.2	74.0	0.4
K	750	18.90	0.0425	1.695	6.67	12.0	97.4	12.2	73.3	0.3
L	750	19.13	0.0348	2.181	7.36	14.7	96.6	14.4	73.6	0.3
M	800	19.32	0.0322	1.180	8.76	15.8	98.2	17.0	75.5	0.3
N	800	19.20	0.0475	2.395	8.49	10.7	96.3	19.6	73.6	0.3
O	850	19.28	0.0398	1.971	7.92	12.8	97.0	21.9	74.4	0.3
P	850	19.48	0.0223	1.758	8.53	22.8	97.3	24.5	75.4	0.3
Q	900	19.52	0.0311	1.939	8.05	16.4	97.1	26.9	75.4	0.3
R	900	19.69	0.0211	2.065	8.92	24.2	96.9	29.5	75.9	0.3
S	950	19.85	0.0329	3.384	7.44	15.5	95.0	31.8	75.0	0.3
T	950	19.92	0.0171	2.729	8.16	29.9	96.0	34.2	76.0	0.3
U	1000	20.30	0.0271	3.670	5.91	18.8	94.7	36.0	76.5	0.4
V	1000	20.43	0.0199	4.059	8.41	25.6	94.1	38.5	76.5	0.3
W	1050	20.62	0.0332	5.556	7.18	15.4	92.0	40.6	75.5	0.4
X	1050	21.12	0.0218	6.420	8.80	23.4	91.0	43.3	76.5	0.3
Y	1100	21.52	0.0325	6.935	7.56	15.7	90.5	45.5	77.4	0.4
Z	1100	21.97	0.0386	8.222	9.18	13.2	89.0	48.3	77.7	0.3
AA	1100	23.61	0.0304	13.50	8.32	16.8	83.1	50.8	78.0	0.4
AB	1100	25.20	0.0329	18.39	10.7	15.5	78.4	54.0	78.6	0.4
AC	1100	28.87	0.0310	30.97	12.0	16.4	68.3	57.5	78.4	0.4
AD	1100	35.81	0.0350	53.08	12.6	14.6	56.2	61.3	80.0	0.6
AE	1200	24.39	0.1067	13.16	3.39	4.8	84.1	62.3	81.5	0.7
AF	1300	21.32	0.0189	4.844	51.3	27.0	93.3	77.7	79.1	0.2
AG	1350	21.65	0.0309	5.587	29.6	16.5	92.4	86.5	79.5	0.2
AH	1550	22.00	0.0664	6.967	44.4	7.7	90.7	99.8	79.3	0.2
AI	1700	546.1	9.074	1759.1	0.696	0.056	5.0	100.0	107.3	13.0
Integrated			n=35		334.6	8.7	K2O=3.75%		77.5	0.2

ID	Temp (°C)	$^{40}Ar/^{39}Ar$	$^{37}Ar/^{39}Ar$	$^{36}Ar/^{39}Ar$ (x 10^{-3})	$^{39}Ar_K$ (x 10^{-15} mol)	K/Ca	$^{40}Ar^*$ (%)	^{39}Ar (%)	Age (Ma)	±1s (Ma)
Km07-06 k1, K-Feldspar, 9.1 mg, J=0.0022513±0.07%, D=1.002±0.001, NM-212A, Lab#=57410-01										
A	500	126.1	0.0662	341.0	3.26	7.7	20.1	0.1	100.1	2.6
B	500	39.57	0.0197	72.90	3.20	25.9	45.6	0.3	71.7	1.1
C	550	23.41	-0.0054	15.13	2.42	-	80.9	0.4	75.3	0.9
D	550	20.57	0.0077	10.19	7.22	66.6	85.4	0.7	69.9	0.3
E	600	22.10	0.0089	9.854	12.9	57.5	86.8	1.3	76.3	0.3
F	600	19.00	0.0083	3.282	12.0	61.7	94.9	1.8	71.8	0.2
G	650	19.15	0.0084	2.281	16.9	60.5	96.5	2.6	73.5	0.2
H	650	18.92	0.0078	1.700	17.9	65.8	97.3	3.4	73.2	0.2
I	700	18.77	0.0075	0.8695	16.5	68.2	98.6	4.1	73.6	0.2
J	700	18.82	0.0085	1.290	24.5	59.8	98.0	5.2	73.3	0.1
K	750	18.89	0.0073	1.069	34.9	69.5	98.3	6.8	73.8	0.1
L	750	18.77	0.0062	0.9388	39.9	81.9	98.5	8.6	73.5	0.1
M	800	18.92	0.0081	0.9654	47.2	63.3	98.5	10.7	74.1	0.2
N	800	18.77	0.0057	0.6090	47.4	88.9	99.0	12.8	73.9	0.2
O	850	18.86	0.0045	0.6321	41.4	112.3	99.0	14.7	74.2	0.2
P	850	18.95	0.0047	0.5317	63.6	107.8	99.2	17.6	74.7	0.2
Q	900	18.96	0.0042	0.6155	44.3	121.6	99.0	19.5	74.7	0.1
R	900	18.99	0.0034	0.5506	57.3	152.1	99.1	22.1	74.9	0.2
S	950	19.01	0.0043	0.5534	52.3	118.4	99.1	24.5	74.9	0.2
T	950	19.08	0.0023	0.4977	56.4	217.3	99.2	27.0	75.3	0.2
U	1000	19.18	0.0032	0.8232	41.9	161.7	98.7	28.9	75.3	0.2
V	1000	19.22	0.0027	0.8483	49.0	192.5	98.7	31.1	75.4	0.2
W	1050	19.53	0.0042	1.716	37.0	121.9	97.4	32.7	75.6	0.1
X	1050	19.46	0.0030	1.784	46.3	168.5	97.3	34.8	75.3	0.2
Y	1100	19.76	0.0073	2.752	39.1	69.8	95.9	36.6	75.3	0.2
Z	1100	19.59	0.0054	2.232	46.7	93.7	96.6	38.7	75.3	0.2
AA	1100	19.78	0.0053	2.742	45.5	97.1	95.9	40.7	75.4	0.2
AB	1100	20.01	0.0054	2.903	55.3	94.6	95.7	43.2	76.1	0.2
AC	1100	20.37	0.0042	4.286	62.8	120.3	93.8	46.0	75.9	0.2
AD	1100	21.09	0.0040	6.300	68.1	127.4	91.2	49.1	76.4	0.1
AE	1200	20.42	0.0077	3.641	21.5	66.0	94.7	50.0	76.9	0.2
AF	1300	20.22	0.0025	3.022	338.8	200.6	95.6	65.2	76.8	0.1
AG	1350	20.58	0.0026	4.362	344.7	195.8	93.7	80.7	76.6	0.1
AH	1550	20.74	0.0036	4.571	425.5	140.3	93.5	99.8	77.1	0.1
AI	1700	52.01	1.484	108.3	4.53	0.34	38.7	100.0	80.0	1.2
Integrated			n=35		2228.2	71.5	K2O=41.78%		75.9	0.1

ID	Temp (°C)	$^{40}Ar/^{39}Ar$	$^{37}Ar/^{39}Ar$	$^{36}Ar/^{39}Ar$ (x 10^{-3})	$^{39}Ar_K$ (x 10^{-15} mol)	K/Ca	$^{40}Ar^*$ (%)	^{39}Ar (%)	Age (Ma)	±1s (Ma)
Pcp07-07 k1, K-Feldspar, 11.7 mg, J=0.0022666±0.06%, D=1.002±0.001, NM-212B, Lab#=57416-01										
A	500	80.71	0.1015	199.2	13.5	5.0	27.1	0.9	87.2	2.2
B	500	35.95	0.0867	74.86	3.60	5.9	38.5	1.1	55.7	2.1
C	550	30.38	0.0635	31.54	7.40	8.0	69.3	1.6	84.1	0.7
D	550	20.31	0.0541	10.36	3.66	9.4	84.9	1.8	69.2	0.6
E	600	22.29	0.0671	13.22	3.69	7.6	82.5	2.1	73.6	0.6
F	600	22.95	0.0618	10.69	9.39	8.3	86.3	2.7	79.2	0.4
G	650	21.06	0.0664	7.338	12.4	7.7	89.7	3.5	75.6	0.3
H	650	18.46	0.0573	1.371	12.8	8.9	97.8	4.3	72.3	0.2
I	700	18.54	0.0605	0.9113	14.2	8.4	98.6	5.2	73.2	0.2
J	700	18.50	0.0522	0.6020	18.4	9.8	99.1	6.4	73.4	0.2
K	750	18.75	0.0518	1.321	23.0	9.8	97.9	7.9	73.5	0.1
L	750	18.51	0.0416	0.5081	28.2	12.3	99.2	9.8	73.6	0.1
M	800	18.63	0.0419	0.6617	26.4	12.2	99.0	11.5	73.8	0.1
N	800	18.68	0.0303	0.5138	38.0	16.8	99.2	13.9	74.2	0.2
O	850	18.59	0.0287	0.6992	45.5	17.8	98.9	16.9	73.6	0.2
P	850	18.58	0.0209	0.3905	46.6	24.4	99.4	19.9	73.9	0.1
Q	900	18.33	0.0225	0.3663	41.0	22.6	99.4	22.6	73.0	0.3
R	900	18.55	0.0205	0.4912	46.8	24.9	99.2	25.6	73.7	0.2
S	950	18.74	0.0278	0.5173	39.4	18.3	99.2	28.2	74.4	0.3
T	950	18.75	0.0226	0.5241	45.4	22.6	99.2	31.1	74.4	0.1
U	1000	18.89	0.0329	0.8933	33.1	15.5	98.6	33.3	74.6	0.1
V	1000	18.89	0.0152	0.7346	39.3	33.7	98.9	35.8	74.7	0.2
W	1050	19.13	0.0246	1.229	31.9	20.8	98.1	37.9	75.1	0.2
X	1050	19.11	0.0210	1.224	39.7	24.3	98.1	40.5	75.1	0.2
Y	1100	19.51	0.0331	1.972	30.8	15.4	97.0	42.5	75.8	0.2
Z	1100	19.57	0.0317	2.073	38.2	16.1	96.9	45.0	75.9	0.2
AA	1150	20.08	0.0555	2.750	25.4	9.2	96.0	46.6	77.1	0.2
AB	1150	20.15	0.0525	2.555	34.4	9.7	96.3	48.9	77.6	0.3
AC	1150	20.17	0.0411	2.906	36.7	12.4	95.8	51.2	77.2	0.2
AD	1150	20.33	0.0318	3.404	49.2	16.0	95.1	54.4	77.3	0.2
AE	1150	20.72	0.0250	4.474	63.2	20.4	93.6	58.6	77.6	0.2
AF	1150	21.50	0.0182	6.619	77.4	28.0	90.9	63.6	78.2	0.1
AG	1200	20.61	0.0291	3.529	7.27	17.6	95.0	64.1	78.3	0.3
AH	1300	20.56	0.0117	3.022	115.1	43.6	95.7	71.5	78.6	0.1
AI	1350	20.61	0.0087	3.171	157.6	58.6	95.5	81.8	78.7	0.1
AJ	1550	20.67	0.0086	3.351	271.2	59.0	95.2	99.4	78.7	0.1
AK	1700	28.09	0.1201	27.63	8.99	4.2	71.0	100.0	79.7	0.5
Integrated			n=37		1538.5	20.3	K2O=22.28%		76.6	0.1

ID	Temp (°C)	$^{40}Ar/^{39}Ar$	$^{37}Ar/^{39}Ar$	$^{36}Ar/^{39}Ar$ (x 10^{-3})	$^{39}Ar_K$ (x 10^{-15} mol)	K/Ca	$^{40}Ar^*$ (%)	^{39}Ar (%)	Age (Ma)	±1s (Ma)
Kl07-02 k1, K-Feldspar, 15.7 mg, J=0.0022815±0.07%, D=1.002±0.001, NM-212C, Lab#=57418-01										
A	500	112.1	0.0248	232.8	8.13	20.6	38.6	0.4	170.1	1.7
B	500	24.42	0.0010	25.65	11.3	507.8	69.0	0.8	68.0	0.4
C	550	22.04	0.0009	10.78	15.8	559.6	85.5	1.5	76.0	0.3
D	550	17.29	-0.0001	3.982	17.2	-	93.2	2.3	65.1	0.2
E	600	24.03	0.0033	10.21	39.3	154.3	87.4	4.0	84.4	0.2
F	600	17.74	0.0012	1.964	27.6	417.6	96.7	5.2	69.2	0.1
G	650	18.47	0.0022	2.125	38.1	227.4	96.6	6.9	72.0	0.2
H	650	18.22	0.0014	1.168	33.1	368.6	98.1	8.3	72.1	0.3
I	700	18.03	0.0022	0.9725	31.8	233.4	98.4	9.7	71.6	0.2
J	700	17.98	-0.0005	0.8617	33.7	-	98.6	11.2	71.5	0.3
K	750	18.18	0.0018	0.9473	34.2	284.1	98.5	12.7	72.2	0.3
L	750	18.01	0.0016	0.9059	36.0	320.2	98.5	14.2	71.5	0.3
M	800	18.17	0.0025	1.118	25.1	202.6	98.2	15.3	71.9	0.1
N	800	17.99	0.0032	1.001	40.2	161.7	98.4	17.1	71.4	0.2
O	850	18.24	0.0013	1.157	31.0	401.4	98.1	18.5	72.1	0.2
P	850	18.27	0.0019	1.122	31.5	268.1	98.2	19.8	72.3	0.2
Q	900	18.37	0.0037	1.203	26.8	137.0	98.1	21.0	72.6	0.1
R	900	18.29	0.0027	1.002	29.0	187.4	98.4	22.3	72.5	0.1
S	950	18.50	0.0062	1.669	31.2	82.1	97.3	23.6	72.6	0.2
T	950	18.45	0.0027	1.333	37.9	191.4	97.9	25.3	72.8	0.2
U	1000	18.81	0.0063	2.002	34.7	81.1	96.9	26.8	73.4	0.1
V	1000	18.67	0.0027	1.891	46.8	186.1	97.0	28.8	73.0	0.2
W	1050	19.09	0.0038	3.034	45.9	132.6	95.3	30.8	73.3	0.2
X	1050	18.96	0.0028	2.241	60.4	184.0	96.5	33.5	73.8	0.2
Y	1100	19.33	0.0041	3.175	57.4	123.7	95.1	36.0	74.1	0.2
Z	1100	19.32	0.0029	2.304	63.3	178.5	96.5	38.7	75.1	0.2
AA	1150	19.41	0.0043	3.189	53.1	117.5	95.1	41.1	74.4	0.2
AB	1150	19.31	0.0051	2.186	59.4	99.7	96.7	43.7	75.2	0.2
AC	1150	19.53	0.0030	2.082	55.7	170.4	96.9	46.1	76.2	0.2
AD	1150	19.74	0.0032	2.589	70.4	161.6	96.1	49.2	76.4	0.1
AE	1150	20.09	0.0027	3.519	85.4	189.2	94.8	52.9	76.7	0.1
AF	1150	20.59	0.0020	5.011	97.2	255.4	92.8	57.1	76.9	0.1
AG	1200	20.69	0.0031	5.415	7.08	166.3	92.3	57.4	76.9	0.3
AH	1300	20.21	0.0019	3.621	129.9	270.7	94.7	63.1	77.1	0.1
AI	1350	20.19	0.0014	3.435	264.1	376.8	95.0	74.7	77.2	0.1
AJ	1550	20.36	0.0018	3.614	562.2	283.7	94.8	99.2	77.7	0.1
AK	1700	22.70	0.0324	11.71	18.4	15.7	84.8	100.0	77.5	0.2
Integrated			n=37		2290.3	190.3	K2O=24.56%		75.9	0.1

ID	Temp (°C)	$^{40}Ar/^{39}Ar$	$^{37}Ar/^{39}Ar$	$^{36}Ar/^{39}Ar$ (x 10^{-3})	$^{39}Ar_K$ (x 10^{-15} mol)	K/Ca	$^{40}Ar^*$ (%)	^{39}Ar (%)	Age (Ma)	±1s (Ma)
Kl07-01 k1, K-Feldspar, 9 mg, J=0.0007955±0.06%, D=1.0032±0.0012, NM-215B, Lab#=57607-01										
B	460	507.1	-0.0980	1629.5	0.093	-	5.0	0.0	36.2	8.9
C	460	67.04	-0.0549	102.2	0.247	-	55.0	0.1	52.1	2.0
D	510	90.16	-0.0125	62.17	0.599	-	79.6	0.4	100.2	1.2
E	510	42.04	0.0073	11.23	0.866	70.3	92.1	0.7	54.7	0.7
F	560	53.23	0.0043	17.52	1.97	118.0	90.3	1.5	67.7	0.4
G	560	44.95	-0.0046	4.917	1.57	-	96.8	2.1	61.4	0.5
H	610	50.60	0.0046	8.697	2.83	109.9	94.9	3.2	67.6	0.2
I	610	49.36	0.0089	5.390	3.09	57.2	96.8	4.4	67.3	0.3
J	660	52.69	0.0025	7.627	3.27	208.0	95.7	5.6	71.0	0.2
K	660	51.69	0.0049	3.536	3.58	103.7	98.0	7.0	71.3	0.2
L	710	52.18	0.0022	4.242	3.99	228.7	97.6	8.6	71.6	0.2
M	710	51.73	0.0034	2.775	4.80	151.7	98.4	10.4	71.6	0.2
N	760	51.93	0.0014	2.059	5.00	368.9	98.8	12.4	72.2	0.2
O	760	51.63	0.0043	2.103	5.76	118.8	98.8	14.6	71.8	0.2
P	810	52.04	0.0042	2.873	5.21	120.9	98.4	16.6	72.0	0.2
Q	810	52.11	0.0049	1.805	5.36	103.1	99.0	18.7	72.5	0.2
R	860	51.97	0.0057	2.754	4.21	89.0	98.4	20.3	72.0	0.2
S	860	52.50	0.0064	2.655	4.51	79.5	98.5	22.1	72.7	0.2
T	910	52.53	0.0035	2.330	3.50	147.2	98.7	23.4	72.9	0.2
U	910	53.17	0.0036	2.969	4.25	140.9	98.4	25.1	73.5	0.2
V	960	52.96	0.0029	4.165	3.64	178.7	97.7	26.5	72.7	0.2
W	960	53.41	0.0024	3.562	4.87	211.2	98.0	28.3	73.6	0.2
X	1010	53.60	0.0067	5.347	4.25	76.2	97.1	30.0	73.2	0.2
Y	1010	54.31	0.0020	5.329	5.99	260.6	97.1	32.3	74.1	0.2
Z	1060	55.38	0.0021	7.363	5.36	237.4	96.1	34.4	74.8	0.2
AA	1060	55.52	0.0027	7.151	7.63	190.3	96.2	37.3	75.1	0.2
AB	1110	57.12	0.0062	11.12	6.95	82.9	94.2	40.0	75.7	0.2
AC	1110	57.09	0.0061	9.232	8.80	83.9	95.2	43.4	76.4	0.2
AD	1110	57.44	0.0048	9.456	8.24	106.3	95.1	46.6	76.8	0.2
AE	1110	58.49	0.0040	12.25	9.70	127.2	93.8	50.4	77.1	0.2
AF	1110	60.17	0.0027	16.41	10.9	185.6	91.9	54.6	77.7	0.2
AG	1110	63.47	0.0020	25.18	11.3	260.9	88.3	59.0	78.7	0.2
AH	1210	62.28	0.0050	22.60	4.95	102.3	89.3	60.9	78.1	0.3
AI	1310	64.08	0.0025	25.39	74.6	202.3	88.3	89.8	79.4	0.2
AJ	1360	65.98	0.0043	33.78	17.3	119.1	84.9	96.5	78.6	0.2
AK	1560	73.80	0.0126	58.85	7.02	40.3	76.4	99.2	79.2	0.3
AL	1710	136.5	-0.0064	274.8	2.07	-	40.5	100.0	77.7	0.9
Integrated			n=37		258.3	144.3	K2O=13.86%		76.1	0.1

ID	Temp (°C)	$^{40}Ar/^{39}Ar$	$^{37}Ar/^{39}Ar$	$^{36}Ar/^{39}Ar$ (x 10^{-3})	$^{39}Ar_K$ (x 10^{-15} mol)	K/Ca	$^{40}Ar^*$ (%)	^{39}Ar (%)	Age (Ma)	±1s (Ma)
Km07-08 k1, K-Feldspar, 15 mg, J=0.0007908±0.05%, D=1.004±0.001, NM-215B, Lab#=57610-01										
B	460	1692.3	-0.2001	5576.7	0.037	-	2.6	0.0	62.2	28.6
C	460	152.2	-0.0691	361.9	0.134	-	29.8	0.0	63.5	4.9
D	510	93.49	0.0097	89.36	0.303	52.6	71.8	0.1	93.3	2.1
E	510	49.82	0.0081	19.59	0.623	63.0	88.4	0.2	61.7	0.9
F	560	54.02	0.0093	14.98	1.16	55.0	91.8	0.5	69.4	0.6
G	560	49.35	0.0144	5.324	1.90	35.4	96.8	0.9	66.9	0.4
H	610	51.93	0.0150	7.126	2.60	34.1	95.9	1.5	69.7	0.3
I	610	51.46	0.0175	1.561	3.62	29.2	99.1	2.3	71.3	0.3
J	660	52.64	0.0207	3.393	4.28	24.6	98.1	3.3	72.2	0.2
K	660	52.28	0.0171	1.603	5.64	29.8	99.1	4.5	72.4	0.2
L	710	52.70	0.0215	1.567	6.33	23.7	99.1	5.9	73.0	0.2
M	710	52.26	0.0157	0.3647	8.53	32.4	99.8	7.8	72.9	0.2
N	760	52.66	0.0154	0.7039	8.94	33.1	99.6	9.8	73.3	0.2
O	760	52.57	0.0132	0.3574	11.6	38.7	99.8	12.4	73.3	0.1
P	810	52.90	0.0115	0.8515	10.9	44.5	99.5	14.8	73.6	0.2
Q	810	53.10	0.0096	0.1749	13.2	52.9	99.9	17.8	74.1	0.1
R	860	53.35	0.0111	0.4524	11.3	46.0	99.8	20.3	74.4	0.1
S	860	53.47	0.0090	0.3320	13.0	56.9	99.8	23.2	74.6	0.1
T	910	53.37	0.0094	0.3712	10.0	54.4	99.8	25.4	74.4	0.2
U	910	53.51	0.0070	0.4948	11.7	72.9	99.7	28.0	74.6	0.1
V	960	53.87	0.0075	1.090	9.01	67.6	99.4	30.0	74.8	0.2
W	960	54.32	0.0072	1.159	10.5	70.8	99.4	32.4	75.4	0.1
X	1010	54.75	0.0068	2.706	8.13	75.5	98.5	34.2	75.4	0.2
Y	1010	55.08	0.0045	3.688	10.5	114.4	98.0	36.5	75.4	0.1
Z	1060	56.13	0.0046	6.986	8.84	110.9	96.3	38.5	75.5	0.2
AA	1060	56.22	0.0053	7.101	12.2	96.1	96.3	41.2	75.6	0.1
AB	1110	57.32	0.0060	10.99	11.0	85.6	94.3	43.7	75.5	0.2
AC	1110	57.00	0.0077	9.480	14.4	66.6	95.1	46.9	75.7	0.1
AD	1110	56.74	0.0071	8.633	13.8	72.1	95.5	49.9	75.7	0.1
AE	1110	57.10	0.0092	9.670	16.8	55.7	95.0	53.7	75.8	0.1
AF	1110	58.27	0.0086	12.04	16.3	59.4	93.9	57.3	76.4	0.1
AG	1110	59.93	0.0072	16.54	18.5	71.2	91.8	61.4	76.9	0.1
AH	1210	59.57	0.0105	16.91	10.2	48.4	91.6	63.7	76.2	0.2
AI	1310	60.94	0.0023	19.38	111.4	223.0	90.6	88.5	77.1	0.1
AJ	1360	61.24	0.0031	21.24	17.9	164.8	89.8	92.5	76.8	0.2
AK	1560	63.68	0.0036	29.92	26.6	142.8	86.1	98.4	76.6	0.2
AL	1710	86.94	0.0024	105.5	7.22	209.4	64.2	100.0	77.9	0.4
Integrated			n=37		449.2	73.2	K2O=14.54%		75.6	0.1

ID	Temp (°C)	$^{40}Ar/^{39}Ar$	$^{37}Ar/^{39}Ar$	$^{36}Ar/^{39}Ar$ (x 10^{-3})	$^{39}Ar_K$ (x 10^{-15} mol)	K/Ca	$^{40}Ar^*$ (%)	^{39}Ar (%)	Age (Ma)	±1s (Ma)
Db05-04 k1, K-Feldspar, 13 mg, J=0.0007918±0.06%, D=1.004±0.001, NM-215B, Lab#=57611-01										
B	460	457.3	-0.0294	1441.5	0.044	-	6.8	0.0	44.2	16.4
C	460	51.42	0.1628	21.73	0.093	3.1	87.5	0.0	63.2	5.9
D	510	141.9	0.0170	38.81	0.336	30.1	91.9	0.1	177.4	2.3
E	510	46.89	0.0271	-2.7243	0.588	18.8	101.7	0.3	66.9	0.9
F	560	58.49	0.0160	6.828	1.31	31.9	96.6	0.7	78.9	0.5
G	560	51.27	0.0157	3.004	1.88	32.4	98.3	1.2	70.6	0.4
H	610	53.41	0.0114	3.560	2.97	44.6	98.0	2.0	73.3	0.3
I	610	52.95	0.0093	1.791	3.95	55.0	99.0	3.1	73.4	0.2
J	660	54.17	0.0107	2.976	5.07	47.7	98.4	4.5	74.6	0.2
K	660	53.72	0.0104	2.068	6.17	49.2	98.9	6.2	74.3	0.2
L	710	54.26	0.0107	2.026	7.43	47.5	98.9	8.3	75.1	0.2
M	710	54.12	0.0092	1.775	8.69	55.6	99.0	10.7	75.0	0.2
N	760	54.11	0.0089	1.755	9.18	57.3	99.0	13.2	75.0	0.1
O	760	54.23	0.0064	1.548	10.9	79.9	99.2	16.3	75.2	0.1
P	810	54.30	0.0062	1.661	10.3	81.8	99.1	19.1	75.3	0.2
Q	810	54.36	0.0066	1.574	12.1	77.5	99.1	22.5	75.4	0.1
R	860	54.56	0.0073	1.009	10.4	69.9	99.5	25.4	75.9	0.2
S	860	54.66	0.0057	1.505	12.6	90.3	99.2	28.9	75.8	0.1
T	910	54.76	0.0067	1.520	10.9	76.3	99.2	31.9	76.0	0.1
U	910	55.05	0.0055	1.601	12.7	92.1	99.1	35.4	76.3	0.1
V	960	55.16	0.0059	2.012	9.47	85.8	98.9	38.1	76.3	0.2
W	960	55.42	0.0026	1.707	11.2	194.6	99.1	41.2	76.8	0.2
X	1010	55.53	0.0042	2.880	8.72	122.7	98.5	43.6	76.5	0.2
Y	1010	55.62	0.0034	3.321	11.1	148.2	98.2	46.7	76.4	0.1
Z	1060	56.72	0.0049	4.276	9.16	103.6	97.8	49.2	77.5	0.2
AA	1060	56.97	0.0050	4.860	12.1	101.4	97.5	52.6	77.6	0.2
AB	1110	57.57	0.0063	6.132	10.6	81.2	96.9	55.5	77.9	0.1
AC	1110	58.15	0.0061	6.224	13.6	84.2	96.8	59.3	78.7	0.1
AD	1110	58.61	0.0061	7.020	12.4	83.2	96.5	62.7	79.0	0.2
AE	1110	59.22	0.0065	7.897	14.6	78.1	96.1	66.8	79.5	0.2
AF	1110	60.89	0.0054	11.77	13.7	94.0	94.3	70.6	80.2	0.2
AG	1110	62.89	0.0039	18.17	14.7	131.7	91.5	74.7	80.4	0.2
AH	1210	62.48	0.0099	13.77	5.84	51.6	93.5	76.3	81.6	0.2
AI	1310	62.77	0.0018	14.92	69.5	284.4	93.0	95.6	81.5	0.1
AJ	1360	63.44	0.0043	18.99	9.50	117.7	91.2	98.3	80.8	0.2
AK	1560	75.99	0.0075	63.13	3.28	67.6	75.5	99.2	80.1	0.4
AL	1710	125.3	0.0055	234.1	2.99	92.8	44.8	100.0	78.5	0.7
Integrated			n=37		360.1	91.7	K2O=13.44%		78.1	0.1

ID	Temp (°C)	$^{40}Ar/^{39}Ar$	$^{37}Ar/^{39}Ar$	$^{36}Ar/^{39}Ar$ (x 10^{-3})	$^{39}Ar_K$ (x 10^{-15} mol)	K/Ca	$^{40}Ar^*$ (%)	^{39}Ar (%)	Age (Ma)	±1s (Ma)

Notes:

Isotopic ratios corrected for blank, radioactive decay, and mass discrimination, not corrected for interfering reactions.

Errors quoted for individual analyses include analytical error only, without interfering reaction or J uncertainties.

Integrated age calculated by summing isotopic measurements of all steps.

Integrated age error calculated by quadratically combining errors of isotopic measurements of all steps.

Plateau age is inverse-variance-weighted mean of selected steps.

Plateau age error is inverse-variance-weighted mean error (Taylor, 1982) times root MSWD where MSWD>1.

Plateau error is weighted error of Taylor (1982).

Decay constants and isotopic abundances after Steiger and Jäger (1977).

symbol preceding sample ID denotes analyses excluded from plateau age calculations.

Weight percent K_2O calculated from ^{39}Ar signal, sample weight, and instrument sensitivity.

Ages calculated relative to FC-2 Fish Canyon Tuff sanidine interlaboratory standard at 28.02 Ma

Decay Constant (LambdaK (total)) = 5.543e-10/a

Correction factors:

$(^{39}Ar/^{37}Ar)_{Ca}$ = 0.00068 ± 5e-05

$(^{36}Ar/^{37}Ar)_{Ca}$ = 0.00028 ± 2e-05

$(^{38}Ar/^{39}Ar)_K$ = 0.0125

$(^{40}Ar/^{39}Ar)_K$ = 0 ± 0.0004

REFERENCES

Ague JJ, Brimhall GH (1988) Magmatic arc asymmetry and distribution of anomalous plutonic belts in the batholiths of California: Effects of assimilation, crustal thickness, and depth of crystallization. Geol Soc Am Bull 100:912-927

Annen C (2007) The growth of magma bodies by amalgamation of discrete sheet intrusions: Implications for the formation of magma chambers. Eos Trans AGU (program and abstracts)

Annen C (2009) From plutons to magma chambers: Thermal constraints on the accumulation of eruptible silicic magma in the upper crust. Earth Planet Sci Lett 284:409-416

Annen C, Scaillet B, Sparks RSJ (2006) Thermal constraints of the emplacement rate of a large intrusive complex: the Manaslu Leucogranite, Nepal Himalaya. J Petrol 47:71-95

Annen C, Pichavant M, Bachmann O, Burgisser A (2008) Conditions for growth of a long-lived shallow crustal magma chamber below Mount Pelee volcano (Martinique, Lesser Antilles Arc). J Geophys Res 113

Bachmann O, Miller CF, de Silva SL (2007) The volcanic-plutonic connection as a stage for understanding crustal magmatism. J Volcanol Geotherm Res 167:1-23

Bartley JM, Glazner AF, Coleman DS, Kylander-Clark ARC, Friedrich AM (2007) Large Laramide dextral offset across Owens Valley, California, and its possible relation to tectonic unroofing of the southern Sierra Nevada. In: Till AB, Roeske SM, Foster DA, Sample JC (eds) Exhumation Processes Along Major Continental Strike-slip Fault Systems. Geol Soc Am Spec Pap 434:129-148

Bartley JM, Coleman DS, Glazner AF (2008) Incremental emplacement of granitic plutons by magmatic crack-seal. In: Petford N, Sparks S (eds) Plutons and Batholiths (Wallace Pitcher Memorial Issue). Trans R Soc Edinb Earth Sci 97:383-396

Barton MD, Hanson RB (1989) Magmatism and the development of low-pressure metamorphic belts: Implications from the western United States and thermal modeling. Geol Soc Am Bull 101:1051-1065

Barton KE, Howell DG, Vigil, JF (2003) The North America Tapestry of Time and Terrain. US Geol Surv I-2781

Bateman PC (1965) Geologic Map of the Blackcap Mountain quadrangle, Fresno County, California. US Geol Surv Rep GQ-0529

Bateman PC (1992) Plutonism in the central part of the Sierra Nevada batholith, California. US Geol Surv Prof Pap 1483

Bateman PC, Moore JG (1965) Geologic Map of the Mount Goddard quadrangle, Fresno and Inyo counties, California. US Geol Surv Rep GQ-0429

Bateman PC, Dodge FCW (1970) Variations of major chemical constituents across the central Sierra Nevada batholith. Geol Soc Am Bull 81:409-420

Bateman PC, Carman MF, Clark LC, Jackson ED, Parker RL (1964) Geologic Map of the Big Pine 15-minute quadrangle, California

Bateman PC, Pakiser LC, Kane MF (1965) Geology and tungsten mineralization of the Bishop District California. US Geol Surv Prof Pap 470

Berger GW (1975) $^{40}Ar/^{39}Ar$ step heating of thermally overprinted biotite, hornblende and potassium feldspar from Eldora, Colorado. Earth Planet Sci Lett 26:387-408

Chen JH, Moore JG (1982) Uranium-lead isotopic ages from the Sierra Nevada batholith, California. J Geophys Res 87B:4761-4784

Clark MK, Maheo G, Saleeby J, Farley KA (2005) The non-equilibrium landscape of the southern Sierra Nevada, California. Geol Soc Am Today 15:4-9

Coleman DS, Glazner AF, Miller JS, Bradford KJ, Frost TP, Joye JL, Bachl CA (1995) Exposure of a Late Cretaceous layered mafic-felsic magma system in the central Sierra Nevada batholith, California. Contrib Mineral Petrol 120:129-136

Coleman DS, Glazner AF (1998) The Sierra Crest magmatic event; rapid formation of juvenile crust during the Late Cretaceous in California. In: Ernst WG, Nelson CA (eds) Integrated Earth and Environmental Evolution of the Southwestern United States; the Clarence A. Hall, Jr. volume. Bellwether Publishing, USA, pp. 253-272

Coleman DS, Gray W, Glazner AF (2004) Rethinking the emplacement and evolution of zoned plutons: Geochronologic evidence for incremental assembly of the Tuolumne Intrusive Suite, California. Geology 32:433-436

Costa F (2008) Residence times of silicic magmas associated with calderas. In: Gottsmann J, Martí J (eds) Developments in Volcanology 10. Caldera Volcanism: analysis, modeling, and response. Elsevier, pp. 1-55

Cross TA, Pilger RH (1982) Controls of subduction geometry, locations of magmatic arcs and tectonics of arc and back-arc regions. Geol Soc Am Bull 93:545-562

Crowley JL, Schoene B, Bowring SA (2007) U-Pb dating of zircon in the Bishop Tuff at the millennial scale. Geology 35:1123-1126

de Silva SL, Gosnold WD (2007) Episodic construction of batholiths: Insights from the spatiotemporal development of an ignimbrite flare-up. J Volcanol Geotherm Res 167:320-335

Dodson MH (1973) Closure temperature in cooling geochronological and petrological systems. Contrib Mineral Petrol 40:259-274

du Bray EA, Moore JG (1985) Geologic map of the Olancha quadrangle, southern Sierra Nevada, California. US Geol Surv Rep MF-1734

Ducea MN, Saleeby JB (1998) The age and origin of a thick mafic-ultramafic keel from beneath the Sierra Nevada batholith. Contrib Mineral Pet 133:169-185

Dumitru TA (1990) Subnormal Cenozoic geothermal gradients in the extinct Sierra Nevada magmatic arc: consequences of the Laramide and post-Laramide shallow-angle subduction. J Geophys Res 95:4925-4941

Engebretson DC, Cox A, Gordon RG (1985) Relative motions between oceanic and continental plates in the Pacific Basin. Boulder, Colorado, Geol Soc Am Spec Pap 206

Farley KA, Wolf RA, Silver LT (1996) The effects of long alpha-stopping distances on (U-Th)/He ages. Geochim Cosmochim Acta. 60:4223-4229

Frost TP, Mahood GA (1987) Field, chemical, and physical constraints on mafic-felsic magma interaction in the Lamarck Granodiorite, Sierra Nevada, California. Geol Soc Am Bull 99:272-291

Frost TP, Mattinson JM (1988) Late Cretaceous U-Pb age of a mafic intrusion from the eastern Sierra Nevada, California. Isochron West 51:15-18

Frost TP, Mattinson JM, (1993) Age and tectonic implications of mid-Mesozoic calc-alkalic hornblende-rich mafic plutonic rocks of the eastern Sierra Nevada, California. Isochron West 59:11-16

García A, Contreras E, Viggiano JC (1989) Establishment of an empirical correlation for estimating the thermal conductivity of igneous rocks. Int J Thermophys 10:1063-1974

Gaschnig RM (2005) Cause, timing, and significance of brittle deformation in Little Lakes Valley, eastern Sierra Nevada, California. MS Thesis, University of North Carolina at Chapel Hill

Glazner AF, Bartley JM, Coleman DS, Gray W, Taylor RZ (2004) Are plutons assembled over millions of years by amalgamation from small magma chambers? Geol Soc Am Today 14:4-11

Gracely JT (2006) Rapid pluton emplacement via multiple discrete processes, Lamarck Granodiorite, Central Sierra Nevada, California. MS Thesis, University of North Carolina at Chapel Hill

Greene DC, Schweickert RA (1995) The Gem Lake shear zone: Cretaceous dextral transpression in the Northern Ritter Range pendant, eastern Sierra Nevada, California. Tecton 14:945-961

Grove M, Lovera OM, Harrison TM (2003) Late Cretaceous cooling of the east-central Peninsular Ranges batholith (33°N): Relationships to La Posta pluton emplacement, Laramide shallow subduction, and forearc sedimentation. In: Johnson SE, Paterson SR, Fletcher JM, Girty GH, Kimbrough DL, Martín-Barajas A (eds) Tectonic evolution of north-western Mexico and southwestern USA. Geol Soc Am Spec Pap 374:355-379

Grunder AL, Klemetti EW, Feeley TC, McKee Cm (2008) Eleven million years of arc volcanism at the Aucanquilcha Volcanic Cluster, northern Chilean Andes: implications for the life span and emplacement of plutons. Trans R Soc Edinb Earth Sci 97:415-436

Gutscher M, Maury R, Eissen J, Bourdon E (2000) Can slab melting be caused by flat subduction? Geology 28:535-538

Hanson RB, Barton MD (1989) Thermal development of low-pressure metamorphic belts: Results from two-dimensional numerical models. J Geophys Res 94:10,363-10,377

Harrison TM (1981) Diffusion of ^{40}Ar in hornblende. Contrib Mineral Petrol 78:324-331

Harrison TM, Clarke GKC (1979) A model of the thermal effects of igneous intrusion and uplift as applied to Quottoon pluton, British Columbia. Can J Earth Sci 16:411-420

Harrison TM, Duncan I, McDougall I (1985) Diffusion of ^{40}Ar in biotite: temperature, pressure, and compositional effects. Geochim Cosmochim Acta 49:2461-2468

Harrison TM, Grove M, Lovera OM, Zeitler PK (2005) Continuous thermal histories from inversion of closure profiles. Rev Mineral Geochem 58:389-409

Hathaway M (2002) Geology of the Inconsolable Range, east-central Sierra Nevada, Kings Canyon National Park and John Muir Wilderness, California; magmatic emplacement and the dynamic evolution of composite intrusions. PhD Dissertation, University of California at Los Angeles

Heizler MT, Lux DR, Decker ER (1988) The age and cooling history of the Chain of Ponds and Big Island Pond plutons and the Spider Lake Granite, west-central Maine and Quebec. Am J Sci 288:925-952

Hildreth W (2004) Volcanological perspectives on long Valley, Mammoth Mountain, and Mono Craters: several contiguous but discrete systems. J Volcanol Geotherm Res 136:169-198

Hirt WH (1989) The petrological and mineralogical zonation of the Mount Whitney Intrusive Suite, eastern Sierra Nevada, California. PhD Dissertation, University of California-Santa Barbara

Hirt WH (2006) Emplacement pressure differences across the granodiorite of Sugarloaf: Implications for pluton architecture and uplift of the central Sierra Nevada, California. Eos Trans AGU (program and abstracts, fall meeting V31B-0582)

Hirt WH (2007) Petrology of the Mount Whitney Intrusive Suite, eastern Sierra Nevada, California: Implications for the emplacement and differentiation of the composite felsic intrusion. Geol Soc Am Bull 119:1185-1200

House MA, Wernicke BP, Farley KA, Dumitru TA (1997) Cenozoic thermal evolution of the central Sierra Nevada, California, from (U-Th)/He thermochronometry. Earth Planet Sci Lett 151:167-179

House MA, Wernicke BP, Farley KA (2001) Paleo-geomorphology of the Sierra Nevada, California, from (U-Th)/He ages in apatite. Am J Sci 301:77-102

Hutton DHW (1988) Granite emplacement mechanisms and tectonic controls: inferences from deformation studies. Trans R Soc Edinb Earth Sci 79:245-255

Iyer HM (1984) Geophysical evidence for the locations, shapes and sizes, and internal structures of magma chambers beneath regions of Quaternary volcanism. Philo Trans R Soc Lond Math Phys Sci 310:473-510

Jaffey AH, Flynn KF, Glendenin LE, Bentley WC, Essling AM (1971) Precision measurement of half-lives and specific activities of ^{235}U and ^{238}U. Phys Rev C4:1889-1906

Kies RP, Abbott PL (1983) Rhyolite clast populations and tectonics in California continental borderland. J Sed Petrol 53:461-475

Kistler RW, Chappell BW, Peck BL, Bateman PC (1986) Isotopic variation in the Tuolumne intrusive suite, central Sierra Nevada, California. Contrib Mineral Petrol 94:205-220

Kistler RW (1990) Two different lithosphere types in the Sierra Nevada, California. In: Anderson JL (ed) The nature and origin of Cordilleran magmatism. Geol Soc Am Mem 174:271-281

Krogh TE (1973) A low-contamination method for hydrothermal decomposition of zircon and extraction of U and Pb for isotopic age determinations. Geochim Cosmochim Acta 37:485-494

Lanphere MA, Dalrymple GB (1976) Identification of excess ^{40}Ar by the $^{40}Ar/^{39}Ar$ age spectrum technique. Earth Planet Sci Lett 32:141-148

Lee C, Yin Q, Rudnick RL, Chesley JT, Jacobsen SB (2000) Osmium isotope for Mesozoic removal of lithospheric mantle beneath the Sierra Nevada, California. Science 289:1912-1916

Lipman PW (2007) Incremental assembly and prolonged consolidation of Cordilleran magma chambers: Evidence from the Southern Rocky Mountain volcanic field. Geosphere 3:42-70

Lo C, Onstott TC (1989) ^{39}Ar recoil artifacts in chloritized biotite. Geochim Cosmochim Acta 53:2697-2711

Lockwood JP, Lydon PA (1975) Geologic map of the Mount Abbot quadrangle, central Sierra Nevada, California. US Geol Sur Rep GQ-1155

Lovera OM, Richter FM, Harrison TM (1989) $^{40}Ar/^{39}Ar$ geothermometry for slowly cooled samples having a distribution of diffusion domain sizes. J Geophys Res 94:17,917-17,935

Lovera OM, Richter FM, Harrison TM (1991) Diffusion domains determined by ^{39}Ar release during step heating. J Geophys Res 96:2057-2069

Lovera OM, Grove M, Harrison TM, Mahon KI (1997) Systematic analysis of K-feldspar $^{40}Ar/^{39}Ar$ step heating experiments I: Significance of activation energy determinations. Geochimica Cosmochim Acta 61:3171-3192

Lovera OM, Grove M, Harrison TM (2002) Systematic analysis of K-feldspar $^{40}Ar/^{39}Ar$ step heating results II: Relevance of laboratory argon diffusion properties to nature. Geochimica Cosmochim Acta 66:1237-1255

Ludwig KR (1980) Calculation of uncertainties of U-Pb isotope data. Earth Planet Sci Lett 46:212-220

Ludwig KR (1998) On the treatment of concordant uranium-lead ages. Geochim Cosmochim Acta 62:665-676

Ludwig KR (2003) Isoplot 3.00; A geochronological toolkit for Microsoft Excel. Berkley Geochronology Center Spec Pub 4

Mahan KH, Bartley JM, Coleman DS, Glazner AF, Carl BS (2003) Sheeted intrusion of the synkinematic McDoogle pluton, Sierra Nevada, California. Geol Soc Am Bull 115:1570-1582

Mansfield CF (1979) Upper Mesozoic subsea fan deposits in the southern Diablo Range, California: Record of the Sierra Nevada magmatic arc. Geol Soc Am Bull 90:1025-1046

Masturyono, McCaffrey R, Wark DA, Roecker SW, Fauzi, Ibrahim G, Sukhyar (2001) Distribution of magma beneath the Toba caldera complex, north Sumatra, Indonesia, constrained by three-dimensional *P* wave velocities, seismicity, and gravity data. Geochem Geophy Geosys 2000GC000096

Mattinson JM (2005) Zircon U-Pb chemical abrasion ("CA-TIMS") method: combining annealing and multi-step partial dissolution analysis for improved precision and accuracy of zircon ages. Chem Geol 220:47-66

Matzel JEP, Bowring SA, Miller RB (2006) Time scales of pluton construction at differing crustal levels: Examples from the Mount Stuart and Tenpeak intrusions, North Cascades, Washington. Geol Soc Am Bull 118:1412-1430

McDougall I, Harrison TM (1999) Geochronology and thermochronology by the $^{40}Ar/^{39}Ar$ method: Second Edition. Oxford University Press, New York

Menand T (2008) The emplacement depth of sills and larger magma bodies: what are the physical controls and how are emplacement depths determined? Geophys Res Abstracts (EGU2008-A-03538)

Michel J, Baumgartner L, Putlitz B, Schaltegger U, Ovtcharova M (2008) Incremental growth of the Patagonian Torres del Paine laccolith over 90 k.y. Geology 36:459-462

Miller WM, Fallick AE, Leake BE, Macintyre RM, Jenkin GRT (1991) Fluid disturbed hornblende K-Ar ages from the Dalradian rocks of Connemara, Western Ireland. J Geol Soc Lond 148:985-992

Miller JS, Wooden JL (2004) Residence, resorption, and recycling of zircons in Devils Kitchen Rhyolite, Coso Volcanic Field, California. J Petrol 45:2155-2170

Miller JS, Matzel JEP, Miller CF, Burgess SD, Miller RB (2007) Zircon growth and recycling during the assembly of large, composite arc plutons. J Volcanol Geotherm Res 167:282-299

Moore JG (1963) Geology of the Mount Pinchot quadrangle, southern Sierra Nevada, California. US Geol Surv Bull 1130

Moore JG (1978) Geologic map of the Marion Peak quadrangle, Fresno County, California. US Geol Surv Rep GQ-1399

Moore JG (1981) Geologic map of the Mount Whitney quadrangle, Inyo and Tulare counties, California. US Geol Surv Rep GQ-1545

Moore JG, Sisson TW (1985) Geologic map of the Kern Peak quadrangle, Tulare County, California. US Geol Surv Rep GQ-1584

Moore JG, Sisson TW (1987) Geologic map of the Triple Divide Peak quadrangle, Tulare County, California. US Geol Surv Rep GQ-1636

Moran SC, Lees JM, Malone SD (1999) *P* wave crustal velocity structure in the greater Mount Rainier area from local earthquake tomography. J Geophys Res 104:10,775-10,786

Mundil R, Ludwig KR, Metcalfe I, Renne PR (2004) Age and timing of the Permian mass extinctions: U/Pb dating of closed-system zircons. Science 305:1760-1763

Murase T, McBirney AR (1973) Properties of some common igneous rocks and their melts at high temperatures. Geol Soc Am Bull 84:3563-3592

Ortega-Rivera A (2003) Geochronological constraints on the tectonic history of the Peninsular Ranges batholith of Alta and Baja California: Tectonic implications for western Mexico. In: Johnson SE, Paterson SR, Fletcher JM, Girty GH, Kimbrough DL, Martín-Barajas A (eds) Tectonic evolution of north-western Mexico and southwestern USA. Geol Soc Am Spec Pap 374:297-335

Parrish RP (1987) An improved micro-capsule for zircon dissolution in U-Pb geochronology. Chem Geol 66:99-102

Parrish RP, Krogh TE (1987) Synthesis and purification of ^{205}Pb for U-Pb geochronology. Chem Geol 66:103-110

Parsons I, Brown WL, Smith JV (1999) ^{40}Ar/^{39}Ar thermochronology using alkali feldspars: real thermal history or mathematical mirage of microtexture? Contrib Mineral Petrol 136:92-110

Pertermann M, Whittington AG, Hofmeister AM, Spera FJ, Zayak J (2008) Transport properties of low-sanidine single-crystals, glasses and melts at high temperatures. Contrib Mineral Petrol 155:689-702

Petford N, Cruden AR, McCaffrey KJW, Vigneresse JL (2000) Granite magma formation, transport and emplacement in the Earth's crust. Nature 408:669-673

Pickett DA, Saleeby JB (1993) Thermobarometric constraints on the depth of the exposure and conditions of plutonism and metamorphism at deep levels in the Sierra Nevada batholith, Tehachapi Mountains, California. J Geophys Res 98:609-629

Pritchard ME, Simons M (2004) An InSAR-based survey of volcanic deformation in the southern Andes. Geophys Res Lett 31:1-4

Quidelleur X, Grove M, Lovera OM, Harrison TM, Yin A (1997) Thermal evolution and slip history of the Renbu Zedong thrust, southeastern Tibet. J Geophys Res 102:2659-2679

Reiners PW, Zanetti KA, Spell TL, Nicolescu S (2004) Zircon (U-Th)/He thermochronometry: He diffusion and comparisons with $^{40}Ar/^{39}Ar$ dating. Geochim Cosomochim Acta 68:1857-1887

Renne PR (2006) Progress and challenges in K-Ar and $^{40}Ar/^{39}Ar$ geochronology. In: Olszewski T (ed) Geochronology: Emerging Opportunities. Paleont Soc Pap 12:47-66

Renne PR, Tobisch OT, Saleeby JB (1993) Thermochronologic record of pluton emplacement, deformation, and exhumation at Courtright shear zone, central Sierra Nevada, California. Geology 21:331-334

Renne PR, Swisher CC, Deino AL, Karner DB, Owens TL, DePaolo DJ (1998) Intercalibration of standards, absolute ages and uncertainties in $^{40}Ar/^{39}Ar$ dating. Chem Geol 145:117-152

Renne PR, Mundil R, Balco G, Min K (2009) Simultaneous determination of ^{40}K decay constants and age of the Fish Canyon sanidine $^{40}Ar/^{39}Ar$ standard. Geol Soc Am (abstracts with programs)

Robertson EC (1988) Thermal properties of rocks. US Geol Surv Open File Rep 88-441

Saint-Blanquat M, Tikoff B (1997) Development of magmatic to solid-state fabrics during syntectonic emplacement of the Mono Creek Granite, Sierra Nevada batholith. In: Bouchez JL, Hutton DHW, Stephens WE (eds) Granite: From Segregation of Melt to Emplacement Fabrics. Kluwer, Netherlands, pp 231-252

Saleeby J (2003) Segmentation of the Laramide Slab–evidence from the southern Sierra Nevada region. Geol Soc Am Bull 115:655-668

Saleeby J, Kistler RW, Longiaru S, Moore JG, Nokleberg WJ (1990) Middle Cretaceous silic metavolcanic rocks in the Kings Canyon area, central Sierra Nevada, California. In: Anderson JL (ed) The nature and origin of the Cordilleran magmatism. Geol Soc Am Mem 174:251-270

Saleeby J, Ducea M, Clemens-Knott D (2003) Production and loss of high-density batholithic root, southern Sierra Nevada, California. Tecton 22:1-23

Saleeby J, Farley KA, Kistler RW, Fleck RJ (2007) Thermal evolution and exhumation of deep-level batholithic exposures, southernmost Sierra Nevada, California. In: Cloos M, Carlson WD, Gilbert MC, Liou JG, Sorensen SS (eds) Convergent Margin Terranes and Associated Regions: A Tribute to W. G. Ernst. Geol Soc Am Spec Pap 419:39-66

Saleeby J, Ducea MN, Busby C, Nadin E, Wetmore PH (2008) Chronology of pluton emplacement and regional deformation in the southern Sierra Nevada batholith, California. In: Wright JE, Shervais JW (eds) Ophiolites, Arcs, and Batholiths. Geol Soc Am Spec Pap 438:1-31

Saleeby J, Saleeby Z, Liu L, Maheo G (2010) Mid-Cretaceous regional exhumation of the Sierra Nevada-Great Valley batholith and a possible tectonic driving mechanism. Geol Soc Am (abstracts with programs) 42:67

Sanders RE, Heizler MT, Goodwin LB (2006) $^{40}Ar/^{39}Ar$ thermochronology constraints on the timing of Proterozoic basement exhumation and fault ancestry, southern Sangre de Cristo Range, New Mexico. Geol Soc Am Bull 118:1489-1506

Schmitz MD (2010) Boise State Isotope Geology laboratory LABSHARE. http://earth.boisestate.edu/isotope/labshare.html

Schmitz MD, Bowring SA (2001) U-Pb zircon and titanite systematics of the Fish Canyon Tuff: an assessment of high precision U-Pb geochronology and its application to young volcanic rocks. Geochim Cosmochim Acta 65:2571-2587

Scott DJ, St-Onge MR (1995) Constraints on Pb closure temperature in titanite based rocks from Ungava orogen, Canada: Implications for U-Pb geochronology and P-T-t path determinations. Geology 23:1123-1126

Simon JI, Renne PR, Mundil R (2008) Implications of pre-eruptive magmatic histories of zircons for U-Pb geochronology of silicic extrusions. Earth Planet Sci Lett 266:182-194.

Singer BS, Pringle MS (1996) Age and duration of the Matuyama-Brunhes geomagnetic polarity reversal from $^{40}Ar/^{39}Ar$ incremental heating analyses of lavas. Earth Planet Sci Lett 139:47-61

Sisson VB, Onstott T (1986) Dating blueschist metamorphism: A combined $^{40}Ar/^{39}Ar$ and electron microprobe approach. Geochim Cosmochim Acta 50:2111-2117

Spear F (1993) Metamorphic phase equilibria and pressure-temperature-time paths. Mineral Soc Am, Washington

Stacey JS, Kramers JD (1975) Approximation of terrestrial lead isotope evolution by a two stage model. Earth Planet Sci Lett 26:207-221

Stearns MA, Bartley JM (2010) Refinement of the crack-seal model: insights from the McDoogle pluton, Sierra Nevada, CA. Geol Soc Am Bull (submitted)

Steiger RH, Jäger E (1977) Subcommission on geochronology; convention on the use of decay constants in geo- and cosmochemistry. Earth Planet Sci Lett 36:359-362

Stern TW, Bateman PC, Morgan BA, Newell MF, Peck DL (1981) Isotopic U-Pb ages of zircon from granitoids of the central Sierra Nevada, California. US Geol Surv Prof Pap 1185:1-17

Stimac JA, Fraser G, Wohletz K (2001) Thermal modeling of the Clear Lake magmatic-hydrothermal system, California, USA. Geothermics 30:349-390

Stone P, Dunne GC, Moore JG, Smith GI (2000) Geologic map of the Lone Pine 15' quadrangle, Inyo County, California. US Geol Surv Rep I-2617

Taylor JR (1982) An Introduction to Error Analysis: The Study of Uncertainties in Physical Measurements. Univ Sci Books, California

Tera F, Wasserburg, GJ (1972) U-Th-Pb systematics in three Apollo 14 basalts and the problem of initial Pb in lunar rocks. Earth Planet Sci Lett 14:281-304

Tikoff B, Teyssier C (1992) Crustal-scale, en echelon "P-shear" tensional bridges: A possible solution to the batholithic room problem. Geology 20:927-930

Tikoff B, Saint Blanquat M (1997) Transpressional shearing and strike-slip partitioning in the Late Cretaceous Sierra Nevada magmatic arc, California. Tecton 16:442-459

Tobisch OT, Saleeby JB, Renne PR, McNulty B, Tong W (1995) Variations in deformation fields during development of a large-volume magmatic arc, central Sierra Nevada, California. Geol Soc Am Bull 107:148-166

Turcotte DL, Schubert G (2002) Geodynamics. Cambridge University Press, Cambridge

Waite GP, Moran SC (2009) *Vp* structure of Mount St. Helens, Washington, USA, imaged with local earthquake tomography. J Volcanol Geotherm Res 182:113-122

Wartho J (1995) Apparent argon diffusive loss $^{40}Ar/^{39}Ar$ age spectra in amphiboles. Earth Planet Sci Lett 134:393-407

Wartho J, Dodson MH, Rex DC, Guise PG (1991) Mechanisms of Ar release from Himalayan metamorphic hornblende. Am Mineral 76:1446-1448

Watabayashi J, Sawyer TL (2001) Stream incision, tectonics, uplift, and evolution of topography of the Sierra Nevada, California. J Geology 109:539-562

Watson EB, Harrison TM (1983) Zircon saturation revisited: temperature and composition effects in a variety of crustal magma types. Earth Planet Sci Lett 64:295-304

Whittington AG, Hofmeister AM, Nabelek PI (2009) Temperature-dependent thermal diffusivity of the Earth's crust and implications for magmatism. Nature 458:319-321

Wohletz K (2008) Kware HEAT 3D. http: //www.ees1.lanl.gov/Wohletz/Heat.htm